Warm Inflationary Universe at the Large and the Small Scales

A thesis submitted in partial fulfilment of
the requirements for the degree of

Doctor of Philosophy

by

Richa Arya

(Roll No. 15330011)

Under the supervision of

Prof. Raghavan Rangarajan

School of Arts and Sciences, Ahmedabad University

and programme supervisor

Prof. Namit Mahajan

Theoretical Physics Division

Physical Research Laboratory, Ahmedabad, India.

DISCIPLINE OF PHYSICS

INDIAN INSTITUTE OF TECHNOLOGY GANDHINAGAR

2020

Dedicated to

my beloved family

Declaration

I declare that this written submission represents my ideas in my own words and where others' ideas or words have been included, I have adequately cited and referenced the original sources. I also declare that I have adhered to all principles of academic honesty and integrity and have not misrepresented or fabricated or falsified any idea/data/fact/source in my submission. I understand that any violation of the above will be cause for disciplinary action by the Institute and can also evoke penal action from the sources which have thus not been properly cited or from whom proper permission has not been taken when needed.

Signature

Name: Richa Arya

(Roll No: 15330011)

Date:

CERTIFICATE

It is certified that the work contained in the thesis titled **"Warm Inflationary Universe at the Large and the Small Scales"** by Ms. Richa Arya (Roll No. 15330011), has been carried out under my supervision and that this work has not been submitted elsewhere for a degree.

Prof. Raghavan Rangarajan
School of Arts and Sciences,
Ahmedabad University,
Ahmedabad, India.

(Thesis Supervisor)

Date:

Thesis Approval

The thesis entitled

Warm Inflationary Universe at the Large and the Small Scales

by

Richa Arya

(Roll No. 15330011)

is approved for the degree of

Doctor of Philosophy

Examiner	Examiner
Supervisor	Chairman

Date: ____________________

Place: ____________________

Acknowledgments

"The journey matters more than the destination."

My Ph.D. journey could be accomplished because of the blessings, motivation, and belief of many people. I take this opportunity to express my sincere gratitude to all those who helped and supported me to make it possible.

To begin with, I am extremely grateful to my supervisor Prof. Raghavan Rangarajan for his guidance, encouragement, and support throughout my Ph.D. Working with him was a great learning experience for me in all respects. The discussions with him have always benefited me in getting a better understanding of the subject. I am very thankful to him for improving me by correcting my mistakes and for being so understanding and cooperative always.

I am very grateful to my programme supervisor and DSC member Prof. Namit Mahajan for his immense help and support. His advices and suggestions have always benefited and motivated me to move ahead. I am very thankful to him for the field theory discussions that helped me in my understanding. I would also like to express my gratitude to my DSC members Prof. Jitesh Bhatt and Prof. Hiranmaya Mishra, for their insightful discussions, encouragement and support throughout my Ph.D. I sincerely thank Prof. Srubabati Goswami and Prof. Subhendra Mohanty for their teaching and guidance during the coursework projects. I have enjoyed learning and working under their supervision. I also sincerely thank Prof. Saurabh D Rindani, Prof. Angom Dilip Kumar, Prof. Partha Konar, Prof. Navinder Singh, Prof. Bijaya Sahoo and Prof. Jay Banerjee for their teaching during my coursework.

I am very thankful to my collaborators Dr. Arnab Dasgupta, Dr. Gaurav Goswami, and Dr. Jayanti Prasad, for all the discussions and the teamwork we carried out. Working with them, I learned many new numerical codes and techniques. I deeply thank Arnab for being so encouraging and helpful, like my elder brother. I am extremely thankful to my friend Prakrut for helping me in installing CosmoMC software and Planck likelihood on HPC cluster.

I am also very thankful to Prof. Arjun Berera, Prof. Mar Bastero Gil, and Prof. Rudnei Ramos and Luis B. Ventura for the email discussions and clarifications to my doubts.

I am very thankful to all the staff members of the theory division, library, administration, and computer center for their assistance and support throughout. A special thanks to Mr. Jigar Raval for conducting the HPC cluster training programme and for assistance in troubleshooting cluster related issues at various times.

I am also grateful to all my seniors, especially Luxmi didi, Lata didi, Anjali didi, Deepak bhaiya, Uday bhaiya, Krishna bhaiya, Bhavesh, Vishnu, Aman, Navpreet, Rukmani, for their support and encouragement. Also, it would have been an incomplete journey without my friends and batchmates - Arvind, Naman, Subir, Archita, Aarthy, Rahul, Akanksha, Ranadeep, Nidhi, Shefali, Shivangi, Varun, Kaustav, Balbeer, Ashish, Harsh Oza, Harsh Raj. Thank you so much for being there and sharing good times and celebrations. I want to express my thanks to all my juniors, especially, Nisha, Deepika, Priyank, Harish, Shivani, Surendra, Hrushikesh, Deepak, Sarika, Anshika, Tanmay, Naval, Anju, Namita, for being so supportive and friendly.

A big thanks to my best friends - Arvind and Naman, for always being there to help, support, and motivate me. Thanks a lot for always taking care of me. I will always cherish the memorable trips we planned at the last minutes, the home parties we had, the driving practice sessions, and so much fun that is hard to express in words.

I am also very thankful to my friends and well-wishers, Raza and Vikram, for always remembering my birthday. A special thanks to my dear friends, Komal, Dilpreet, Ruchi, Shifa, Aastha, Vishal, for supporting and inspiring me at all the times.

I am highly obliged to all my school and college teachers for instilling in me the curiosity towards science. Special thanks to Prof. Patrick Das Gupta and Prof. T.R. Seshadri for introducing me to the subject of Einstein's Theory of General Relativity and Cosmology.

Above all, I am immensely grateful to my parents and grandparents for their blessings, encouragement, and belief in me throughout my life. I am greatly thankful to my brother & bhabhi for the love and care they have provided me. Thank you so much for your patience and the support you have given me to accomplish this.

Richa Arya

Abstract

The Standard Big-Bang Model (SM) of Cosmology has been a widely accepted and successful framework in describing the post Big-Bang Nucleosynthesis (BBN) evolution of our Universe. But certain difficulties arise when one tries to explain the observations of the early Universe, like the extreme homogeneity and isotropy of the cosmic microwave background radiation, within this description. Thus, to overcome these shortcomings and probe an insight to the early Universe, a phenomenon known as '*Inflation*', is introduced. Inflation is a phase of a rapid accelerated expansion of the early Universe during which the physical distance between any two spatial points in the Universe grows tremendously (nearly exponentially) within a brief time. It is proposed to have taken place when the Universe was in its initial stages (within 1 second of its formation). The inflationary paradigm of the early Universe efficiently resolves the problems faced by the SM, as well as explains the current observations very precisely. As an additional feature, it also provides a mechanism to generate the density inhomogeneities that become the seeds of the Large Scale Structure (LSS) at late times, which supplements its importance and success.

There are two approaches to explain the dynamics of inflation. The first one is the standard cold inflation. In this description, as the Universe inflates, the number densities of all the species present at that time dilute away, and the Universe attains an almost supercooled state during the inflationary phase. On the other hand, there is a second description, known as *Warm Inflation*, in which the dissipation processes during the inflationary phase are taken in account. During expansion, a thermal bath of particles (radiation) is created from the inflaton dissipation and thus, the Universe has a non-zero temperature during warm inflation.

The two descriptions of inflation have different microphysics that governs them. In warm inflation, one accounts for the inflaton couplings to the other fields during inflation, unlike in cold inflation where they are neglected. Because of these couplings, the inflaton dissipates its energy, which is quantified in terms of a dissipation coefficient. Thus, warm inflation is a broader and more general description, with cold inflation as its limiting case. The dynamics of the Universe are different in the two scenarios and lead to significant distinctions in the theoretical predictions of the cosmological

observables. In this thesis, I consider a few models of warm inflation and discuss their signatures in the large and small scale observations.

The observational test of any inflationary model is carried out by examining the imprints of inflation on the Cosmic Microwave Background (CMB) radiation. CMB radiation - the earliest signals of the Universe, refers to the primordial photons present in all directions of the sky. The CMB temperature is observed to be uniform over the entire sky to high precision, with some tiny anisotropies of the order of 1 part in 10^5. The anisotropies in the CMB temperature is evidence for the existence of fluctuations in the energy density of the primordial Universe and is studied using the linear theory of cosmological perturbations. The origin of these anisotropies is attributed to the inflationary phase, therefore features in the CMB act as a probe to the physics of inflation. The correlations in the CMB anisotropies are described in terms of a primordial power spectrum, and are quantified by the amplitude of the primordial power spectrum, A_s, the scalar spectral index, n_s, and the tensor-to-scalar ratio, r. With the precision measurements of the CMB, stringent bounds have been put on the parameters n_s and r. Hence, in order that any inflationary model is a viable one, its theoretical estimates of the cosmological parameters must be consistent with the observational measurements.

Constructing a model of inflation from fundamental particle physics has always been elusive. The ultimate goal of model builders is to make a connection between the inflationary theory and the elementary particle physics theory of the early Universe. This requires a knowledge of the parameters of the inflation model such as the masses, couplings, and multiplicities of the fields involved. Therefore, an estimation of the model parameters consistent with the observations is essential for the inflation model building. In the first part of the thesis, I consider some models of warm inflation with monomial potentials and explore their microphysics in terms of the inflaton self-coupling, and its dissipation to other fields characterized by a dissipation parameter. Using the CosmoMC numerical code, I estimate the values of these model parameters for which these models are consistent with the CMB observations. In our analysis, it is seen that for some parameter values, these models are viable models of inflation. Further, I also calculate the n_s and r values for the mean values of the parameters and show that for the weak dissipative regime, r is within the sensitivity of the next generation CMB polarization experiments, which is an important observational test for these models.

In the second part of the thesis, I discuss the growth of small scale fluctuations generated during warm inflation in the context of Primordial Black Holes (PBHs), i.e., black holes with a primordial origin. PBHs are one of the exotic and remarkable probes to the physics of the early Universe. They are a very unique and efficient means to investigate various inflation models. PBHs can form in the early Universe when primordial small scale overdense fluctuations, generated during inflation, reenter the horizon and collapse by gravitational instability. In my thesis, I study a model of warm inflation and find that for certain parameter space, it has the features that it is consistent with the CMB as well as has a large amplitude of the primordial power spectrum at the small scales to form a significant abundance of PBHs. Further, I calculate the mass and the initial mass fraction of the generated PBHs and discuss the observational bounds on the abundance and other implications of the PBHs formed in our warm inflation model.

Keywords: Cosmic inflation, Warm inflation, Dissipation coefficient, Primordial power spectrum, Primordial black holes, Initial mass fraction of black holes

Abbreviations

BBN	Big-Bang Nucleosynthesis
CAMB	Code for Anisotropies in the Microwave Background
CDM	Cold Dark Matter
CMB	Cosmic Microwave Background
CosmoMC	Cosmological Monte Carlo
DE	Dark Energy
GR	Theory of General Relativity
GUT	Grand Unified Theory
LSS	Large Scale Structure
PBH	Primordial Black Hole
SM	Standard Model

Contents

Acknowledgements **i**

Abstract **iii**

Abbreviations **vii**

Contents **ix**

List of Figures **xiii**

1 Introduction **1**

1.1 Timeline of our Universe 1

1.2 Standard Model of Cosmology 4

1.3 Basics of Cosmology 5

1.4 Shortcomings of the Standard Model 8

1.4.1 Horizon problem 8

1.4.2 Flatness problem 10

1.4.3 Monopole and unwanted relics problem 11

1.5 Solution to the problems - Inflation 11

1.6 Thesis Overview 13

2 Cosmic inflation - the standard cold description **15**

2.1 Introduction 15

2.2 Kinematics of inflation 18

2.2.1 Slow roll approximation 19

2.2.2 Duration of inflation 20

2.3 Cosmological perturbations during inflation 20
2.3.1 Linear Cosmological Perturbation Theory 20
2.3.2 Perturbed Einstein equations for the scalar perturbations . . . 22
2.3.3 Gauge Choice 23
2.3.4 Gauge transformations 24
2.3.5 Gauge invariant quantities constructed from metric and scalar field perturbations 25
2.4 Primordial curvature power spectrum 26
2.4.1 Dynamics of perturbations during inflation 26
2.4.2 Evolution of comoving curvature perturbation 27
2.5 Tensor power spectrum 28
2.6 Observational imprints of inflation on the CMB 29
2.6.1 Cosmic Microwave Background Radiation 29
2.6.2 Angular Power Spectrum of CMB temperature fluctuations . . 31
2.7 Current status of cold inflation models from CMB 32
2.8 Numerical codes in Cosmology 33

3 Warm Inflation 37

3.1 Introduction 37
3.2 Model Building in Warm Inflation 40
3.3 The theory of warm inflation 42
3.3.1 Evolution equations for the inflaton and radiation 42
3.3.2 Slow roll parameters and conditions 44
3.3.3 Dissipation coefficient 45
3.3.4 Primordial curvature power spectrum 49
3.3.5 Primordial tensor power spectrum 51
3.4 Summary 52

4 Warm inflation models with $\lambda\phi^4$ potential 53

4.1 Models of warm inflation studied 53
4.2 Parameterization of the primordial power spectrum 55
4.2.1 When the dissipation coefficient $\Upsilon = C_\phi T^3/\phi^2$ 55

4.2.2 When the dissipation coefficient $\Upsilon = C_T T$ 57
4.3 Dissipation parameter evolution during inflation Q_k 57
4.3.1 Calculation of dQ/dN 58
4.3.2 Calculation of dN/dx 59
4.4 Analysis 60
4.4.1 Evolution of the inflaton and the radiation 60
4.4.2 Thermal equilibrium and a lower bound on Q_P 61
4.4.3 Primordial power spectrum 63
4.4.4 Scalar Index 64
4.5 Model Parameters 64
4.5.1 Choice of priors for model parameters 65
4.6 CMB angular power spectrum 66
4.6.1 When λ is fixed, and Q_P is variable 66
4.6.2 When Q_P is fixed, and λ is variable 66
4.6.3 Effect of the inflaton non-zero particle number distribution . . 67
4.7 CosmoMC results 69
4.7.1 Constraints on the parameters of the warm inflation model $V(\phi) = \lambda\phi^4$ with a cubic dissipation coefficient $\Upsilon = C_\phi T^3/\phi^2$ 70
4.7.2 Constraints on the parameters of the warm inflation model $V(\phi) = \lambda\phi^4$ with a linear dissipation coefficient $\Upsilon = C_T T$ . . 74
4.8 Summary 78

5 Warm inflation models with $\lambda\phi^6/M_{Pl}^2$ potential **81**
5.1 Parameterization of the primordial power spectrum 82
5.1.1 When the dissipation coefficient $\Upsilon = C_\phi T^3/\phi^2$ 82
5.1.2 When the dissipation coefficient $\Upsilon = C_T T$ 83
5.2 Dissipation parameter, Q_k 83
5.3 Model parameters and their priors 84
5.4 CosmoMC results 86
5.4.1 Constraints on the parameters of the warm inflation model $V(\phi) = \lambda\phi^6/M_{Pl}^2$ with dissipation coefficient $\Upsilon = C_\phi T^3/\phi^2$. 86

5.4.2 Constraints on the parameters of the warm inflation model $V(\phi) = \lambda\phi^6/M_{Pl}^2$ with dissipation coefficient $\Upsilon = C_T T$ . . . 89

5.5 Comparison of results with the $\lambda\phi^4$ model 93

5.6 Summary 94

6 Primordial Black Hole formation from warm inflation 95

6.1 Introduction 95

6.2 Formation of Primordial Black Holes 97

6.2.1 Mass of the generated primordial black holes 97

6.2.2 Initial mass fraction of PBHs 100

6.2.3 Press-Schechter theory for the PBH formation 104

6.3 PBH formation from various models of inflation 105

6.4 Formation of PBHs from warm inflation 107

6.4.1 Features in the primordial power spectrum 108

6.4.2 Relevant range of the dissipation parameter 110

6.5 Results and Discussion 111

6.5.1 Mass and the Initial mass fraction of the PBHs formed 111

6.5.2 Constraints on the abundance of generated PBHs 112

6.5.3 PBH relics as a constituent of dark matter 114

6.6 Summary 115

7 Summary and Conclusions 117

A Thermal Field Theory 121

B Dissipation parameter at the end of inflation, Q_e 125

C Integral Function of dN/dQ 127

D Spectral index 129

Bibliography 131

List of publications 157

List of Figures

1.1 Timeline of our Universe with different epochs and energy scale during evolution are shown here. *Source:* Particle Data Group 2015. 2

1.2 The present energy budget of the Universe from Planck satellite observations. *Source*: https://sci.esa.int/web/planck/-/51557-planck-new-cosmic-recipe 5

1.3 Horizon problem: At the time of recombination or last scattering, there are causally disconnected regions in the sky. *Source*: https://favpng.com/. 9

1.4 Geometry of the Universe (*Top to Bottom:* closed, open, and flat). *Source*: Wikipedia 11

1.5 Phase of cosmic inflation in the early Universe shown here. *Source:* https://commons.wikimedia.org 12

1.6 A pictorial representation of the solution to the Horizon problem [1]. . 13

2.1 Pictorial representation of the old inflation model *Source*: *Left figure*: [2] and *Right figure*: https://ned.ipac.caltech.edu/ 16

2.2 Pictorial representation of the new inflation model. *Source*: *Left figure*: https://ned.ipac.caltech.edu/ and *Right figure*: [3]. 16

2.3 Pictorial representation of the chaotic inflation model. *Source*: [4]. . . 17

2.4 Pictorial representation of inflaton slowly rolling down a potential $V(\phi)$ leading to the cosmic inflation [5]. 17

2.5 Evolution of the physical wavelength of the fluctuation modes generated during inflation, as a function of scale factor. *Source*: [6]. 26

2.6 *Left*: Full sky map of CMB with the anisotropies, as seen by the Planck satellite. The color coding (red to blue) represents a temperature value above or below the mean value of 2.725 K. *Source*: https://sci.esa.int/ and *Right*: A black body spectrum of the CMB radiation, as seen by the COBE satellite. *Source*: Wikipedia 30

2.7 Angular power spectrum of the CMB from Planck 2018 results [7]. The blue curve represents the ΛCDM best fit to the data points for Planck TT, TE, EE+ low E + lensing. The lower panel shows the residuals with respect to the best fit. 32

2.8 Joint 68% and 95% confidence limits on the parameters n_s and r for various inflationary models from Planck 2018 results. The band of values for various models corresponds to the number of inflationary efolds between 50 to 60. *Source*: [7]. 33

4.1 The allowed values of n_s and r from the WMAP Seven-year observations are shown here [8]. 54

4.2 Plot showing how the dissipation parameter changes as a function of the number of efolds of inflation. For this plot, we have fixed $N_P = 50$ and considered the mean values for this model as $Q_P = 10^{-2.4}$, $\lambda = 1.68 \times 10^{-14}$, and $C_\phi = 8.8 \times 10^6$. 58

4.3 *(a)* The evolution of the inflaton field, *(b)* the energy density in inflaton and radiation, and *(c)* the temperature of the thermal bath of radiation, as a function of the number of efoldings. Here we have fixed $N_P = 50$ and chosen the mean values of parameters for this model as $Q_P = 10^{-2.4}$, $\lambda = 1.68 \times 10^{-14}$, and $C_\phi = 8.8 \times 10^6$. 61

4.4 Plots showing the variation of T_k/H_k as a function of the number of efolds for different values of Q_P. 62

4.5 Plot of $\log_{10}\Delta^2_{\mathcal{R}}(k)$ vs $\ln(k/kp)$ for different values of Q_P for the model with cubic dissipation. Here $N_P = 50$ and A_s is fixed to obtain the corresponding λ for each Q_P. The standard power law with $n_s = 0.9645$ is also plotted as a solid (black) line. 63

4.6 The spectral index, n_s as a function of the dissipation parameter, $\log_{10} Q_P$ are plotted for (a) the model with cubic dissipation coefficient on the left, and, (b) the model with a linear dissipation coefficient on the right. The colored band shows the allowed n_s values from *Planck* 2015 TT, TE, EE + low P results for a power law power spectrum with 68% and 95% C.L.. 65

4.7 The TT angular power spectrum of the CMB for various values of Q_P, with $\lambda = 10^{-13.7746}$ and $N_P = 50$. In the plots, low ℓ refers to the range $\ell = 2 - 49$ while high ℓ refers to the range $\ell = 50 - 2500$. . . 67

4.8 The TT angular power spectrum of the CMB for various values of λ, fixed $Q_P = 10^{-2.4}$ and $N_P = 50$. 67

4.9 Angular power spectra for warm inflation with the coth term retained in the primordial power spectrum and with the coth term set to 1 $(n_k = 0)$. 68

4.10 *Left:* Plot of the tensor-to-scalar ratio r vs $\log_{10} Q_P$ indicates that for larger dissipation (larger Q_P value), the r value is smaller. *Right:* Plot of $n_s - r$, where different points on the curve represent different Q_P values (and the corresponding λ). The Q_P value increases as we move from left to right on the plot, whereas as λ is inversely correlated to Q_P, it therefore decreases. Here we fix $N_P = 60$. 71

4.11 The joint probability distribution and the marginalized distributions of the cosmological parameters for the model $V(\phi) = \lambda\phi^4$ with $\Upsilon = C_\phi T^3/\phi^2$ in the weak dissipative regime for $N_P = 50$. The CosmoMC analysis is carried out with the *Planck* 2015 TT, TE, EE + low P dataset. 72

4.12 Plot of $\log_{10} C_\phi$ vs $\log_{10} Q_P$ for the weak dissipative regime shows that $C_\phi \sim \mathcal{O}(10^7)$ for this model of warm inflation. Here also $N_P = 60$. . 73

4.13 The joint probability distribution and the marginalized distributions of the cosmological parameters for the case $V(\phi) = \lambda\phi^4$ with $\Upsilon = C_\phi T^3/\phi^2$ in the weak dissipative regime for $N_P = 60$. To obtain this, we carry out the CosmoMC analysis using the *Planck* 2015 TT, TE, EE + low P dataset. 73

4.14 *Left*: Plot of r vs $\log_{10} Q_P$ indicates that the r value is smaller for the strong dissipation (large Q_P) case than the weak dissipation. *Right:* Plot of $n_s - r$, where different points on the curve represent different Q_P values (and the corresponding λ). The value of Q_P increases from left to right on the plot, whereas λ decreases. For the strong dissipation, r value is nearly 0. 74

4.15 The joint probability distribution and the marginalized distributions of the cosmological parameters for the case $V(\phi) = \lambda\phi^4$, with $\Upsilon = C_T T$ in the weak dissipative regime, obtained using the *Planck* 2015 TT, TE, EE + low P dataset. 76

4.16 *Left*: Plot of $\log_{10} C_T$ vs $\log_{10} Q_P$ for the weak dissipative regime, and *Right*: for the strong dissipative regime is shown. The value of C_T is smaller in the weak dissipation regime than in the strong dissipation regime. 77

4.17 The joint probability distribution and the marginalized distributions of the cosmological parameters for the case $V(\phi) = \lambda\phi^4$, with $\Upsilon = C_T T$ in the strong dissipative regime. The CosmoMC analysis is carried out with the *Planck* 2015 TT, TE, EE + low P dataset. 77

5.1 The spectral index, n_s as a function of the dissipation parameter, $\log_{10} Q_P$ are plotted for (a) the model with cubic dissipation coefficient, and, (b) the model with linear dissipation coefficient. The band shows the allowed n_s values from *Planck* 2015 TT, TE, EE + low P results for a power law power spectrum with 68% and 95% C.L.. 85

5.2 The joint probability distribution of $-\log_{10}\lambda$ and $-\log_{10} Q_P$ for the case $V(\phi) = \lambda\phi^6/M_{Pl}^2$, with $\Upsilon = C_\phi T^3/\phi^2$ in the weak dissipative regime. The plot shows that there are two convergence regions for the parameters. 86

5.3 *Left:* Plot of the tensor-to-scalar ratio r vs $\log_{10} Q_P$ indicates that for larger dissipation (larger Q_P value), the r value is smaller. *Right:* Plot of $n_s - r$, where different points on the curve represent different Q_P values (and corresponding λ). Q_P increases from left to right on the plot, whereas λ decreases. 87

5.4 The joint probability distribution and the marginalized distributions of the cosmological parameters for the case $V(\phi) = \lambda\phi^6/M_{Pl}^2$, with $\Upsilon = C_\phi T^3/\phi^2$ in the weak dissipative regime, obtained using the *Planck* 2015 TT, TE, EE + low P dataset.. 88

5.5 Plot of $\log_{10} C_\phi$ vs $\log_{10} Q_P$ for the weak dissipative regime shows that $C_\phi \sim \mathcal{O}(10^7 - 10^8)$ for this model of warm inflation. 89

5.6 *Left*: Plot of r vs $\log_{10} Q_P$ indicates that the r value is smaller for the strong dissipation (large Q_P) case than the weak dissipation. *Right:* Plot of $n_s - r$, where different points on the curve represent different Q_P values (and λ). The Q_P value increases from left to right on the plot, while λ decreases. For the strong dissipation, r value is nearly 0. 90

5.7 The joint probability distribution and the marginalized distributions of the cosmological parameters for the case $V(\phi) = \lambda\phi^6/M_{Pl}^2$, with $\Upsilon = C_T T$ in the weak dissipative regime, obtained using the *Planck* 2015 TT, TE, EE + low P dataset. 91

5.8 The joint probability distribution and the marginalized distributions of the cosmological parameters for the case $V(\phi) = \lambda\phi^6/M_{Pl}^2$, with $\Upsilon = C_T T$ in the strong dissipative regime, obtained using the *Planck* 2015 TT, TE, EE + low P dataset. 92

5.9 *Left*: Plot of $\log_{10} C_T$ vs $\log_{10} Q_P$ for the weak dissipative regime, and *Right*: for the strong dissipative regime is shown here. The value of C_T is smaller in the weak dissipation than in the strong dissipation. . 93

6.1 Constraints on the initial mass fraction $\beta(M_{PBH})$ versus the mass of PBH is shown here [9]. The acronyms stand for: the lightest supersymmetric paricle (LSP), big-bang nucleosynthesis (BBN), galactic gamma-ray background (GGB), extagalactic gamma-ray background (EGB), cosmic ray (CR), gravitational lensing (GL), gravitational waves (GW), X-ray binary (XB), dynamical friction (DF), large scale structure (LSS). 101
6.2 The fraction of PBH energy density contributing as the dark matter, as constrained from various observations [10]. 103
6.3 Gaussian probability distribution $p(\delta)$ of the density fluctuation δ is plotted here [11]. The width of the distribution shown here $\sigma(M_H)$ can be related to $\sigma(R)$ in the text, as M_H and R are related. 104
6.4 Upper bound on the primordial power spectrum obtained from observations for various mass of PBHs corresponding to comoving wavenumber k. *Source*: [9]. 106
6.5 Plot of the growth functions in the primordial power spectrum for $\Upsilon \propto T^3, T$ and $1/T$. 108
6.6 Plot of the primordial power spectrum $\Delta^2_{\mathcal{R}}(k)$ versus k for our warm inflation model with different values of Q_P. Here the black line represents the standard power law parameterization considered in cold inflation. 109
6.7 Plot of the initial mass fraction of the generated PBH, $\beta(M_{PBH})$, versus its mass $M_{PBH}(g)$. 112

A.1 Schwinger-Keldysh contour in the complex time plane. Figure taken from Ref. [12]. 122

Chapter 1

Introduction

Cosmology - the study of the origin, evolution, and fate of our Universe - is a subject based on observations. By looking at the state of the Universe at present, we postulate about the various phases attained in its evolution. Inflation is one such speculated period in the cosmic evolution, which has a remarkable importance in the cosmic history. To begin with, firstly I give a brief introduction to the timeline of our Universe, followed by the Standard Model and basics of cosmology. Then, I discuss the shortcomings in the Standard Model and how inflation can provide a solution to these problems.

1.1 Timeline of our Universe

From numerous observational studies, we have arrived at the following understanding of the timeline of our Universe in the Standard Big-Bang Model of cosmology, as shown in Fig. 1.1 (see standard texts [13–23] and lectures [24–30]; also see Ref. [31] for a comprehensive list of references.).

According to the Standard Model of cosmology, the present age of our Universe is found to be around 13.8 billion years. From observations of Hubble [32], we have inferred that our Universe is expanding. As it expands, it cools down and the number density of particles dilutes, which indicates that the early Universe was extremely hot and dense. In the Big-Bang model, the Universe is assumed to originate from an infinite energy density at time $t = 0$, known as the Big-Bang singularity. The cause

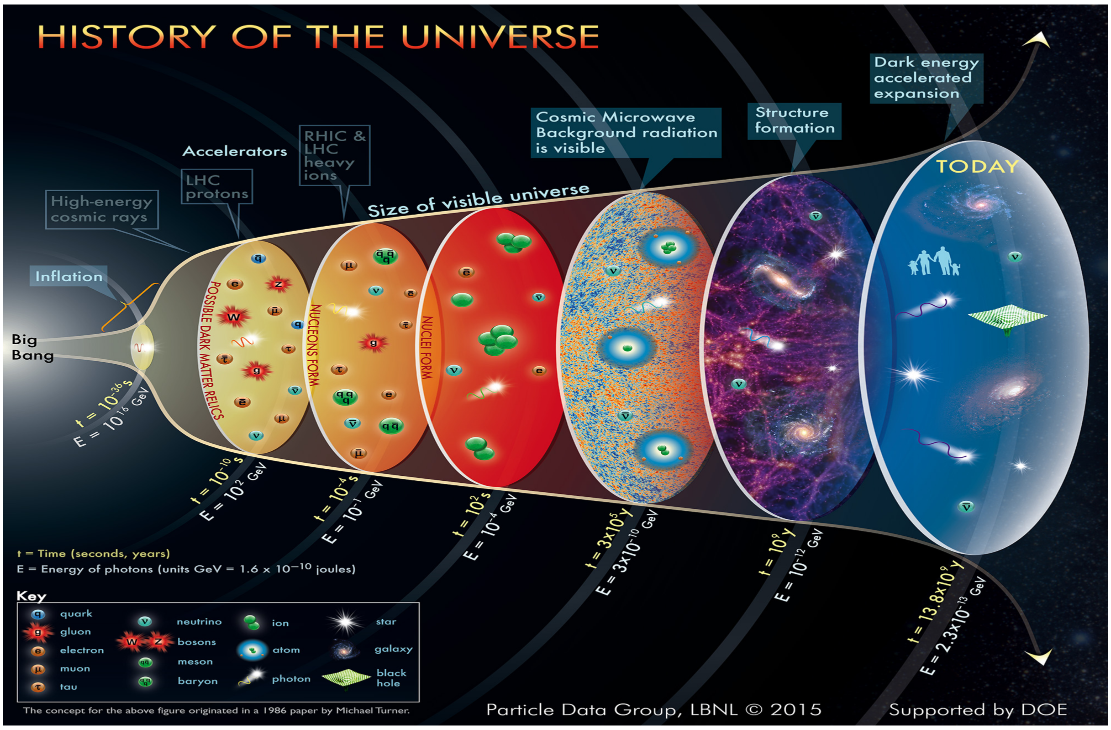

Figure 1.1: Timeline of our Universe with different epochs and energy scale during evolution are shown here. *Source:* Particle Data Group 2015.

and the nature of this singularity are still open questions in cosmology. Followed by that is the epoch when quantum gravity effects are important, and the energy density in the Universe is above the scale of Planck energy $M_{Pl} \sim 10^{19}$ GeV. Till date, we do not have a complete understanding of the quantum gravity era, and our concept of spacetime from the classical Theory of General Relativity (GR) does not hold at such epochs.

At the energy scale of $\sim 10^{15}$ GeV or below, there is a proposed phase of cosmic inflation, which is the subject of this thesis. Cosmic Inflation [33–39] is a phase of accelerated expansion of the early Universe for a very brief duration of time. It is speculated to happen in the Universe when the age of the Universe was 10^{-34} seconds (for Grand Unified Theory (GUT) scale inflation) or later. This phase was introduced to resolve some issues faced by the Standard Model of cosmology, as will be discussed in Section 1.4. The inflationary paradigm is very powerful and successful, as it provides a solution to problems in the Standard Model, as well as its predictions satisfy observations to high precision.

Inflation ends with a production of elementary particles into a radiation dominated Universe. Subsequently, the Universe is like a hot soup of plasma with quarks, leptons, gauge bosons, dark matter particles, etc. Then, at around an energy scale ~ 200 MeV (time nearly 10^{-6} second), the quarks hadronize into protons and neutrons. With further expansion and cooling, when the temperature of the Universe corresponds to the nuclear binding energy ~ 1 MeV (time around ~ 1 second after the big-bang), the protons and neutrons begin to combine and form nuclei. Light nuclei - Helium ^{4}He, traces of deuterium ^{2}H, Helium ^{3}He, Lithium ^{7}Li, are formed during this epoch, known as the Big-Bang Nucleosynthesis (BBN), and takes place within the first 3 minutes after the Big-Bang [40].

Further, when the temperature of the Universe is about 0.3 eV, neutral Hydrogen atoms begin to form (the Universe at this stage is almost $380,000$ years old). As a consequence, the photons which earlier underwent Thomson scattering with the charged particles, now do not scatter efficiently with the neutral atoms. After the last scattering, these photons free stream, and this phase is also known as decoupling, as the photons decouple from the thermal plasma. These relic photons are now seen in all directions of the sky as the primordial Cosmic Microwave Background (CMB) radiation [41–45]. The CMB is isotropic to a high degree with an average temperature of 2.725 K but also has tiny anisotropies of 1 part in 10^5. (For a review, see Refs. [46, 47].) The origin of these anisotropies is attributed to the early inflationary phase.

For long periods after the photon decoupling, the Universe remains in the dark ages. At around an age of 200 million years, when the density fluctuations in the Universe grew sufficiently, the first stars, galaxies, and quasars came into existence. The radiation emitted from these sources ionized the neutral intergalactic medium, and this phase is known as the epoch of reionization. As the Universe expanded and diluted further, this epoch gradually ended. The density inhomogeneities continued to grow, linearly and then non-linearly, and collapsed to form all the structures - galaxies, clusters, superclusters, voids, etc. in the Universe.

After about 10 billion years of cosmic time, the Universe became dominated by dark energy, which resulted in its accelerated expansion. The present age of the Universe is nearly 13.8 billion years and is the outcome of all the phases attained during its evolution.

The above timeline of the Universe is in good accordance with the observational evidence from the Big-Bang Nucleosynthesis epoch till the present. However, the physics of the Universe within the first second of the Universe formation is not well tested.

The phase of inflation in the early Universe is interesting and vital as it can well explain the isotropy of the CMB temperature and the correlations in its tiny anisotropies. The quantum fluctuations generated during inflation are also considered to become the seeds of the density inhomogeneities that grow and subsequently become the structures at late times. Thus, inflation simultaneously explains the features in the CMB and the formation of Large Scale Structure (LSS) seen today, thus its remarkable success as a cosmological theory.

1.2 Standard Model of Cosmology

The Standard Model of cosmology, also called ΛCDM (Lambda Cold Dark Matter), is a theoretical framework for understanding the composition and evolution of our Universe. According to this, our present Universe is composed of baryonic matter, invisible Cold Dark Matter (CDM), and Dark Energy (DE). The radiation density had dominant contributions in the early Universe but has diluted by today. The baryonic and the dark matter contribute to the structure formation, whereas the dark energy, or cosmological constant Λ, is responsible for the present-day accelerated expansion of the Universe. The energy budget of the present day Universe from the recent observations is shown in Fig. 1.2. At present, the majority of the energy content of the Universe, 68.3%, is in the form of dark energy, 26.8% is cold dark matter, and the rest 4.9% is the baryonic matter.

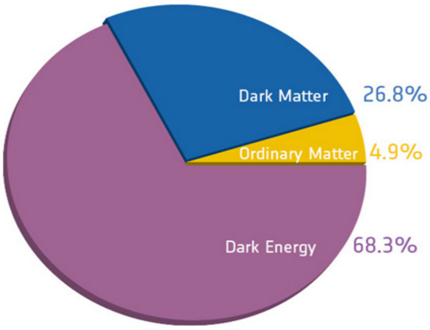

Figure 1.2: The present energy budget of the Universe from Planck satellite observations. *Source*: https://sci.esa.int/web/planck/-/51557-planck-new-cosmic-recipe .

1.3 Basics of Cosmology

Friedmann-Lemaître-Robertson-Walker (FLRW) metric

By the cosmological principle, our Universe is homogeneous and isotropic on large scales (above 100 Mpc), i.e. the large scale properties are independent of the position of the observer. The geometry of the $(3+1)$ space-time is expressed in terms of the metric $g_{\mu\nu}$, given by the line element $ds^2 = g_{\mu\nu}dx^\mu dx^\nu$. In our notation, the greek alphabets, μ, ν, etc., run over time, space coordinates, $(t, \boldsymbol{x})$ and have the values $(0, 1, 2, 3)$, respectively.

From observations, it is well established that our Universe is expanding spatially. The metric for the expanding Universe is given by the FLRW metric (we follow the notation of Ref. [1]) as

$$ds^2 = -dt^2 + a^2(t)\left[\frac{dr^2}{1-kr^2} + r^2(d\theta^2 + sin^2\theta\, d\phi^2)\right], \tag{1.1}$$

where t is the proper time, (r, θ, ϕ) are the comoving spherical coordinates, $a(t)$ is the scale factor which indicates how the physical distance between any two positions in the Universe scales with time and k is a measure of the spatial curvature and is equal to $0, -1, +1$ for a flat, open, and a closed Universe, respectively.

Observations also indicate that the spatial geometry of our Universe is almost flat. For a flat Universe, we can also write the FLRW metric in terms of conformal time $\left(\eta = \int \frac{dt}{a(t)}\right)$ as

$$ds^2 = a^2(t)\left[-d\eta^2 + d\boldsymbol{x}^2\right]. \tag{1.2}$$

Here the term in brackets is like the metric of the Minkowski spacetime.

Hubble expansion rate

The rate of expansion of the Universe at any epoch is measured in terms of the Hubble expansion rate, defined as

$$H(t) \equiv \frac{\dot{a}(t)}{a(t)} \,, \tag{1.3}$$

where a dot represents the derivative w.r.t. the proper time.

Einstein equation

The dynamics of the Universe is studied using Einstein's Theory of General Relativity. According to it, the geometry of the spacetime is related to the energy density of the Universe, which is mathematically formulated in the Einstein equation, as

$$G_{\mu\nu} \equiv R_{\mu\nu} - \frac{1}{2} g_{\mu\nu} R = 8\pi G_N T_{\mu\nu} \tag{1.4}$$

where $R_{\mu\nu}$ is the Ricci tensor which depends on the metric and its derivatives, $R = g^{\mu\nu} R_{\mu\nu}$ is the Ricci scalar, G_N is the Newton's gravitational constant, and $T_{\mu\nu}$ is the stress-energy tensor. The quantities on the left represent the geometry part, and the energy-momentum components are written on the right-hand side.

The Ricci tensor is constructed from the Christoffel symbols as

$$R_{\mu\nu} = \Gamma^{\alpha}{}_{\mu\nu,\alpha} - \Gamma^{\alpha}{}_{\mu\alpha,\nu} + \Gamma^{\alpha}{}_{\beta\alpha}\Gamma^{\beta}{}_{\mu\nu} - \Gamma^{\alpha}{}_{\beta\nu}\Gamma^{\beta}{}_{\mu\alpha} \,, \tag{1.5}$$

where the subscript $_{,\alpha}$ denotes $\frac{\partial}{\partial x^{\alpha}}$. For any metric, the Christoffel symbols are given as,

$$\Gamma^{\mu}{}_{\alpha\beta} = \frac{g^{\mu\nu}}{2} \left[g_{\alpha\nu,\beta} + g_{\beta\nu,\alpha} - g_{\alpha\beta,\nu} \right] . \tag{1.6}$$

For the FLRW metric given in Eq. (1.1), the Ricci tensor components are obtained to be

$$\begin{aligned}
R_{00} &= -3\frac{\ddot{a}}{a} \\
R_{0i} &= 0 \\
R_{ij} &= \left[\frac{\ddot{a}}{a} + 2\frac{\dot{a}^2}{a^2} + 2\frac{k}{a^2} \right] g_{ij},
\end{aligned} \tag{1.7}$$

and the Ricci scalar is calculated to be

$$\mathcal{R} = 6\left[\frac{\ddot{a}}{a} + \frac{\dot{a}^2}{a^2} + \frac{k}{a^2}\right]. \tag{1.8}$$

Stress Energy Tensor

The stress energy tensor for a perfect fluid in its rest frame is a diagonal matrix, given as

$$T^{\mu}{}_{\nu} = \mathrm{diag}\,(-\rho, p, p, p), \tag{1.9}$$

where the 00 component represents the energy density ρ, and the diagonal elements give the pressure p. The off-diagonal elements are 0, as the fluid is considered as a perfect one. The conservation of the stress energy demands $T^{\mu\nu}_{\ \ ;\mu} = 0$, which gives the energy conservation equation for the expanding Universe as

$$\dot{\rho} + 3H(\rho + p) = 0. \tag{1.10}$$

For a fluid with $p = w\rho$, where w is called the equation of state, Eq. (1.10) can be rewritten as,

$$\dot{\rho} + 3\,\frac{\dot{a}}{a}\,(1+w)\,\rho = 0. \tag{1.11}$$

The solution of this turns out as $\rho \propto a^{-3(1+w)}$. For a radiation fluid, $w = \frac{1}{3}$, and thus $\rho \propto a^{-4}$. For the pressureless dust or matter, $w = 0$, and the solution is obtained as $\rho \propto a^{-3}$. Thus, the energy density of the radiation and the matter decreases as the Universe expands. However, for a fluid with $w = -1$, it can be found that $\rho =$ constant, independent of the expansion of the Universe.

Friedmann equations

Using the Eqs. (1.7) and (1.8) in the Einstein equation given in Eq. (1.4), we obtain the following two independent equations, known as the Friedmann equations, as

$$\left(\frac{\dot{a}}{a}\right)^2 + \frac{k}{a^2} = \frac{8\pi G_N}{3}\rho\,, \tag{1.12}$$

and

$$2\frac{\ddot{a}}{a} + \left(\frac{\dot{a}}{a}\right)^2 + \frac{k}{a^2} = -8\pi G_N\,p\,. \tag{1.13}$$

On combining these two equations, we get

$$\frac{\ddot{a}}{a} = -\frac{4\pi G_N}{3}(3p + \rho) = -\frac{4\pi G_N}{3}\rho\,(3w + 1)\,. \tag{1.14}$$

It can be seen that for the radiation ($w = 1/3$), or the matter fields ($w = 0$), $\ddot{a}$ turns out to be negative, which implies a decelerated expansion of the Universe. But in the case when $w < -1/3$, the Universe has an accelerated expansion, as in the present time (dark energy dominated Universe, $w \approx -1$), as well as during the early phase of inflation.

1.4 Shortcomings of the Standard Model

Despite its success in explaining the post-BBN Universe, the Standard Model fails to explain certain issues of the early Universe. These shortcomings are listed below:

1.4.1 Horizon problem

The horizon problem is related to the uniform temperature of the observed cosmic microwave background radiation. CMB is measured to have a black body spectrum with an average temperature of 2.725 K in all the directions over the entire sky. But by looking at our past light cone, it is seen that there are nearly 10^4 uncorrelated or causally disconnected patches in the sky at the time of the last scattering from when the CMB photons free stream. A pictorial representation of the horizon problem is shown in Fig. 1.3. The horizon size at the epoch of last scattering ($t \sim 380,000$ year), subtends an angle of $\sim 1^\circ$ on the sky today, which means that no microphysics could equilibrate the CMB photons at angles greater than 1°. Despite this, the CMB has a uniform temperature in all the directions. This raises the question of why temperature is the same for any two causally disconnected regions or how thermal equilibrium is attained between the two separated regions.

Mathematically, it can be understood as follows. The photons or any particle travel a physical distance from the epoch of the Big-Bang ($t = 0$) till any time t, known as the *particle horizon*, $d_H(t)$. It is the measure of the maximum size of the Universe that can be in causal contact at any epoch. Since the trajectory of the photons is a null

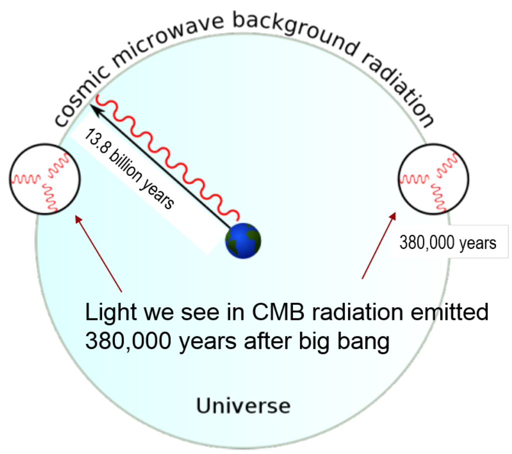

Figure 1.3: Horizon problem: At the time of recombination or last scattering, there are causally disconnected regions in the sky. *Source*: https://favpng.com/.

geodsic $ds^2 = 0$, for radial propagation $dr = dt/a(t)$, which gives the particle horizon as,

$$d_H(t) = a(t)\int_0^t \frac{dt}{a(t)} = \begin{cases} 2t, & \text{radiation dominated era} \\ 3t, & \text{matter dominated era} \end{cases} \tag{1.15}$$

Since we see the CMB photons from the last scattering surface, as illustrated in Fig. 1.3, the physical distance travelled by the CMB photons from the surface of the last scattering (t_{LSS}) till today (t_0) can be calculated as

$$r_{CMB}(t_0) = a_0 \int_{t_{LSS}}^{t_0} \frac{dt}{a(t)}.$$

Then at the CMB epoch, this distance would have been rescaled according to the scale factor at that time a_{LSS}, so that

$$r_{CMB}(t_{LSS}) = a_{LSS} \int_{t_{LSS}}^{t_0} \frac{dt}{a(t)}.$$

Assuming a matter dominated era ($a \propto t^{2/3}$) from the epoch of last scattering till today, and $t_0 \gg t_{LSS}$, the integral gives

$$r_{CMB}(t_{LSS}) = 3\, t_{LSS}^{2/3}\, t_0^{1/3}. \tag{1.16}$$

The particle horizon or the size of the causally connected Universe at the CMB epoch, as calculated in Eq. (1.15) is,

$$d_H(t_{LSS}) = 2t_{LSS}. \tag{1.17}$$

Then from Eqs. (1.16) and (1.17), it can be seen that

$$\frac{r_{CMB}(t_{LSS})}{d_H(t_{LSS})} = \frac{3}{2}\left(\frac{t_o}{t_{LSS}}\right)^{1/3} \sim \frac{3}{2}\left(\frac{10^{10}}{10^5}\right)^{1/3} \sim 70. \tag{1.18}$$

This implies that at the time of last scattering, the size of the Universe in causal connection was smaller than the rescaled size of current CMB sky. Then how is the temperature uniform in all directions of the sky today? This is the horizon problem.

1.4.2 Flatness problem

The flatness problem in cosmology is the problem of an extreme fine tuning of the early Universe, in order to have the present Universe as spatially flat. This can be understood as below. From the Friedmann equation, for a Universe with total energy density ρ at any time t, the Hubble rate of expansion is given as

$$H^2(t) + \frac{k}{a(t)^2} = \frac{8\pi}{3M_{Pl}^2}\rho(t), \tag{1.19}$$

where k/a^2 is the measure of spatial curvature, and $M_{Pl} = 1/\sqrt{G_N} = 1.2 \times 10^{19}$ GeV is the Planck mass in our notation. The critical energy density at any time is defined as the energy density of the Universe for which its geometry is flat, i.e. $k = 0$,

$$H^2(t) = \frac{8\pi}{3M_{Pl}^2}\rho_{cr}(t). \tag{1.20}$$

Substituting this in Eq. (1.19), we get

$$1 + \frac{k}{a(t)^2 H(t)^2} = \frac{\rho(t)}{\rho_{cr}(t)} \equiv \Omega(t), \tag{1.21}$$

where $\Omega(t)$ is known as the density parameter, and is the ratio of energy density of the Universe to the critical energy density at that epoch. From observations, it is found that at present $\Omega_0 \approx 1$, corresponding to the flat geometry, shown in Fig. 1.4.

The ratio of $|\Omega(t) - 1|$ at an earlier time, say Planck scale, to the present value

$$\frac{|\Omega(t_{Pl}) - 1|}{|\Omega_0 - 1|} = \frac{a_0^2 H_0^2}{a_{Pl}^2 H_{Pl}^2}. \tag{1.22}$$

The comoving horizon, $(aH)^{-1}$ increases as time proceeds (ignoring late time acceleration), which implies that $a_0 H_0 \ll a_{Pl} H_{Pl}$, and hence $|\Omega(t_{Pl}) - 1| < \mathcal{O}(10^{-61})$, or

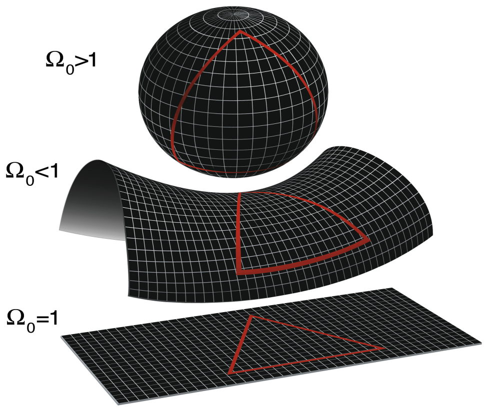

Figure 1.4: Geometry of the Universe (*Top to Bottom:* closed, open, and flat). *Source*: Wikipedia

an extreme fine tuning of the density parameter of the early Universe. This is puzzling as it is very unnatural and raises a question to how can it be explained.

1.4.3 Monopole and unwanted relics problem

Monopoles are point-like topological defects produced in phase transitions. When the GUT symmetry breaks down to a lower symmetry, then during this transition, magnetic monopoles are produced. These are very massive and stable, but are unwanted, as they contribute to the present energy density and overclose it. However, they are not observed, and their non-detection raises a question as to where are such predicted unwanted relics.

1.5 Solution to the problems - Inflation

The solution to all the above-listed problems can be provided by introducing a phase of inflation in the very early Universe.

Cosmic Inflation [33–39] is a phenomenon of a rapid accelerated expansion in the early Universe. It is speculated to have taken place at the energy scale of GUT or below when the Universe was 10^{-34} seconds old. During this phase, the physical distances between any two points in the Universe grew nearly exponentially by at least 50 to 60 efolds, i.e., $e^{50}(\approx 10^{21})$ to $e^{60}(\approx 10^{26})$ (if the scale of inflation is the GUT scale), as shown in Fig. 1.5. For a review on inflation, see Refs. [1, 48–53].

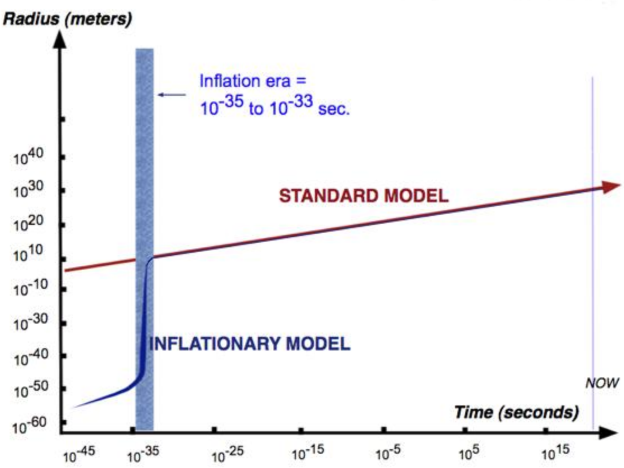

Figure 1.5: Phase of cosmic inflation in the early Universe shown here. *Source:* https://commons.wikimedia.org

Now we explain how inflation can solve all these problems simultaneously. During the inflationary phase, the Hubble rate of expansion is nearly a constant, but as the scale factor increases nearly exponentially, the comoving Hubble radius, $(aH)^{-1}$ shrinks as the Universe inflates. The comoving Hubble radius at any time represent the causally connected region of the Universe, and the fact that it decreases during the inflation provides a solution to the horizon problem. The regions in the sky that appear to be causally disconnected on the last scattering surface were connected in the early Universe, but were taken out of the causal contact due to the shrinking comoving radius during the inflationary phase, as shown in Fig. 1.6. In this way, the two far away regions at the last scattering surface were in causal contact before inflation, but separated as the physical lengths grew nearly exponentially during inflation. Thus, the uniform temperature of the CMB is explained, and the horizon problem is solved with inflation.

Next, we consider the flatness of the Universe, and the extreme fine-tuning required to achieve it. During inflation, the scale factor increases exponentially and the curvature term on the right-hand side of Eq. (1.22) goes to almost 0, thereby solving the flatness problem without any fine-tuning requirement.

During inflation, due to the exponential expansion, the number densities of all the

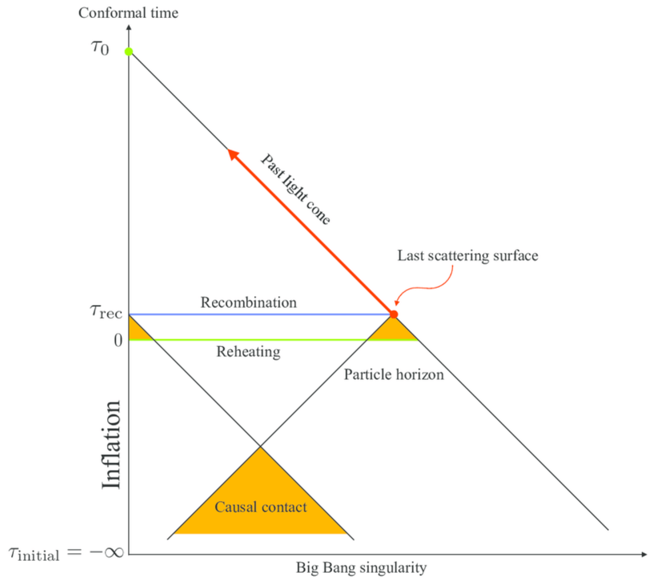

Figure 1.6: A pictorial representation of the solution to the Horizon problem [1].

particles dilute away, and thus the monopoles or other unwanted relics become too scarce to detect. Thus inflation resolves the monopole problem as well.

All these successes make inflation a very compelling and relevant phase of cosmic history. Besides resolving these shortcomings, inflation, as a bonus, also provides a mechanism to explain the tiny anisotropies in the CMB and the formation of structures at the late time.

1.6 Thesis Overview

The main focus of this thesis is on the Warm Inflation description of inflation, and its implications on the large and small scales observations.

The thesis is organized as follows. In Chapter 2, I first give an overview of the standard cold inflation and the dynamics associated with it. Then I describe the fluctuations generated during cold inflation and the primordial curvature power spectrum. After that, I discuss the observational imprints of inflation on the cosmic microwave background radiation and the current status of various cold inflation models.

In Chapter 3, I give a review of the warm inflation description of inflation and the motivation for it. I discuss the features of warm inflation that make it distinct from cold inflation. Then I describe the dissipation coefficient and the primordial scalar and tensor power spectrum of warm inflation.

In Chapters 4 and 5, I discuss the warm inflationary models considered in our study and calculate the primordial power spectrum for all the models. Then using the MCMC technique, I constrain the parameter space of these models from the CMB observations.

After that, in Chapter 6, I discuss the small scale features of inflation in the context of the formation of Primordial Black Holes (PBHs). I consider a model of warm inflation and calculate the initial mass fraction of PBHs that are generated in this model. Further, I also discuss the theoretical and observational constraints on the abundance of the generated PBHs.

In the last Chapter, I summarize and conclude this thesis with some future directions for research.

Chapter 2

Cosmic inflation - the standard cold description

As discussed in the previous Chapter, the inflationary scenario can successfully resolve the problems in the Standard Model of cosmology. Now I discuss the field theoretical description of inflation and the associated observables in the CMB anisotropies. In the literature, there are two realizations for the dynamics of inflation - cold inflation and warm inflation. In this Chapter, I give a brief review of the standard cold inflation and the dynamics that govern it. From the next Chapter onwards, the focus will be on warm inflation.

2.1 Introduction

The idea of an expanding early Universe was independently studied by Refs. [33–35] before the term 'Inflationary Universe' was first coined by Alan Guth [36]. Guth's 1981 'old inflation' [36] model was based on a first-order symmetry breaking phase transition at the GUT scale. Above the GUT scale energy ($T_{GUT} > 10^{15}$ GeV), the symmetry is restored, and there is a single minimum of the potential $V(\phi)$, as shown in Fig. 2.1. The inflaton field is trapped in a metastable 'false vacuum' with a constant energy density in the Universe, leading to exponential expansion. As the temperature falls below the T_{GUT}, a 'true minimum' emerges in the potential $V(\phi)$. During the phase transition, bubbles of 'true vacuum' emerge in the sea of false vacuua, which

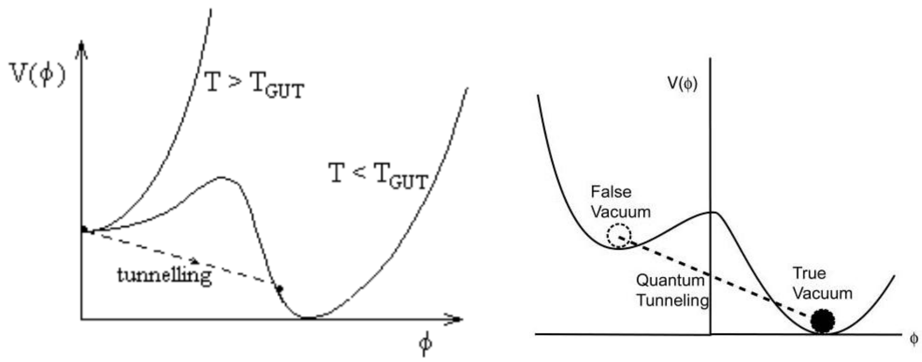

Figure 2.1: Pictorial representation of the old inflation model *Source*: *Left figure*: [2] and *Right figure*: https://ned.ipac.caltech.edu/

expand and then collide to complete the phase transition and reheat the Universe. The inflationary phase lasts till the inflaton tunnels and rolls down to the true minima. But this model encounters a problem that the process of bubble nucleation and collision was rare in the expanding background, and a sufficient reheating of the Universe could not be achieved at the end of inflation. This is known as the 'graceful exit' problem of old inflation.

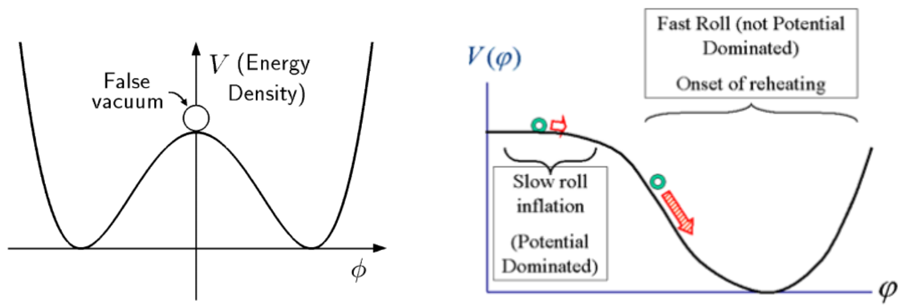

Figure 2.2: Pictorial representation of the new inflation model. *Source*: *Left figure*: https://ned.ipac.caltech.edu/ and *Right figure*: [3].

Thereafter, a 'new inflation' model was proposed by Linde [37, 54], and independently by Albrecht and Steinhardt [38] in which this problem was resolved by considering the phase transition to be second order. In the new inflation or the 'slow roll inflation', the inflaton field starts near $\phi = 0$ and evolves very slowly down a potential $V(\phi)$ initially taken to be Coleman-Weinberg potential. During this slow-roll phase, the energy density of the Universe remains nearly constant and causes the Universe to inflate, as pictorially shown in Fig. 2.2. A separate 'reheating' phase is needed at the end of inflation in which the inflaton oscillates about the minima and decays into particles, and the Universe enters the radiation dominated epoch.

Both old and new inflation models were based on a phase transition in the early Universe, with the initial field value tuned near 0. Thereafter, in 1983, Linde [39] proposed the idea that inflation could even be achieved without a phase transition with a sufficiently flat potential and initial conditions where the inflaton field value $\phi \gg M_{Pl}$, as pictorially represented in Fig. 2.3. This model was named as the 'chaotic model' of inflation.

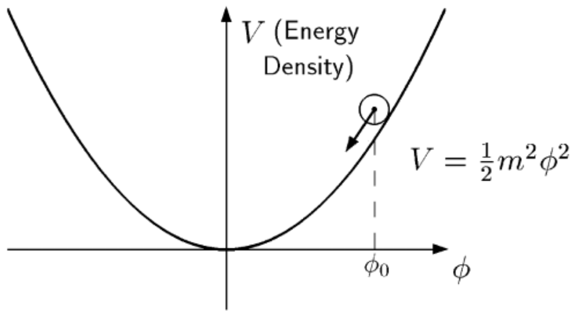

Figure 2.3: Pictorial representation of the chaotic inflation model. *Source*: [4].

Inflation takes place when the energy density of the inflaton field dominates the energy density of the Universe, $\rho_{total} \approx \rho_\phi$. As the field rolls down a potential $V(\phi)$ slowly, the Universe undergoes an accelerated expansion. A pictorial representation of the phenomenon of inflation is shown in Fig. 2.4.

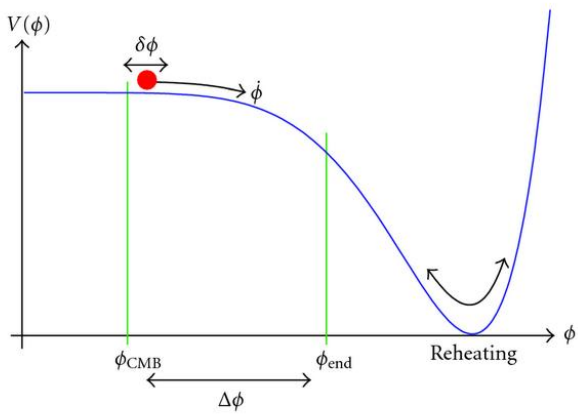

Figure 2.4: Pictorial representation of inflaton slowly rolling down a potential $V(\phi)$ leading to the cosmic inflation [5].

In the standard *cold inflation* description, it is presumed that the inflaton's coupling to other fields is ineffective during the inflationary phase. Therefore, because of the nearly exponential expansion of the Universe during inflation, the number densities of all the species present at that epoch dilute away, and the Universe enters into a supercooled state. Further, when the inflationary phase ends, the Universe undergoes a reheating phase in which the inflaton oscillates and decays into particles [55].

2.2 Kinematics of inflation

In the simplest form, inflation is assumed to be driven by a scalar field, inflaton ϕ, minimally coupled to the gravity. Some standard texts and good reviews on inflation include Refs. [1, 4, 48–53, 56–63]. The Lagrangian density for the inflaton field in a potential $V(\phi)$ is given as,

$$\mathcal{L}(\phi) = \frac{1}{2}(\partial_\mu \phi)(\partial^\mu \phi) - V(\phi), \tag{2.1}$$

and the action governing its dynamics is given as

$$\mathcal{S}_\phi = \int d^4x\sqrt{-g}\left[\frac{1}{2}(\partial_\mu \phi)(\partial^\mu \phi) - V(\phi)\right], \tag{2.2}$$

where g is the determinant of the metric $g_{\mu\nu}$.

By varying the action with respect to the metric, we obtain the stress energy tensor for the inflaton field as

$$T^\mu_\nu = (\partial^\mu \phi)(\partial_\nu \phi) - \mathcal{L}\, \delta^\mu_\nu. \tag{2.3}$$

The diagonal components of T^μ_ν gives the energy density and the pressure for the inflaton field, as

$$\rho_\phi = \frac{\dot{\phi}^2}{2} + V(\phi) + \frac{(\nabla\phi)^2}{2a^2} \tag{2.4}$$

$$p_\phi = \frac{\dot{\phi}^2}{2} - V(\phi) - \frac{(\nabla\phi)^2}{6a^2}. \tag{2.5}$$

For a spatially homogeneous inflaton field, $\nabla\phi = 0$ in these equations. As shown in Eq. (1.14), an accelerated expansion takes place in the cosmic fluid when $3p + \rho < 0$. For the homogeneous inflaton field responsible for the accelerated expansion, from Eqs. (2.4) and (2.5), this implies that $\dot{\phi}^2 < V(\phi)$, i.e., the field has smaller kinetic energy than the potential energy.

The inflaton evolution equation is obtained by varying the action given in Eq. (2.2) with respect to ϕ, as

$$\ddot{\phi} + 3H\dot{\phi} + V'(\phi) = 0. \tag{2.6}$$

In our notation, overdot represents derivative w.r.t. time and prime represents derivative w.r.t. ϕ. The second term, $3H\dot{\phi}$, arises because of the Hubble expansion of the Universe and acts as friction to the inflaton motion. For different forms of the potential $V(\phi)$, the inflaton equation of motion is solved to get the trajectory of the inflaton.

Thus from the Friedmann equation, the Hubble parameter for the homogeneous inflaton field is given as

$$H^2 = \frac{8\pi}{3M_{Pl}^2}\left(\frac{\dot{\phi}^2}{2} + V(\phi)\right). \tag{2.7}$$

As the field is slowly rolling $\dot{\phi}^2/2 \ll V(\phi)$, this can be approximated as,

$$H^2 \approx \frac{8\pi}{3M_{Pl}^2}V(\phi). \tag{2.8}$$

2.2.1 Slow roll approximation

In the approximation that the kinetic energy of the inflaton field is very small, $\ddot{\phi}$ can be taken to 0, and thus the Eq. (2.6) reduces to,

$$\dot{\phi} \approx \frac{-V'(\phi)}{3H}. \tag{2.9}$$

The slow roll motion of the inflaton is maintained by a flat potential, which is quantified in terms of the slow roll parameters,

$$\epsilon_\phi = \frac{M_{Pl}^2}{16\pi}\left(\frac{V'(\phi)}{V(\phi)}\right)^2, \qquad \eta_\phi = \frac{M_{Pl}^2}{8\pi}\left(\frac{V''(\phi)}{V(\phi)}\right). \tag{2.10}$$

The first slow roll parameter, ϵ_ϕ, measures the slope of the potential, and the second slow roll parameter, η_ϕ, measures the curvature of the potential. The slow roll conditions demand that during inflation,

$$\epsilon_\phi \ll 1, \qquad |\eta_\phi| \ll 1. \tag{2.11}$$

2.2.2 Duration of inflation

The scale factor during inflation increases almost exponentially during inflation. To quantify this growth, we define a parameter called number of efolds

$$N(t) \equiv \ln \frac{a(t_e)}{a(t)},$$

where $a(t_e)$ is the scale factor at the end of inflation and $a(t)$ is the scale factor at any time. In our notation, the number of efolds are counted from the end of inflation ($N(t_e) = 0$). From its definition, the Hubble parameter can also be written as

$$H = \frac{\dot{a}}{a} = \frac{d \ln a}{dt},$$

which gives $dN = -H dt$.

For the inflaton field moving in a potential $V(\phi)$, the equation of motion in the slow roll approximation

$$\frac{d\phi}{dN} = \frac{V'(\phi)}{3H^2}. \tag{2.12}$$

Thus, the number of efolds of inflation can be calculated as,

$$N = \frac{8\pi}{M_{Pl}^2} \int_{\phi_e}^{\phi} \frac{V}{V'(\phi)} d\phi. \tag{2.13}$$

2.3 Cosmological perturbations during inflation

As previously mentioned, the generation of density and metric fluctuations is also attributed to inflation. These fluctuations are imprinted as the anisotropies in the CMB and further become the seeds of structures at late times. Having discussed the background dynamics of the inflaton field, we now discuss the quantum fluctuations during inflation, which lead to density and metric fluctuations.

2.3.1 Linear Cosmological Perturbation Theory

The perturbations generated during inflation are small and are treated using linear perturbation theory. In this approach, the inhomogeneities in any physical observable can be treated as linear perturbations around a homogeneous background [1, 6, 48, 64–67]. All the physical quantities $X(t, \mathbf{x})$ (metric $g_{\mu\nu}$ and stress energy tensor $T_{\mu\nu}(\phi, \rho, p)$)

can be decomposed into a homogeneous background $\bar{X}(t)$ which is a function of time only, and inhomogeneous perturbations dependent on both space and time, as

$$X(t, \mathbf{x}) = \bar{X}(t) + \delta X(t, \mathbf{x}).$$

Metric perturbations

We first discuss the perturbations in the components of the metric of the Universe. The full metric can be written as

$$g_{\mu\nu}(t, \mathbf{x}) = \bar{g}_{\mu\nu}(t) + \delta g_{\mu\nu}(t, \mathbf{x}),$$

where the unperturbed metric $\bar{g}_{\mu\nu}(t) = \begin{pmatrix} -1 & 0 \\ 0 & a^2(t)\delta_{ij} \end{pmatrix}$ and the metric perturbations are given as

$$\delta g_{00} = -2\Phi \tag{2.14}$$

$$\delta g_{0i} = a(t)B_i \tag{2.15}$$

$$\delta g_{ij} = 2a(t)^2 C_{ij}. \tag{2.16}$$

We further write

$$B_i \equiv B_{,i} - S_i$$

$$C_{ij} \equiv -\Psi\delta_{ij} + E_{,ij} + F_{i,j} + \frac{1}{2}h_{ij},$$

where a subscript $_{,i}$ represents $\dfrac{\partial}{\partial x^i}$. Here Φ, B, Ψ, E are called the **scalar metric perturbations** constructed from scalars or their derivatives. $S_i,\ F_i$ are called the **vector metric perturbations** which satisfy the condition that they are divergence free $\partial^i S_i = 0$ and $\partial^i F_i = 0$. The **tensor metric perturbation** h_{ij} satisfy the condition that it is transverse $\partial^i h_{ij} = 0$ and traceless $h^i_i = 0$.

Decomposition Theorem

At linear order, the scalar, vector, and tensor perturbations decouple and can be studied independently. The scalar perturbations are related to the density fluctuations, while the tensor perturbations contribute to the primordial gravitational waves. The vector perturbations are related to the vorticity effects, which are damped during inflation, and hence not interesting. Here we discuss the scalar perturbations only.

Scalar metric perturbations

Considering only the scalar perturbations in the line element $ds^2 = g_{\mu\nu}dx^\mu dx^\nu$, we get

$$ds^2 = -(1+2\Phi)\, dt^2 + 2\, a(t)B_{,i}\, dt\, dx^i + a(t)^2 \left[(1-2\Psi)\,\delta_{ij} + 2E_{,ij}\right] dx^i dx^j. \quad (2.17)$$

We can see that there are 4 scalar degrees of freedom in the metric Φ, B, Ψ, E.

Matter perturbations

Now we discuss the perturbations in the components of the stress energy tensor. For a perfect fluid, the unperturbed stress energy tensor is given as

$$\bar{T}^\mu{}_\nu = (\bar{\rho} + \bar{p})\, u^\mu\, u_\nu + \delta^\mu_\nu\, \bar{p}, \quad (2.18)$$

where the 4-velocity satisfy $g_{\mu\nu}u^\mu u^\nu = -1$. The perturbed 4-velocity is given as,

$$u_\mu = (-1-\Phi, av_i), \qquad u^\mu = (1-\Phi, a^{-1}(v^i - B^i)).$$

The unperturbed stress energy tensor can be expressed as $\bar{T}^\mu{}_\nu = \begin{pmatrix} -\bar{\rho} & 0 \\ 0 & \bar{p}\,\delta^i_j \end{pmatrix}$ and the perturbations are given as

$$\delta T^0_0 = -\delta\rho \quad (2.19)$$

$$\delta T^0_i \equiv \delta q_{,i} = (\bar{\rho} + \bar{p})\, av_i \quad (2.20)$$

$$\delta T^i_0 = -(\bar{\rho} + \bar{p})(v^i - B^i)/a \quad (2.21)$$

$$\delta T^i_j = \delta p\, \delta^i_j. \quad (2.22)$$

Here we have assumed that no anisotropic stresses are present.

2.3.2 Perturbed Einstein equations for the scalar perturbations

The Einstein's equations relate the geometry part with the matter energy density as

$$G_{\mu\nu} \equiv R_{\mu\nu} - \frac{1}{2}g_{\mu\nu}R = 8\pi G_N T_{\mu\nu}.$$

Similarly, the perturbations in the metric (Φ, B, Ψ, E) are related to the stress energy tensor perturbations $(\delta\rho, \delta q, \delta p)$, at linear order as

$$\delta G_{\mu\nu} = 8\pi G_N\, \delta T_{\mu\nu}.$$

On expanding the perturbed Einstein equation for the perturbed metric given in Eq. (2.17), we obtain the following equations

$$3H(\dot{\Psi} + H\Phi) + \frac{k^2}{a^2}\left[\Psi + H(a^2\dot{E} - aB)\right] = -4\pi G_N \delta\rho$$

$$\dot{\Psi} + H\Phi = -4\pi G_N \delta q$$

$$\ddot{\Psi} + 3H\dot{\Psi} + H\dot{\Phi} + (3H^2 + 2\dot{H}\Phi) = 4\pi G_N \delta p.$$

2.3.3 Gauge Choice

Gauge choice refers to a *slicing and threading* of the spacetime. Spacelike hypersurfaces of constant time t are called slices, and timelike worldlines of constant $\mathbf{x}$ are called threads. A choice of gauge is not unique, and spurious perturbations can be generated by a transformation of coordinates. Thus, it is important to work either in a specific gauge or construct gauge-invariant quantities.

Types of Gauges

A list of popular gauge choices and their respective definitions is given here. For details on the perturbed Einstein and continuity equations for the different gauges, see the Appendix A of Ref. [1].

- **Longitudinal or Conformal Newtonian Gauge**: $B = 0,\ E = 0$
- **Spatially Flat Gauge**: $E = 0,\ \Psi = 0$
- **Comoving Gauge**: $E = 0,\ \delta q = 0$
- **Uniform Density Gauge**: $E = 0,\ \delta\rho = 0$
- **Synchronous Gauge**: $B = 0,\ \Phi = 0$

A gauge choice reduces the degrees of freedom by 2.

2.3.4 Gauge transformations

Under a gauge transformation, $x^\alpha \to \tilde{x}^\alpha = x^\alpha + \epsilon^\alpha$, we can write

$$\tilde{x}^0 = x^0 + \epsilon^0\,, \qquad \tilde{x}^i = x^i + \delta^{ij}\epsilon^s_{,j} \tag{2.23}$$

where we separate the scalar and vector parts as $\epsilon^i = \epsilon^s_{,i} + \epsilon^v$ and consider only the scalar perturbation.

Under the coordinate transformation defined in Eq. (2.23), the scalar metric perturbations transform as the following,

$$\begin{aligned}
\tilde{\Phi} &\to \Phi - \dot{\epsilon}^0 \\
\tilde{B} &\to B + \frac{\epsilon^0}{a} - a\dot{\epsilon}^s \\
\tilde{E} &\to E - \epsilon^s \\
\tilde{\Psi} &\to \Psi + H\epsilon^0.
\end{aligned}$$

From the combination of these scalar metric perturbations, two gauge invariant quantities known as **Bardeen potentials** are constructed as

$$\Phi_B = \Phi + \frac{d}{dt}[a(B - a\dot{E})] \tag{2.24}$$

$$\Psi_B = \Psi - [aH(B - a\dot{E})]. \tag{2.25}$$

The quantity $(B - a\dot{E})$ is a function of time only.

The stress energy tensor perturbations transform under the gauge transformations in Eq. (2.23) as follows,

$$\begin{aligned}
\delta\tilde{\rho} &\to \delta\rho - \dot{\rho}\epsilon^0 \\
\delta\tilde{q} &\to \delta q + (\bar{\rho} + \bar{p})\epsilon^0 \\
\delta\tilde{p} &\to \delta p - \dot{p}\epsilon^0.
\end{aligned}$$

Some gauge invariant quantities formed for the stress energy tensor perturbations are

$$\delta\rho^{(gi)} = \delta\rho + \dot{\bar{\rho}}a[(B - a\dot{E})] \tag{2.26}$$

$$\delta q^{(gi)} = \delta q + (\bar{\rho} + \bar{p})[a(B - a\dot{E})] \tag{2.27}$$

$$\delta p^{(gi)} = \delta p + \dot{\bar{p}}a(B - a\dot{E}). \tag{2.28}$$

The inflaton field perturbations also transform under the gauge transformation as

$$\delta\tilde{\phi} \to \delta\phi - \dot{\rho}\epsilon^0,$$

and the corresponding gauge invariant quantity constructed from it is given as

$$\delta\phi^{(gi)} = \delta\phi + \dot{\phi}a[(B - a\dot{E})]. \tag{2.29}$$

2.3.5 Gauge invariant quantities constructed from metric and scalar field perturbations

- **Comoving curvature perturbation**

$$\mathcal{R} \equiv \Psi - \frac{H}{\bar{\rho} + \bar{p}}\delta q,$$

where δq is defined in Eq. (2.20). During inflation $\delta T^0_i = -\dot{\bar{\phi}}\,\partial_i\delta\phi$ from Eq. (2.3), which gives

$$\mathcal{R} = \Psi + \frac{H}{\dot{\bar{\phi}}}\delta\phi. \tag{2.30}$$

Geometrically, it measures the spatial curvature of comoving (during inflation $\delta\phi = 0$) hypersurface, i.e. $\mathcal{R} = \Psi|_{\delta q=0}$, where the spatial curvature of constant conformal time hypersurface ${}^{(3)}R = \frac{4}{a^2}\nabla^2\Psi$.

- **Curvature perturbation on uniform energy density hypersurfaces**

$$-\zeta \equiv \Psi + \frac{H}{\dot{\bar{\rho}}}\delta\rho.$$

Geometrically, it measures the spatial curvature of constant density ($\delta\rho = 0$) hypersurface, i.e. $-\zeta = \Psi|_{\delta\rho=0}$. During inflation, ϕ is the dominant field contributing to energy density. Therefore,

$$-\zeta \approx \Psi + \frac{H}{\dot{\bar{\phi}}}\delta\phi. \tag{2.31}$$

From Eqs. (2.30) and (2.31), we see that during inflation, the two gauge invariant quantities $\mathcal{R}$ and $-\zeta$ are equal.

2.4 Primordial curvature power spectrum

In this section, we calculate the primordial power spectrum of the gauge-invariant co-moving curvature perturbation $\mathcal{R}$.

2.4.1 Dynamics of perturbations during inflation

- The curvature perturbations are generated during inflation on **sub Hubble scales** (physical wavelengths of perturbation modes smaller than Hubble radius), i.e. $\lambda_{phys} \ll (H)^{-1}$ or $\frac{k}{a} \gg H$. The physical wavelength of these modes grows like the scale factor.

- When $\lambda_{phys} = (H)^{-1}$ or $\frac{k}{a} = H$, the modes exit the Hubble radius and the amplitude of the fluctuations **freeze-in**.

- The fluctuation modes become **super Hubble** when $\lambda_{phys} > (H)^{-1}$ or $\frac{k}{a} < H$ and no causal physics acts on them.

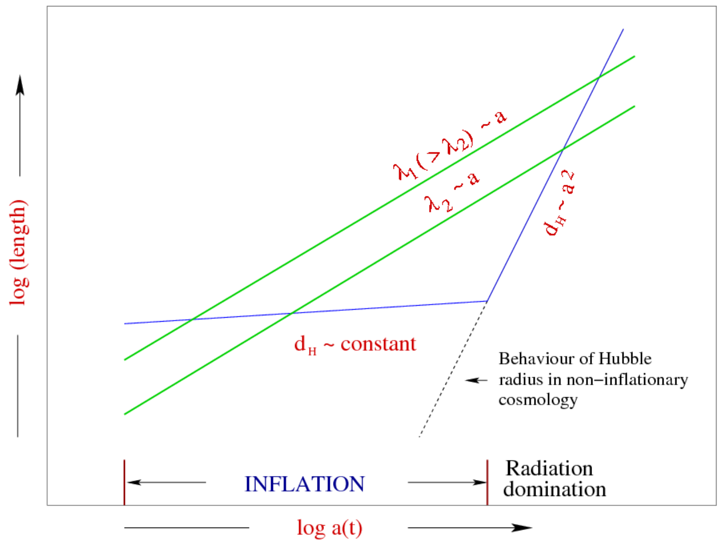

Figure 2.5: Evolution of the physical wavelength of the fluctuation modes generated during inflation, as a function of scale factor. *Source*: [6].

- After inflation ends, the Hubble radius increases. At some time during the radiation or matter-dominated era, these perturbation modes re-enter the Hubble radius.

- These fluctuations are observed in the CMB anisotropies and are also the seeds for density perturbations which grow to form structures at late time.
- For two modes with physical wavelengths, λ_1, λ_2, where $\lambda_1 > \lambda_2$ or $\frac{k_1}{a} < \frac{k_2}{a}$, the mode with larger physical wavelength λ_1 exits the Hubble radius early and re-enters the Hubble radius late - **First Out - Last In**, as shown in Fig. 2.5.

2.4.2 Evolution of comoving curvature perturbation

The action for a canonical single field inflation model can be written as

$$\mathcal{S} = \frac{1}{2}\int d^4x\sqrt{-g}\left[R + (\partial_\mu\phi)(\partial^\mu\phi) - 2V(\phi)\right]. \tag{2.32}$$

Here $8\pi G_N = 1$. To study the perturbations, we choose a comoving gauge, where $\delta\phi = 0$, and $\mathcal{R} = \Psi$. The action is expanded to second order in $\mathcal{R}$, as

$$\mathcal{S}_{(2)} = \frac{1}{2}\int d^4x\, a^3\frac{\dot{\phi}^2}{H^2}\left[\dot{\mathcal{R}}^2 - a^{-2}(\partial_i\mathcal{R})^2\right]. \tag{2.33}$$

By changing the time coordinate to conformal time and defining $v \equiv z\mathcal{R}$, called the *Mukhanov Sasaki* variable, where $z = \frac{a\dot{\phi}}{H}$, we get

$$\mathcal{S}_{(2)} = \frac{1}{2}\int d\eta\, d^3x\left[v'^2 + (\partial_i v)^2 + \frac{z''}{z}v^2\right], \tag{2.34}$$

where a prime denotes a derivative with respect to η. By varying the action in Eq. (2.34) with respect to v, and taking a Fourier transform in k space, we get a parametric oscillator equation for v_k as,

$$v_k'' + \left(k^2 - \frac{z''}{z}\right)v_k = 0. \tag{2.35}$$

The subscript k denotes a mode with wavenumber k. The boundary conditions for solving this equation are obtained (a) from the normalization of quantized v_k, and (b) by selecting a vacuum. By choosing a Bunch-Davies vacuum,

$$\lim_{\eta\to-\infty} v_k = \frac{e^{-ik\eta}}{\sqrt{2k}}$$

and de Sitter space (H = constant), the solution to the mode equation

$$v_k'' + \left(k^2 - \frac{2}{\eta^2}\right)v_k = 0$$

is given as

$$v_k = \frac{e^{-ik\eta}}{\sqrt{2k}}\left(1 - \frac{i}{k\eta}\right). \tag{2.36}$$

Primordial curvature power spectrum

The two point correlation function of the curvature perturbation modes is given by the primordial curvature power spectrum $P_{\mathcal{R}}(k)$, as

$$< \mathcal{R}_{\mathbf{k}}\mathcal{R}_{\mathbf{k}'} >= (2\pi)^3\delta(\mathbf{k}+\mathbf{k}')P_{\mathcal{R}}(k).$$

From the definition of the Mukhanov Sasaki variable, $\mathcal{R} = \frac{v}{z}$. On substituting the solution for v_k given in Eq. (2.36) for a mode at Hubble crossing ($|k\eta| = 1$ or $k = a_* H_*$, where a subscript $_*$ denotes the value of any quantity evaluated at Hubble crossing), we get

$$< \mathcal{R}_{\mathbf{k}}\mathcal{R}_{\mathbf{k}'} >= (2\pi)^3\delta(\mathbf{k}+\mathbf{k}')\frac{H_*^2}{2k^3}\frac{H_*^2}{\dot{\phi}_*^2}.$$

The dimensionless power spectrum $\Delta^2_{\mathcal{R}}(k)$ is thus given as

$$\Delta^2_{\mathcal{R}}(k) \equiv \frac{k^3}{2\pi^2}P_{\mathcal{R}}(k) = \left(\frac{H_*^2}{2\pi\dot{\phi}_*}\right)^2. \tag{2.37}$$

In single field inflation, the primordial curvature power spectrum is a constant quantity for any perturbation mode on the super Hubble scale. In the slow roll approximation, the scalar power spectrum can be written as

$$\Delta^2_{\mathcal{R}}(k) \approx \frac{8}{3}\frac{V}{M_{Pl}^4}\frac{1}{\epsilon_\phi}\bigg|_{k=aH}. \tag{2.38}$$

The slope of the scalar power spectrum at a fiducial scale, called the pivot scale k_P, is given in terms of a *scalar spectral index* n_s, as

$$n_s - 1 \equiv \frac{d\ln\Delta^2_{\mathcal{R}}(k)}{d\ln k}\bigg|_{k=k_P} = 2\eta_\phi - 6\epsilon_\phi. \tag{2.39}$$

2.5 Tensor power spectrum

Similar to the scalar perturbations and the associated dimensionless scalar power spectrum, tensor fluctuations h_{ij} are also generated during inflation. The dimensionless tensor power spectrum is calculated by expanding the Einstein Hilbert action to second order in the tensor fluctuations and is given as

$$\Delta^2_t(k) = \frac{16}{\pi}\frac{H_*^2}{M_{Pl}^2}. \tag{2.40}$$

In the slow roll approximation, the tensor power spectrum can be written as

$$\Delta_t^2(k) \approx \frac{128}{3} \frac{V}{M_{Pl}^4}\bigg|_{k=aH}. \tag{2.41}$$

The slope of the tensor power spectrum at the pivot scale k_P, is given in terms of a *tensor spectral index* n_t, as

$$n_t \equiv \frac{d\ln \Delta_t^2(k)}{d\ln k}\bigg|_{k=k_P} = -2\epsilon_\phi. \tag{2.42}$$

Tensor-to-scalar ratio

The ratio of the amplitude of the tensor power spectrum to the amplitude of the scalar power spectrum at the pivot scale is known as the tensor-to-scalar ratio,

$$r \equiv \frac{\Delta_t^2(k_P)}{\Delta_{\mathcal{R}}^2(k_P)}. \tag{2.43}$$

From Eqs. (2.38) and (2.41), we get

$$r = 16\epsilon_\phi,$$

and further using Eq. (2.42), we obtain the consistency condition, $r = -8n_t$.

The amplitude of the scalar perturbations is known from CMB observations to be $\Delta_{\mathcal{R}}^2(k_P) = 2.1 \times 10^{-9}$, where the pivot scale $k_P = 0.05\,\mathrm{Mpc}^{-1}$. Then using Eq. (2.41), we get

$$V^{1/4} \sim \left(\frac{r}{0.01}\right)^{1/4} 10^{16}\mathrm{GeV}.$$

Thus, the tensor power spectrum or the tensor-to-scalar ratio are the direct measures of the energy scale of inflation.

2.6 Observational imprints of inflation on the CMB

2.6.1 Cosmic Microwave Background Radiation

The cosmic microwave background radiation refers to the relic photons from the epoch of recombination that are present in all the directions of the sky. They are the earliest snapshots of the very early Universe. These photons from the last scattering surface have free streamed and redshifted from $z = 1100$ till today at $z = 0$ and have a

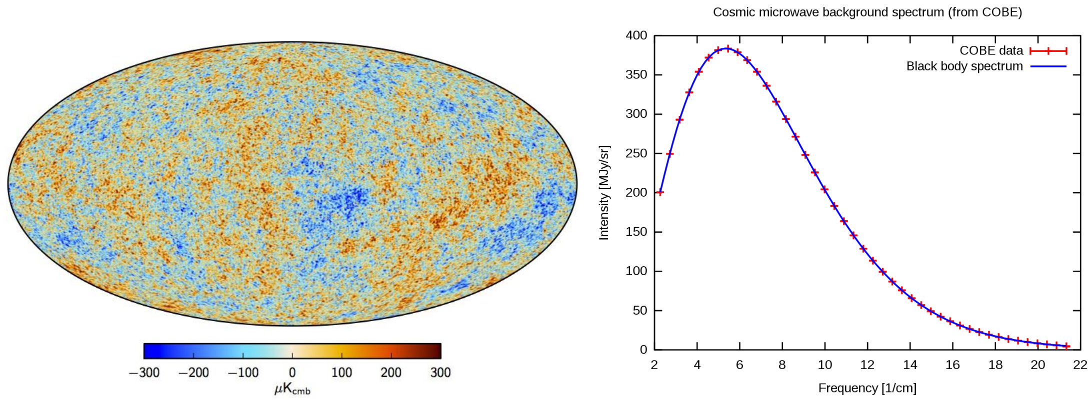

Figure 2.6: *Left*: Full sky map of CMB with the anisotropies, as seen by the Planck satellite. The color coding (red to blue) represents a temperature value above or below the mean value of 2.725 K. *Source*: https://sci.esa.int/ and *Right*: A black body spectrum of the CMB radiation, as seen by the COBE satellite. *Source*: Wikipedia

uniform temperature 2.725 K. The existence of CMB was predicted in 1948 by Ralph Alpher and Robert Herman, but it was serendipitously detected for the first time in 1964 by Arno Penzias and Robert Woodrow Wilson in their radio antenna, for which they received the Nobel prize in 1978 [41]. The temperature of the CMB was measured to be uniform across the sky through a series of ground-based and balloon experiments till the satellite experiments were launched in the 1990s [68].

The spectrum of the CMB was measured to be a perfect black body with the Far Infrared Absolute Spectrophotometer (FIRAS) instrument on COBE (COsmic Background Explorer) satellite [42], as shown in Fig. 2.6. The ansiotropies in the CMB temperature are extremely tiny, 1 part in 10^5, as shown in Fig. 2.6. The different colors in the CMB map denote a value of temperature above or below the mean temperature of 2.725 K. These anisotropies were first detected with the Differential Microwave Radiometer (DMR) instrument on COBE [43]. For these findings, John Mather and George Smoot jointly received the Nobel prize in 2006. After the COBE mission, the WMAP (Wilkinson Microwave Anisotropy Probe) satellite was launched in 2001 with a better sensitivity to measure the CMB anisotropies and polarization, and it operated for 9 years [44]. Thereafter, the *Planck* satellite mission was launched in 2009 with a further high resolution and it completed its exploration in 2018.

2.6.2 Angular Power Spectrum of CMB temperature fluctuations

The temperature anisotropy in the CMB can be expanded in spherical harmonics as

$$\Theta(\mathbf{x},\eta,\hat{n}) \equiv \frac{\Delta T}{T}(\mathbf{x},\eta,\hat{n}) = \sum_{l=1}^{\infty}\sum_{m=-l}^{+l} a_{lm}(\mathbf{x},\eta)Y_{lm}(\hat{n}),$$

where $\hat{n}$ is the direction of observation, l are different multipoles ($l = 0$ monopole, $l = 1$ dipole, $l = 2$ quadrupole), and Y_{lm} are the spherical harmonics on a 2-sphere. Using the orthogonality property of Y_{lm},

$$\int d\Omega\, Y_{lm}(\hat{n})\, Y^{*}_{l'm'}(\hat{n}) = \delta_{ll'}\delta_{mm'},$$

where $d\Omega$ is the solid angle subtended by $\hat{n}$, we get

$$a_{lm}(\mathbf{x},\eta) = \int \frac{d^3k}{(2\pi)^3} e^{i\mathbf{k}.\mathbf{x}} \int d\Omega\, Y^{*}_{lm}(\hat{n})\Theta(\mathbf{k},\eta,\hat{n}). \tag{2.44}$$

The variance of a_{lm} is called the angular power spectrum C_l^{TT}

$$\langle a_{lm}a^{*}_{l'm'}\rangle = \delta_{ll'}\delta_{mm'}C_l^{TT}$$

$$C_l^{TT} = \frac{1}{2l+1}\sum_m \langle a_{lm}a^{*}_{lm}\rangle\,. \tag{2.45}$$

The CMB temperature fluctuations are sourced by the scalar fluctuations $\mathcal{R}$, and are related through the relation [1],

$$C_l^{TT} = \frac{2}{\pi}\int k^2 dk\, P_{\mathcal{R}}(k)\Delta_{Tl}(k)\Delta_{Tl}(k), \tag{2.46}$$

where the transfer function $\Delta_{Tl}(k)$ describes the evolution of perturbations from the horizon reentry epoch till the matter radiation equality. Mathematically, it is the line-of-sight integral of convolution of the source terms and geometric projection factors. For reviews, see Refs. [1, 16, 47].

The angular power spectrum of the CMB from recent Planck 2018 results is shown in Fig. 2.7. The quantity on the y-axis is defined as $\mathcal{D}_l^{TT} \equiv \frac{l(l+1)}{2\pi}C_l^{TT}$. In the figure, the blue curve represents the best fit of the theoretical predictions from ΛCDM to the data. Also, the residuals of the theoretical predictions for the best fit parameters and the data points are shown in the lower panel of Fig. 2.7. For a scale-invariant primordial power spectrum ($n_s = 1$), at the large scales ($l < 30$), the angular power spectrum is independent of l.

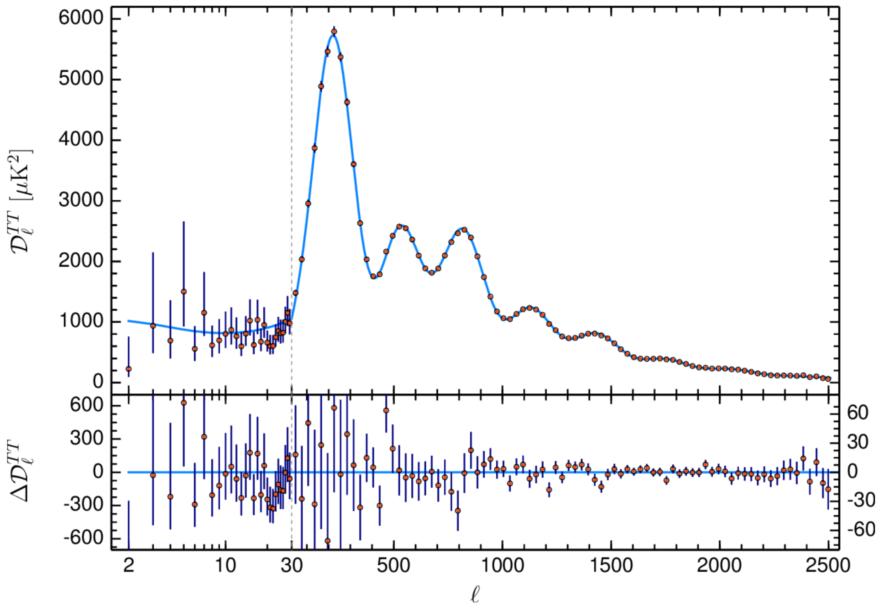

Figure 2.7: Angular power spectrum of the CMB from Planck 2018 results [7]. The blue curve represents the ΛCDM best fit to the data points for Planck TT, TE, EE+ low E + lensing. The lower panel shows the residuals with respect to the best fit.

2.7 Current status of cold inflation models from CMB

CMB is the most pristine probe of the composition and primordial fluctuations of the early Universe. The angular power spectrum of the CMB, and especially its peaks, carry a lot of information and are important for understanding the early Universe. From the CMB, we infer that the spatial geometry of our Universe is flat, and the spectrum of scalar fluctuations is nearly scale-invariant, Gaussian, and adiabatic. Current observations are in good agreement with the inflationary predictions. In the era of precision cosmology, various inflationary models have been stringently tested with the observations. The theoretical estimates of the cosmological parameters, scalar spectral index n_s, and the tensor-to-scalar ratio r for the inflationary models are compared with their allowed range from the measurements.

Inflationary models are classified into various categories, eg. single-field (eg. chaotic inflation, natural inflation, hilltop inflation, power-law inflation) or multiple-field (eg. hybrid inflation, N-inflation) (based on the field driving inflation), large-field or small-field (based on the field evolution, comparable to M_{Pl}), having minimal or non-minimal

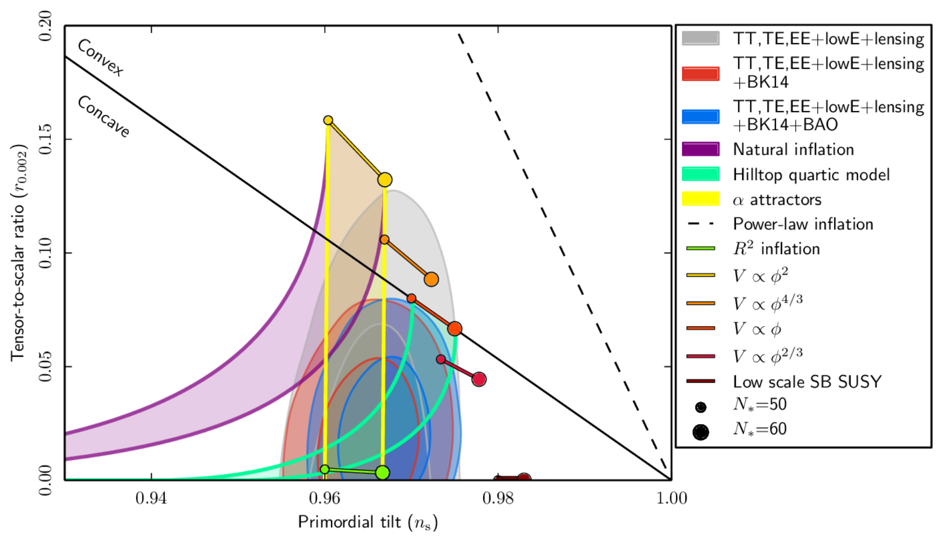

Figure 2.8: Joint 68% and 95% confidence limits on the parameters n_s and r for various inflationary models from Planck 2018 results. The band of values for various models corresponds to the number of inflationary efolds between 50 to 60. *Source*: [7].

kinetic term (eg. K-inflation, DBI inflation, tachyonic inflation), with minimal or non-minimal coupling to gravity (eg. Starobinsky inflation, Higgs inflation), etc. For a detailed review and the current status of various models, see Refs. [69–71].

The future measurements of CMB will focus on the B-mode polarization [72]. The amplitude of B-modes of CMB is a direct measure of the energy scale of inflation. Their detection will provide a unique signature of the inflationary gravitational waves. Some experiments dedicated for CMB B-mode polarization include CMB-S4 [73], LiteBIRD [74], CORE [75]. Also, in the future, studies like HI intensity mapping with BINGO [76], FAST [77] and SKA-I [78], will explore the non-Gaussian signatures in the CMB [79]. Non-Gaussanity is an important aspect to understand the interactions of the inflaton field and therefore demands precision measurements in this direction.

2.8 Numerical codes in Cosmology

The test of any theory in cosmology is its compatibility with observations. For the various epochs of the Universe evolution, there are a variety of observations, like the CMB temperature anisotopies and polarization [44, 45, 80–83], matter power spectrum and baryon acoustic oscillations [84–87], galaxy cluster counts [88], dark ages 21 cm line [89], Lyman-α [90], weak lensing observations [91, 92],Type Ia supernovae [93], Cepheid variables [94, 95] etc. In the era of precision cosmology, powerful numerical tools are required to estimate the theoretical parameters which explain the observations [96]. Here is the list of numerical codes used in this study.

CAMB (Code for Anisotropies in the Microwave Background)

CAMB [97] is a cosmological Boltzmann code, used for calculating the theoretical power spectrum of the cosmological observables [98, 99]. It is written in Fortran and Python languages, and is developed by Antony Lewis and Anthony Challinor. CAMB integrates the Boltzmann equations for various species and has features to compute CMB, CMB lensing, lensing, galaxy count and dark-age 21 cm power spectra, transfer functions and matter power spectra, and background cosmological functions [100–102].

CosmoMC (Cosmological Monte Carlo)

CosmoMC [103, 104] is a Markov Chain Monte Carlo (MCMC) engine for exploring cosmological parameter space. It has been developed by Antony Lewis and Sarah Bridle in Fortran language and has Python codes for analyzing MCMC samples. For notes on installation and running of CosmoMC, see Refs. [105, 106]. CosmoMC is based on the technique of Bayesian inference to estimate the model parameters that best explain the observational data [107–110].

In the Bayesian analysis for cosmological parameter estimation, given a dataset D, and a theoretical model parameter θ, the Baye's Theorem is given as

$$P(\theta|D) = \frac{P(D|\theta)P(\theta)}{P(D)} , \tag{2.47}$$

where,
$P(\theta|D)$ is the *posterior probability* of a value of the parameter θ given the data,
$P(D|\theta)$ is the *likelihood* of the data given a model, i.e. the conditional probability of data given a value of the parameter θ, and is also written as $\mathcal{L}(\theta)$.
$P(\theta)$ is the *prior* probability of the theoretical parameter. It is the degree of belief in the value of theoretical parameter, before the dataset D is observed, and

$P(D)$ is called the *evidence* or marginal likelihood, the probability of observing data under all possible models. It is a normalizing constant obtained by marginalizing the likelihood over all models,

$$P(D) = \int P(D|\theta)P(\theta)d\theta.$$

In statistics, one also computes a quantity called *chi-square*, defined as,

$$\chi^2 = \sum_{ij}(x_i - \mu_i)\, C_{ij}^{-1}\, (x_j - \mu_j). \tag{2.48}$$

Here μ_i and μ_j are the mean values of variables x_i and x_j, respectively, and the covariance matrix,

$$C_{ij} =< (x_i - \mu_i)(x_j - \mu_j) > .$$

For a gaussian distributions, the likelihood is given as

$$\mathcal{L}(\theta) = \exp(-\frac{\chi^2}{2}). \tag{2.49}$$

The best fit point to data is obtained for the theoretical parameters with a maximum likelihood.

For CMB analysis, the Planck likelihoods need to be installed from the Planck Legacy Archive [45]. The CAMB code is inbuilt into CosmoMC for the theoretical computations of power spectra. The output of CosmoMC consists of multiple chains with parameter values, which are then further analyzed.

GetDist GUI

GetDist [111, 112] is a Python package used for analysing CosmoMC chains. It reads the MCMC chains in plain text format, and has a Graphical User Interface (GUI) for easy use [113]. The output of GetDist are marginalized probability distribution (1 D) plots and statistics, joint contour (2 D) plots with $68\%, 95\%$, and 99% confidence limits, three parameter plots (3 D), and triangle plots.

Chapter 3

Warm Inflation

Although the cold inflation description successfully solves the problems faced by the Standard Model of cosmology, it must be scrutinized for its supercooled phase during inflation. This led to the idea of *warm inflation,* where one does not neglect the inflaton dissipative effects during the slow roll, and it results in the production of radiation and hence temperature in the Universe even during the inflationary phase. In this Chapter, I present a review of warm inflation and the dynamics associated with it.

3.1 Introduction

Warm Inflation [114–116] is a description of inflation in which one accounts for the dissipation processes and non-equilibrium effects during inflation. In this scenario, radiation fields are produced simultaneously with the expansion during the inflationary phase [114–118]. The inflaton energy dominates the energy density of the Universe, as required for inflation. However, it also dissipates into the radiation energy density as it evolves during inflation, and therefore, a separate reheating phase may not be required in some warm inflation models [116, 119–121]. In this way, it differs from the cold inflation description, where the particle production occurs only in the reheating phase after the end of inflation [55, 122, 123]. Because of the inflaton dissipation into radiation, the Universe has a temperature throughout the inflationary phase, unlike the supercooled state during cold inflation. (For reviews, see Refs. [124–130].) Thus, warm inflation is a more natural and complete picture of inflation, with the cold inflation as its limiting case [131].

The warm inflation description has the following unique and distinct characteristics from cold inflation. In this picture, the inflaton couplings with other fields are accounted for during the inflationary phase [119, 131–137], unlike in cold inflation where they are overlooked. As a result of its interactions, the inflaton dissipates its energy, and calculations show that even a tiny amount of dissipation can lead to a sufficient particle production and a temperature in the Universe. Therefore, the assumptions of the cold inflation description have to be scrutinized more carefully, and this motivates one to study warm inflation.

In warm inflation, the dynamics of the inflaton is modified and there is an additional friction term in its equation of motion because of its interactions and dissipation into radiation [138–141]. The radiation fields which are produced backreact to affect the fluctuations in the inflaton. These fluctuations are then imprinted on the cosmic microwave background radiation as its temperature anisotropies. Therefore, from the observations of the CMB, we can access the information about the microphysics of the inflationary phase. The friction term in the evolution equation of the inflaton due to the inflaton interactions during warm inflation is quantified as the dissipation coefficient [142–145]. The microphysics of dissipation, such as the channel of decay, the coupling strengths, and the multiplicities of the fields involved, govern the strength of the dissipation coefficient [142, 144, 145], and even a small amount of inflaton dissipation could lead to important cosmological consequences.

The criterion for warm inflation is that $\rho_r^{1/4} \gtrsim H$, where ρ_r is the radiation energy density, and H is the Hubble expansion rate of the Universe [119, 139]. Assuming the thermalization of the radiation, this amounts to the condition that the temperature of the thermal bath $T \gtrsim H$. The perturbations during warm inflation are generated in a statistical state and are thermal [117, 134, 146–150], rather than the quantum vacuum fluctuations in cold inflation. Therefore, the primordial curvature power spectrum for warm inflation is sourced dominantly by the thermal fluctuations [147–151], and depends on the magnitude of the dissipation. This leads to significant differences in the imprints of warm inflation on the Cosmic Microwave Background radiation compared to the standard cold inflation [152, 153]. For warm inflation models, the theoretical predictions of the scalar spectral index n_s, and the tensor-to-scalar ratio r, depends on the strength of the dissipation parameter. Warm inflation predicts a lower value of r, as compared to the standard cold inflation. Therefore, certain inflation models which were ruled out in the cold inflation studies because of r values above the observationally allowed bounds, are now viable from the warm inflation dynamics for some range of dissipation [136, 154–156].

Besides the Gaussian two-point correlations, warm inflation can also lead to non-Gaussianities because of the inflaton interactions. These are studied in Refs. [157–161], where it is shown that the amplitude of the bispectrum, measured in terms of the non-linearity parameter f_{NL}, as well as the shape of the bispectrum are different for the warm inflation models and depends on the dissipation parameter and the temperature of the thermal bath in the weak dissipation case.

Further, warm inflation also predicts interesting features at the small scales. In the model we studied in Ref. [162], it is found that the dissipation parameter is enhanced to a large value by the end of inflation, which leads to a huge growth in the primordial power spectrum at the small scales and the formation of primordial black holes [163–166]. This feature originates naturally in our model of warm inflation because of inflaton dissipation, which makes it interesting to study. It will be discussed in detail in Chapter 6.

Depending on the strength of inflaton dissipation, warm inflation is classified into two dissipative regimes - weak and strong [125, 136]. These are characterized by a dissipation parameter Q, defined as the ratio of the inflaton dissipation rate, Υ to the Hubble expansion rate. When the dissipation parameter is smaller than the Hubble expansion rate ($Q < 1$), it is the weak dissipative regime, and when it is larger ($Q > 1$), then it is the strong dissipative regime of warm inflation.

For the strong dissipation case, warm inflation may relax the η problem [167], which is related with the requirement to have an extremely flat potential during the slow roll phase. In warm inflation, because of the dissipation coefficient term in the inflaton equation of motion, the conditions for slow roll are modified. The presence of the extra friction term slows down the inflaton motion, and thus, even for a non-flat potential, the desired number of efolds of inflationary expansion can be achieved.

Therefore, warm inflation is less restrictive in the flat shape of the potential, and the slow roll conditions are relaxed in this scenario [168].

Furthermore, the warm inflation scenario also offers a resolution to the swampland problems faced by cold inflation [169–173]. As inflation is a low energy effective field theory, it has to obey some criteria, such as the swampland distance and de-Sitter conjectures [174, 175], in order to embed it in a UV complete theory. It has been found [176, 177] that single-field slow roll cold inflation, with a canonical kinetic term and a Bunch Davies vacuum, is not in accordance with the swampland conjectures. However, recent studies [169–173] show that a warm inflation description of inflation can satisfy the swampland conjectures, thus making it in agreement with a high energy theory. This requires warm inflation to be in the strong dissipative regime [170] with a large value of the dissipation parameter [171]. Such a large dissipation may not be consistent to explain the CMB observations for many models, as discussed in Ref. [171]. However, if the bounds in the swampland conjectures are relaxed, then even the weak dissipative regime of many models can simultaneously satisfy both the swampland conjectures as well as the current CMB observations [170, 171].

All these above features arise from the fundamental feature of treating the dynamics of inflaton as that of a dissipative system, and hence makes warm inflation interesting. Thus, a comprehensive study of the warm inflation scenario is significant and necessary to understand the physics of the Universe.

3.2 Model Building in Warm Inflation

A microscopic particle physics construction of inflation has always been elusive. The ultimate aim of the model building is to make a connection between elementary particle physics and the early Universe physics. In the warm inflation description, one considers the dissipative processes during inflation which are based on the principles of non-equilibrium field theory for interacting quantum fields [178–183]. Here the background slow-rolling inflaton field constitutes the system and the radiation fields to which it couples and dissipates its energy, constitute the reservoir or the environment. The inflaton is assumed to be near-equilibrium and evolving slowly as compared to the microphysics timescales in the adiabatic approximation. The inflaton approach to equilibrium can also be described in a linear response theory.

The effective equation of motion of inflaton field is obtained using the Schwinger-Keldysh close time path formalism of thermal field theory (For reviews on this, see Refs. [12, 184–188]). Using this formalism, a Langevin type equation of motion with a dissipation term and a stochastic noise is obtained for the inflaton field coupled to radiation [132, 178, 180].

The microphysics description of warm inflation is described by non-equilibrium field theory [180], based on which a field theoretical model was constructed in Ref. [132] for studying the strong dissipative regime of warm inflation. However, it was indicated in [132] and also pointed out in [189] that it is difficult to obtain a successful strong dissipative regime of warm inflation. The problem was that in the high-temperature limit taken in Ref. [132], the thermal corrections to the effective potential become large, due to which the shape of the potential no longer remains flat, and thus inflation ends quickly without achieving a sufficient number of efolds of expansion [189]. Therefore, subsequent studies considered new models, such as the supersymmetric distributed mass model in the context of string theory [133], or a two-stage decay mechanism of inflaton, where the inflaton couples to a heavy intermediate catalyst field which then further couple to the light radiation fields [119, 131, 135, 139], or recently discrete interchange symmetry in the warm little inflaton model [190, 191] to control these corrections [192], and attain a strong dissipation regime of warm inflation.

There is another difficulty in warm inflation, that it usually requires the inflaton to couple to a very large number of fields [136, 193]. However, such large multiplicities of fields can be achieved through some string theory inspired generation mechanism [194]. Another possible solution to this shortcoming is the recently proposed warm inflation models with the inflaton as a pseudo-Nambu-Goldstone boson which requires a very few additional fields [190, 195] and allow for a well-motivated particle physics description.

In the literature, a number of studies have been carried out for the warm inflation model building. Some examples include, warm supersymmetric hybrid inflation [193, 196–198], warm hilltop potential [156, 193, 198, 199], warm inflation with a SUSY breaking potential [153], warm inflation near an inflection point [200], warm natural inflation [195, 201], tachyonic warm inflation [202], warm inflation with monomial potentials [154–156, 193, 198], warm little inflaton [190, 203], warm psuedoscalar inflation [204], minimal warm inflation with axions [205], etc. Also, inspired from string theory, brane world models of warm inflation are constructed in Refs. [206–209] and in loop quantum cosmology [210]. There are other warm inflation studies which consider non-canonical scalar fields [211–213] or modifications to gravity, such as $f(R)$ theory [214, 215], $f(G)$ gravity [216], teleparallel $f(T)$ gravity [217]. Apart from this, there are studies which also include the viscous pressure contributions in the radiation produced during warm inflation [218–220].

3.3 The theory of warm inflation

In this section, we first review the dynamical equations for the inflaton and the radiation during warm inflation. Then, we define the slow-roll parameters and the slow roll conditions in warm inflation. We then discuss the forms of the dissipation coefficient and their physical interpretation. After that, we describe the primordial scalar and tensor power spectrum for warm inflation.

3.3.1 Evolution equations for the inflaton and radiation

The warm inflation dynamics of inflation involves the evolution of a scalar inflaton field $\phi(x,t)$ coupled with other fields. The system (inflaton) is assumed to be slightly displaced from thermal equilibrium. Dissipative effects, because of its interactions with the environment (fields coupled to inflaton), tend to relax the system to thermal equilibrium within the relaxation time approximation. Using the principles of non-equilibrium field theory, the effective equation of motion of the inflaton is calculated to have a Langevin-like form with dissipation and fluctuation terms, as given by [132, 180]

$$\ddot{\phi}(x,t) + 3H\dot{\phi}(x,t) + \Upsilon\dot{\phi}(x,t) - \frac{1}{a^2(t)}\nabla^2\phi(x,t) + V'(\phi) = \xi_q + \xi_T. \tag{3.1}$$

In this equation, apart from the Hubble friction term $3H\dot{\phi}(x,t)$, due to the expansion of the Universe, there is an additional friction from the dissipative term $\Upsilon\dot{\phi}(x,t)$, which is absent in the cold inflation Eq. (2.6). $\Upsilon(\phi, T)$ is called the dissipation coefficient, and it emerges because of the terms in the Lagrangian involving the inflaton coupling to the other fields. The form of $\Upsilon(\phi, T)$ depend on the microphysics of the inflaton dissipation, and can be calculated as in Refs. [142, 144, 145]. The term $\nabla^2\phi(x,t)/a^2(t)$ represents an inhomogeneous background inflaton field value and is absent for the homogeneous field. Also, there are stochastic gaussian quantum and thermal fluctuations (noise) terms ξ_q and ξ_T [150]. The presence of the noise terms in Eq. (3.1) backreacts on the inflaton fluctuations, which then manifests in the primordial curvature power spectrum.

The evolution of a classical homogeneous (spatial gradients equal to 0) background inflaton field, can be obtained from Eq. (3.1), as

$$\ddot{\phi}(t) + (3H + \Upsilon)\,\dot{\phi}(t) + V'(\phi) = 0. \tag{3.2}$$

We can define a dissipation parameter $Q \equiv \Upsilon/3H$ and rewrite the above equation as

$$\ddot{\phi} + 3H(1+Q)\dot{\phi} + V'(\phi) = 0, \tag{3.3}$$

where the dissipation parameter, Q, is the ratio of the strength of inflaton dissipation to the Hubble rate of expansion. For $Q \gg 1$, the dissipation coefficient is larger than H, and this regime is termed as the strong dissipative regime. In this regime, the dissipative effects have a prominent role during inflation. For $Q \ll 1$, the expansion is faster than dissipation, and this is termed as the weak dissipative regime of warm inflation. In this regime, the dissipative effects are present and affect the dynamics, but are less prominent.

From the continuity equation, we can also express Eq. (3.2) in terms of the energy density of the inflaton as,

$$\dot{\rho_\phi} + 3H(p_\phi + \rho_\phi) = -\Upsilon\dot{\phi}^2. \tag{3.4}$$

The negative sign on the right-hand side of this equation shows that the inflaton dissipates its energy with time. As a result of the dissipation, radiation is produced along with the expansion during warm inflation. From the continuity equation, the radiation energy density is given as

$$\dot{\rho}_r + 4H\rho_r = \Upsilon\dot{\phi}^2 \,. \tag{3.5}$$

In this equation, the right-hand side is positive, implying a gain in the energy density of the radiation with time. Assuming that the radiation thermalizes quickly after being produced, we can write

$$\rho_r = \frac{\pi^2}{30} g_* T^4 \equiv AT^4$$

where T is the temperature of the thermal bath, g_* is the number of relativistic degrees of freedom present during warm inflation, and $A = \pi^2 g_*/30$.

3.3.2 Slow roll parameters and conditions

The flatness of the potential $V(\phi)$ in inflation is measured in terms of the potential slow roll parameters, similar to the ones defined for cold inflation

$$\epsilon_\phi = \frac{M_{Pl}^2}{16\pi}\left(\frac{V'}{V}\right)^2, \qquad \eta_\phi = \frac{M_{Pl}^2}{8\pi}\left(\frac{V''}{V}\right). \tag{3.6}$$

In addition to these, in warm inflation there are other slow roll parameters defined as [148, 168]

$$\beta_\Upsilon = \frac{M_{Pl}^2}{8\pi}\left(\frac{\Upsilon' V'}{\Upsilon V}\right), \qquad b = \frac{TV'_{,T}}{V'}\,, \qquad c = \frac{T\Upsilon_{,T}}{\Upsilon}. \tag{3.7}$$

Here the subscript $_{,T}$ represents derivative of the quantity w.r.t T. These additional slow roll parameters are a measure of the field and temperature dependence in the inflaton potential and the dissipation coefficient.

The thermal corrections to the potential in warm inflation have to be controlled by some symmetry arguments, such as in supersymmetric warm inflation models [119, 139, 192]. In the literature one also defines the horizon flow parameters in terms of the Hubble parameter as

$$\epsilon_H = -\frac{\dot{H}}{H^2}\,, \qquad \eta_H = -\frac{\ddot{H}}{2H\dot{H}}\,. \tag{3.8}$$

The stability analysis of warm inflationary solution shows that the following conditions should be satisfied during the slow roll [168]

$$\epsilon_\phi \ll 1+Q, \qquad |\eta_\phi| \ll 1+Q, \quad |\beta_\Upsilon| \ll 1+Q,$$

$$0 < b \ll \frac{Q}{1+Q}, \qquad |c| < 4. \tag{3.9}$$

As can be clearly seen, for large Q, these conditions relax the requirement for the potential to be extremely flat, as the upper limit on the slow roll parameters ϵ_ϕ, η_ϕ is increased. Therefore, the η problem is not as severe in warm inflation [167].

End of warm inflation

In the standard cold inflation, the violation of slow-roll conditions marks the end of inflation. But in warm inflation, two conditions can bring the inflation to an end : (i) either the slow-roll conditions are violated, or (ii) the radiation energy density dominates the inflaton energy density, i.e., $\rho_r > \rho_\phi$.

Evolution equations in the slow roll approximation

In the slow roll approximation, we can neglect $\ddot{\phi}$ in Eq. (3.3), which gives

$$\dot{\phi} \approx \frac{-V'(\phi)}{3H(1+Q)}, \tag{3.10}$$

and since $\dot{\rho}_r$ is smaller than the other terms in Eq. (3.5) throughout inflation, we can approximate $\dot{\rho}_r \approx 0$ and obtain

$$\rho_r \approx \frac{\Upsilon}{4H}\dot{\phi}^2 = \frac{3}{4}Q\dot{\phi}^2. \tag{3.11}$$

3.3.3 Dissipation coefficient

The microphysics of the inflaton-radiation system, results into dissipation, which is quantified in terms of a dissipation coefficient. For an interacting inflaton, an effective equation of motion is obtained by integrating over the fields coupled to the inflaton, using the Schwinger closed time path formalism of thermal field theory (see Appendix A for details). There is a non-local term in the effective action which corresponds to the dissipative effects in the system and a transfer of energy from the inflaton to the radiation fields. Assuming that the inflaton varies slowly compared to the response timescale of the fields coupled to it in the adiabatic approximation i.e. $\frac{\dot{\phi}}{\phi} \ll \tau^{-1}$, the non-local term can be localized and the resultant effective equation of motion of background homogeneous inflaton is obtained as [144]

$$\ddot{\phi}(t) + 3H\dot{\phi}(t) + \Upsilon\dot{\phi}(t) + V'(\phi) = 0 \tag{3.12}$$

where Υ is the dissipation coefficient which is calculated by accounting all the micro-physical interactions as [144]

$$\Upsilon = \int d^4x' \, \Sigma_R(x, x')(t' - t) \tag{3.13}$$

here the retarded self energy $\Sigma_R(x, x') = \Sigma_\rho(x, x')\theta(t - t')$, and Σ_ρ is given in Appendix A. In this study, we are considering a two-stage decay of the inflaton in a supersymmetric inflation model [142, 144]. In our model, we have three superfields Φ, X, and Y, whose scalar and fermion components are (ϕ, ψ_ϕ), (χ,ψ_χ) and (σ,ψ_σ), respectively. The interacting superpotential is given as

$$W = g\Phi X^2 + hXY^2, \tag{3.14}$$

where g and h are the coupling strengths between $\Phi - X$, and $X - Y$, respectively. The scalar inflaton is coupled with the intermediate bosonic and fermionic components of the X superfield (also called catalyst fields), which subsequently decay into the scalar and fermionic components of the Y superfield (called radiation fields). The radiation fields are considered to be lighter than the catalyst fields. The scatterings of decay products σ, ψ_σ with masses $m_\sigma, m_{\psi_\sigma} \ll T$ is sufficient to keep them thermalized and constitute the thermal bath, as shown in the Appendix C of Ref. [145]. The inflaton particle states are also assumed to thermalize with a same temperature, for some range of effective couplings (see details in Ref. [145]).

The scalar part of the Lagrangian is given as

$$\begin{aligned} -\mathcal{L}_s &= |\partial_\Phi W|^2 + |\partial_X W|^2 + |\partial_Y W|^2 \\ &= g^2|\chi|^4 + h^2|\sigma|^4 + 4g^2|\chi|^2|\phi|^2 + 4ghRe[\phi^\dagger\chi^\dagger\sigma^2] + 4h^2|\chi|^2|\sigma|^2. \end{aligned} \tag{3.15}$$

The scalar fields ϕ, χ, σ are chosen to be complex with real and imaginary components, such as $\chi = (\chi_1 + i\chi_2)/\sqrt{2}$, and similarly for others. When the background scalar field ϕ takes an expectation value $\varphi/\sqrt{2}$, the mass of the χ field is given as:

$$m_{\chi_1} = \sqrt{2}g\varphi \qquad m_{\chi_2} = \sqrt{2}g\varphi.$$

The Yukawa interactions are obtained as

$$-\mathcal{L}_Y = \frac{1}{2}\sum_{n,m}\frac{\partial^2 W}{\partial\zeta_n\,\partial\zeta_m}\bar{\psi}_n P_L\psi_m + \frac{1}{2}\sum_{n,m}\frac{\partial^2 W^\dagger}{\partial\zeta_n^\dagger\,\partial\zeta_m^\dagger}\bar{\psi}_n P_R\psi_m \tag{3.16}$$

where ζ refers to the superfields Φ, X, Y and $P_L = 1 - P_R = (1+\gamma_5)/2$. For the superpotential given in Eq. (3.14), the Yukawa interactions are given as

$$-\mathcal{L}_Y = g\phi\bar{\psi}_\chi P_L\psi_\chi + 2g\chi\bar{\psi}_\phi P_L\psi_\chi + h\chi\bar{\psi}_\sigma P_L\psi_\sigma + 2h\sigma\bar{\psi}_\chi P_L\psi_\sigma + h.c. \tag{3.17}$$

On accounting for these interactions of the inflaton with intermediate scalar boson χ and fermion ψ_χ, the dissipation coefficient at leading order is obtained to be [144]

$$\begin{aligned}\Upsilon =& \frac{2}{T}g^4\phi^2\int\frac{d^4p}{(2\pi)^4}\left[\rho_{\chi_1}(\omega,\boldsymbol{p})^2 + \rho_{\chi_2}(\omega,\boldsymbol{p})^2\right] n_B(\omega)\,(1+n_B(\omega)) \\ &+ \frac{2}{T}g^2\int\frac{d^4p}{(2\pi)^4}\,tr[\rho_{\psi_\chi}(\omega,\boldsymbol{p})^2]\,n_F(\omega)\,(1-n_F(\omega)).\end{aligned} \tag{3.18}$$

Here $n_B(\omega)$, $n_F(\omega)$ are the Bose-Einstein and Fermi-Dirac distributions, respectively, and ρ_χ, ρ_{ψ_χ} are the spectral functions for the intermediate χ, ψ_χ fields.

$$\begin{aligned}\rho_\chi(\omega,\boldsymbol{p}) &= \frac{i}{p^2 + m_{\chi,R}^2 + i\mathrm{Im}\Sigma_\chi} - \frac{i}{p^2 + m_{\chi,R}^2 - i\mathrm{Im}\Sigma_\chi} \\ &= \frac{2\mathrm{Im}\Sigma_\chi}{(p^2 + m_{\chi,R}^2)^2 + (\mathrm{Im}\Sigma_\chi)^2} \\ &= \frac{4\omega_p\Gamma_\chi}{(-\omega^2+\omega_p^2)^2 + 4\,\omega_p^2\,\Gamma_\chi^2},\end{aligned} \tag{3.19}$$

where Γ_χ is the decay width of the χ field and is related to the imaginary component of the self energy Σ_χ, as shown in Appendix A, $\omega_p^2 = |\boldsymbol{p}^2| + m_{\chi,R}^2$ is the dispersion relation of the χ field, and $m_{\chi,R}^2 = m_\chi^2 + \mathrm{Re}\Sigma_\chi$ is the effective, renormalized mass of the χ field. The spectral function for fermionic field ψ_χ is given by

$$\rho_{\psi_\chi}(\omega,\boldsymbol{p}) = \frac{i}{\not{p} + m_{\psi_\chi,R} + i\mathrm{Im}\Sigma_{\psi_\chi}} - \frac{i}{\not{p} + m_{\psi_\chi,R} - i\mathrm{Im}\Sigma_{\psi_\chi}}, \tag{3.20}$$

where $m_{\psi_\chi,R} = m_{\psi_\chi} + \mathrm{Re}\Sigma_{\psi_\chi}$ is the effective, renormalized mass, and Σ_{ψ_χ} is the self energy of the ψ_χ field.

Thus, to calculate the dissipation coefficient, we need to compute the masses of χ, ψ_χ fields and their decay width at finite temperature. The decay width of the χ, ψ_χ fields has contributions from direct, inverse as well as thermal scatterings (Landau damping). The response timescale of the system is associated with the decay width as $\tau \to 1/\Gamma$. For explicit calculations and expressions of the field self energy and decay widths, see Appendix B of Ref. [144].

In certain approximations, the dissipation coefficient given in Eq. (3.18) reduces to some simplified expression, which we analyze in our study. In one regime, the poles of the spectral function dominate the integral and is called the pole approximation. In the other regime, the integration is limited to low-momentum and it is referred to as the low-momentum approximation.

- **Low temperature limit**

  In this regime, the temperature of the thermal bath is much less than the masses of the intermediate catalyst fields, χ and ψ_χ, i.e. $T \ll m_{\chi,R}, m_{\psi_\chi,R}$, but is higher compared to the radiation fields, $T \gg m_{\sigma,R}, m_{\psi_\sigma,R}$. The thermal corrections to the effective masses of the χ, ψ_χ fields can be neglected in this regime, i.e. $m^2_{\chi,R} \simeq m^2_\chi = 2g^2\varphi^2$ and $m^2_{\psi_\chi,R} \simeq m^2_{\psi_\chi} = 2g^2\varphi^2$. For large values of m_χ/T, the dominant contributions to the dissipation coefficient given in Eq. (3.18) come from virtual χ fields with low energy and momentum, ω, $|\boldsymbol{p}| \sim T \ll m_\chi$ which leads to the low-momentum approximation. Then, $(\omega^2 - \omega_p^2)^2 \approx m_\chi^4$, and the spectral function for the scalar boson in Eq. (3.19) becomes

$$\rho_\chi \simeq \frac{4}{m_\chi^3}\Gamma_\chi, \tag{3.21}$$

  which gives a leading order contribution to the dissipation coefficient, given in Eq. (3.18), $\propto T^3/m_\chi^2$ [142, 144, 145]. The fermionic contribution is calculated to be subleading in T in the low temperature limit ($\propto T^5/m^4_{\psi_\chi}$) [142, 144].

  A detailed analysis including thermal corrections to the χ mass and finite decay width of χ field in the spectral function gives [145]

$$\Upsilon = C_\phi \frac{T^3}{\phi^2}, \tag{3.22}$$

  where

$$C_\phi = \frac{h^2}{16\pi} N_Y N_X.$$

  C_ϕ depends on the multiplicities of X and Y superfields and coupling between them. The inflaton couples to N_X types of χ fields and each of them decay into N_Y number of σ, ψ_σ. For this analysis to hold, $h\sqrt{N_Y} \leq 1$.

For $h\sqrt{N_Y} \ll 1$, when the deacy width Γ_χ is sufficiently small, the real on-shell χ fields with $m_\chi \geq T$ can also contribute significantly to the dissipation coefficient in the pole approximation (see Ref. [145] for detailed analysis).

- **High temperature limit**

  In this limit, the intermediate catalyst fields are lighter, $m_{\chi,R}, m_{\psi_\chi,R} \ll T$. The main contribution to the dissipation coefficient comes from the pole in the spectral function at $\omega = \omega_p$ and a resonant production of on-shell χ particles take place. In the pole approximation, the bosonic spectral function becomes

$$\rho_\chi^2 \to \frac{\pi}{2\omega_p^2 \Gamma_\chi} \delta(\omega - \omega_p).$$

  Substituting this in Eq. (3.18) for the scalar field, the dissipation coefficient gets a contribution which is linearly dependent on the temperature of the thermal bath $\Upsilon \approx 0.691\, \frac{g^2}{h^2} T$ [142]. On accounting all the fermionic and bosonic contributions in Eq. (3.18), the total dissipation coefficient is obtained to be [142]

$$\Upsilon \ = \ C_T T, \qquad\qquad C_T \approx 0.97\, \frac{g^2}{h^2}. \tag{3.23}$$

  By knowing the value of C_T, we can calculate the order of ratio of couplings g/h, which is useful in model building.

A general expression for the dissipation coefficient dependent on the inflaton field value ϕ, temperature of the thermal bath T, and the mass of the fields coupled to the inflaton m_X, is given in Ref. [143, 150] as

$$\Upsilon(\phi, T) = C T^c \phi^{2a} / m_X^{2b}, \tag{3.24}$$

where it is required that $c + 2a - 2b = 1$.

3.3.4 Primordial curvature power spectrum

In warm inflation description, there is a temperature in the Universe throughout the inflationary phase. Therefore, the fluctuations in the inflaton field are also sourced by the thermal noise, unlike in the cold inflation where the inflaton has only quantum fluctuations. By the fluctuation-dissipation theorem, the two-point correlation of the thermal fluctuations is related to the dissipation coefficient present in the equation of motion of the inflaton Eq. (3.1) due to its interactions with the other fields.

The total primordial curvature power spectrum for warm inflation by including both quantum and thermal contributions to the inflaton power spectrum is calculated in Refs. [148–150, 221] and developed into the recent expression as in Refs. [156, 190, 222] given as

$$\Delta^2_{\mathcal{R}}(k) = \left(\frac{H_k^2}{2\pi\dot{\phi}_k}\right)^2 \left[1 + 2n_k + \left(\frac{T_k}{H_k}\right)\frac{2\sqrt{3}\pi Q_k}{\sqrt{3+4\pi Q_k}}\right] G(Q_k). \tag{3.25}$$

Here is the description of each term present in this equation:

- The prefactor $\left(\frac{H_k^2}{2\pi\dot{\phi}_k}\right)^2$ is the primordial curvature power spectrum in the cold inflation. It shows that in the limit $Q \to 0$ and $T \to 0$, we recover the standard cold inflation from warm inflation.

- Due to the presence of the radiation bath in warm inflation, the inflaton can also be excited from its vacuum state to some Bose-Einstein distribution, given as

$$n_k = \frac{1}{\exp(\frac{k/a_k}{T_k}) - 1}\,, \tag{3.26}$$

  which gives

$$1 + 2n_k = \coth\frac{H_k}{2T_k}. \tag{3.27}$$

  The system of inflaton particles and radiation fields is assumed to thermalize with a same temperature, and the scattering rates are shown in Appendix of Ref. [145]. The $\coth(H_k/2T_k)$ factor emerges from the quantum contributions to the inflaton fluctuations [150].

- In addition, due to the thermal noise contributions to the inflaton fluctuations, the primordial power spectrum has terms dependent on the dissipation coefficient and the temperature of the thermal bath, as given by the third term in the square bracket.

- In the strong dissipation limit $Q \gg 1$, the two-point correlation of inflaton fluctuations $\langle|\delta\phi_k|^2\rangle \propto (\Upsilon H)^{1/2} T$ [148].

- In the weak dissipation limit, $Q \ll 1$, the two-point correlation is given by $\langle|\delta\phi_k|^2\rangle \propto HT$, which was proposed in Ref. [117].

- The perturbations in the radiation can also couple to the inflaton perturbations and lead to a growth in the primordial power spectrum [149]. This growth factor $G(Q_k)$ depends on the form of dissipation coefficient and is obtained numerically. As given in Refs. [156, 190]

$$\text{For } \Upsilon \propto T, \quad G(Q_k)_{linear} = 1 + 0.0185\, Q_k^{2.315} + 0.335\, Q_k^{1.364}.$$

$$\text{For } \Upsilon \propto T^3, \quad G(Q_k)_{cubic} = 1 + 4.981\, Q_k^{1.946} + 0.127\, Q_k^{4.330}.$$

- In the weak dissipation regime (small Q), the growth factor does not enhance the power spectrum significantly. But in the strong dissipation regime (large Q), the power spectrum is considerably enhanced due to the growth factor.

- In the strong dissipation regime, the shear effects in radiation also become important which cause damping of the power spectrum [221], and therefore the overall growth in the power spectrum is reduced. In the expression for the primordial power spectrum given above, we do not account for any shear effects.

3.3.5 Primordial tensor power spectrum

Furthermore, the tensor fluctuations of the metric during warm inflation give rise to a primordial tensor power spectrum [222] similar to cold inflation

$$\Delta_t^2(k) = \frac{16}{\pi}\left(\frac{H_k}{M_{Pl}}\right)^2, \tag{3.28}$$

and the ratio of the tensor to the scalar power spectrum, given by the tensor-to-scalar ratio,

$$r = \frac{\Delta_t^2(k_P)}{\Delta_{\mathcal{R}}^2(k_P)}. \tag{3.29}$$

Monomial potentials of cold inflation predict a large value of the tensor-to-scalar ratio, greater than the upper limit on r from CMB observations. Hence, the non-detection of the primordial gravitational waves rule out the monomial potentials of cold inflation. But for our warm inflation models, we find that this ratio gets reduced to values within the allowed upper bound on r from *Planck* 2015 observations, and hence these warm inflation models are viable.

3.4 Summary

Warm inflation is a well-motivated and general description of inflation, in which the dissipation and non-equilibrium effects during inflation are considered. The inflaton couplings to the other fields are considered in the inflation phase, unlike in cold inflation where they are overlooked. Due to inflaton dissipation, there is particle production simultaneously with the expansion phase, and hence there is a non-zero temperature in the Universe.

The dynamics of the inflaton is modified with an additional friction term due to its coupling with the other fields. The microphysics of dissipation and the channel of decay govern the form of the dissipation coefficient in the dissipative term. It is quantified in terms of a dissipation parameter, Q, which can play a dominant (for strong dissipation $Q \gg 1$) or a subdominant role (for weak dissipation $Q < 1$) during warm inflation. From the kinematic equations of warm inflation, we infer that as the inflaton field evolves, the magnitude of the dissipation parameter Q increases. Therefore, even if the dissipation is weak initially, it can become strong by the end of inflation, and cause a growth in the primordial power spectrum.

The primordial curvature power spectrum during warm inflation is dominated by the thermal fluctuations and has distinct signatures on the CMB, compared to cold inflation. The tensor-to-scalar ratio for the warm inflation models is lowered, and as a result, some potentials of inflation, which were ruled out in cold inflation studies, become viable models to describe inflation.

Chapter 4

Warm inflation models with $\lambda\phi^4$ potential

Given the importance of warm inflation, now I present my study on the warm inflation models carried out in this thesis. Firstly, I calculate the primordial power spectrum for the large scale fluctuations generated during inflation in these warm inflation models. Then using the MCMC technique, I estimate the parameters for these models, for which the theoretical predictions of the cosmological observables are consistent with the CMB measurements.

4.1 Models of warm inflation studied

The monomial potentials ($V(\phi) \propto \phi^p$) of warm inflation are chosen in this study, as they are the simplest, one parameter models. Being large field models, they predict a large value of the tensor-to-scalar ratio, which can be used to test these models. The CMB B-mode polarization detection, if possible, in the future experiments, would be a smoking gun test for the various inflationary models.

Here we have considered two models of warm inflation with the $\lambda\phi^4$ potential. As shown in Fig. 4.1, the WMAP observations of CMB temperature anisotropies have ruled out the $\lambda\phi^4$ potential of cold inflation, as its prediction for the tensor-to-scalar ratio is larger than that allowed from the observations. However, it is indicated in some warm inflation studies [154–156, 193, 198] that for certain parameter values of

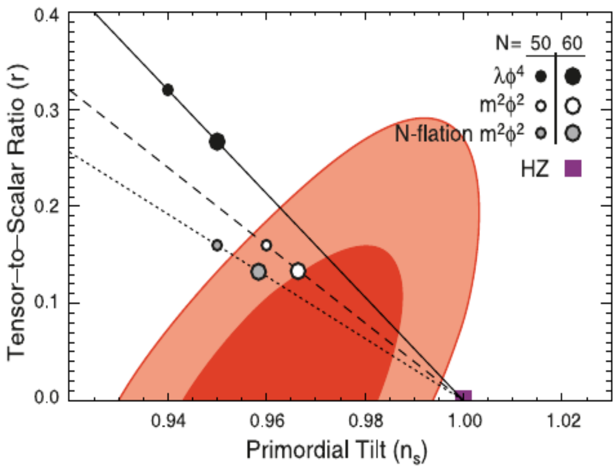

Figure 4.1: The allowed values of n_s and r from the WMAP Seven-year observations are shown here [8].

the monomial potentials, the tensor-to-scalar ratio may be lowered, and hence these potentials may also be consistent with the CMB. Therefore, a detailed analysis for the parameter space of the warm inflation models with monomial potentials is essential to test their viability.

The warm inflation description is motivated from its completeness and its origin from the fundamental principles, as was discussed in detail in Chapter 3. In this description, the equation of motion of the inflaton is modified with an additional friction term, arising from its interactions with the other fields. The inflaton dissipates its energy into radiation as it evolves during inflation, which is quantified by a parameter called the dissipation parameter. Thus, apart from the inflaton self-coupling, there is an extra model parameter in warm inflation, namely the dissipation parameter, and our goal is to compute the range of values it can have to consistently explain the observations.

The observational signatures of warm inflation on the CMB anisotropies differ from cold inflation. As the Universe during warm inflation has a temperature, the fluctuations generated in warm inflation are dominantly thermal in origin, which thus leads to a significant modification of the primordial curvature power spectrum. This may result in the lowering of the tensor-to-scalar ratio predictions for some warm inflation models. Therefore, it is important to determine how much dissipation may be allowed in any warm inflation model, in order that it satisfies the CMB measurements. The following models of warm inflation with the two forms of dissipation coefficient, as explained in the previous Chapter, are considered here:

- $V(\phi) = \lambda\phi^4$ with the dissipation coefficient $\Upsilon = C_\phi T^3/\phi^2$.
- $V(\phi) = \lambda\phi^4$ with the dissipation coefficient $\Upsilon = C_T T$.

We study both the cases, when the dissipation is weak ($Q \ll 1$), and when it is strong ($Q \gg 1$), and find the correlations in the model parameters for both the regimes.

4.2 Parameterization of the primordial power spectrum

Firstly we parameterize the primordial power spectrum, as given in Chapter 3 for all the models. By doing so, we express the primordial power spectrum in terms of only a few model parameters. As can be seen, the primordial power spectrum has many terms,

$$\Delta^2_{\mathcal{R}}(k) = \left(\frac{H_k^2}{2\pi\dot{\phi}_k}\right)^2 \left[1 + 2n_k + \left(\frac{T_k}{H_k}\right)\frac{2\sqrt{3}\pi Q_k}{\sqrt{3+4\pi Q_k}}\right] G(Q_k). \tag{4.1}$$

We expand on each term for our models here.

4.2.1 When the dissipation coefficient $\Upsilon = C_\phi T^3/\phi^2$

In this model, the dissipation coefficient has a cubic dependence on the temperature of the radiation bath.

- The energy density during inflation is largely the potential of the inflaton field. Therefore we can write the Einstein equation for this potential from Eq. (1.12) (for a flat Universe $k = 0$) as

$$H^2 = \frac{8\pi}{3}\frac{\lambda\phi^4}{M_{Pl}^2}. \tag{4.2}$$

For the slow rolling inflaton field, the evolution equation given in Eq. (3.10) can be written as,

$$\dot{\phi} \approx \frac{-V'(\phi)}{3H(1+Q)} = -\frac{4}{3}\sqrt{\frac{3}{8\pi}}\sqrt{\lambda}\frac{\phi M_{Pl}}{(1+Q)}. \tag{4.3}$$

On combining the above two equations, we obtain

$$\frac{H_k^2}{2\pi\dot{\phi}_k} = -\sqrt{\frac{8\pi}{3}}\sqrt{\lambda}\left(\frac{\phi_k}{M_{Pl}}\right)^3 (1+Q_k). \tag{4.4}$$

Thus, for this model, Eq. (4.4) is the prefactor of the primordial power spectrum in Eq. (4.1).

- Now we look for the terms in the square bracket of the primordial power spectrum. The temperature of the thermal bath of radiation in the slow-roll approximation can be obtained from Eq. (3.11) as,

$$\rho_r = AT^4 = \frac{3}{4}Q\dot{\phi}^2, \tag{4.5}$$

where $A \equiv (\pi^2/30)g_*$. Thus on substituting $\dot{\phi}$ from Eq. (4.3) into this, we get

$$T_k = \left(\frac{15}{\pi^3 g_*}\frac{Q_k}{(1+Q_k)^2}\lambda\,\phi_k^2 M_{Pl}^2\right)^{\frac{1}{4}}, \tag{4.6}$$

and further using Eq. (4.2), we get

$$\frac{T_k}{H_k} = \left(\frac{15}{\pi^3 g_*}\right)^{\frac{1}{4}}\sqrt{\frac{3}{8\pi}}\lambda^{-\frac{1}{4}}\frac{Q_k^{\frac{1}{4}}}{(1+Q_k)^{\frac{1}{2}}}\left(\frac{\phi_k}{M_{Pl}}\right)^{-3/2}. \tag{4.7}$$

Throughout warm inflation, this factor T_k/H_k has to be greater than 1 for all the fluctuation modes.

- As mentioned before, the non-zero inflaton particle number, n_k, is represented by a Bose-Einstein distribution, which gives $1 + 2n_k = \coth(H_k/2T_k)$. Using Eq. (4.7), we calculate this factor.

- We now evaluate the inflaton field value, ϕ_k. In this model, the dissipation coefficient is taken as $\Upsilon = C_\phi\frac{T^3}{\phi^2}$. Thus, from this, we can write the inflaton field value

$$\phi = \left(\frac{C_\phi T^3}{3QH}\right)^{1/2}.$$

Then, on substituting Eqs. (4.6) and (4.2) into this, we get

$$\frac{\phi_k}{M_{\rm Pl}} = \sqrt{\frac{1}{8\pi}}\left(\frac{64C_\phi^4\lambda}{9A^3}\frac{1}{Q_k(1+Q_k)^6}\right)^{\frac{1}{10}}. \tag{4.8}$$

This is then substituted in the prefactor, and the T_k/H_k, to express the primordial power spectrum in terms of variables λ, Q_k and C_ϕ.

We also parameterize the tensor power spectrum by substituting Eq. (4.2) in the expression for tensor power spectrum,

$$\Delta_t^2(k) = \frac{16}{\pi}\left(\frac{H_k}{M_{Pl}}\right)^2 = \frac{128}{3}\lambda\left(\frac{\phi_k}{M_{Pl}}\right)^4. \tag{4.9}$$

By substituting Eq. (4.8) into this, we obtain $\Delta_t^2(k)$ in terms of λ, Q_k and C_ϕ.

4.2.2 When the dissipation coefficient $\Upsilon = C_T T$

In this model, the dissipation coefficient is taken to be linearly dependent on the temperature, but the inflaton potential is the same as the previous model. The equations (4.4), (4.7), and (4.9) hold for this model as they are not explicitly dependent on the form of the dissipation coefficient. However, as the field value ϕ_k depends on the Υ, we now evaluate it. In this model, we have taken the dissipation coefficient $\Upsilon = C_T T$, which gives $\dfrac{T}{H} = \dfrac{3Q}{C_T}$. On equating this with Eq. (4.7), we obtain

$$\left(\frac{\phi_k}{M_{Pl}}\right) = \sqrt{\frac{1}{8\pi}}\left(\frac{4C_T^4}{9\lambda A}\frac{1}{Q_k^3(1+Q_k)^2}\right)^{\frac{1}{6}}. \tag{4.10}$$

This is then used to express the primordial scalar and tensor power spectrum for this model in terms of the variables λ, Q_k and C_T.

4.3 Dissipation parameter evolution during inflation Q_k

The dissipation parameter $Q \equiv \dfrac{\Upsilon(\phi,T)}{3H}$ changes during inflation, as the inflaton rolls down in the field space during inflation. In this section, we calculate the evolution of the dissipation parameter during inflation. In our notation, $N = \ln(a_e/a)$, is the number of efolds counted from the end of inflation ($N = 0$). As inflation proceeds, N decreases, and at the pivot scale, $N = N_P$. We define a variable $x = \ln(k/k_P)$, where k_P corresponds to the pivot scale, and write

$$\frac{dQ}{dx} = \left(\frac{dQ}{dN}\right)\left(\frac{dN_k}{dx}\right). \tag{4.11}$$

We first calculate both the terms on the r.h.s. of this equation in the subsections below. After that, we integrate Eq. (4.11) to obtain Q_k, and further $\Delta_{\mathcal{R}}^2(k)$.

4.3.1 Calculation of dQ/dN

In Eqs. (4.8) and (4.10), we separate the functions of Q on the left hand side, and then take the derivative with respect to N. We can then write $\frac{d\phi}{dN} = \left(\frac{d\phi}{dt}\right)\left(\frac{dt}{dN}\right) = -\frac{\dot\phi}{H}$ and use the expressions for $\dot\phi$ and H for both the models calculated in the previous section. The expressions for dQ/dN thus obtained are the following. For cubic dissipation, we get

$$\frac{dQ}{dN} = -40\left(\frac{9A^3}{64C_\phi^4\lambda}\right)^{\frac{1}{5}}\frac{Q^{6/5}(1+Q)^{6/5}}{(1+7Q)}, \tag{4.12}$$

and for linear dissipation, we have

$$\frac{dQ}{dN} = -24\left(\frac{9A\lambda}{4C_T^4}\right)^{\frac{1}{3}}\frac{Q^2(1+Q)^{2/3}}{(3+5Q)}. \tag{4.13}$$

The negative sign of dQ/dN implies that the dissipation parameter Q increases as the inflation proceeds (N decreases) for the models considered in this study.

In Fig. 4.2, we plot the solution of Eq. (4.12) for the cubic dissipation model as a function of the number of efolds of inflation. We find that though initially the dissipation is weak (the mean value obtained for this model as $Q_P = 10^{-2.4}$) at the pivot scale ($N_P = 50$), it can become very large by the end of inflation. As Q crosses 1 during inflation the model transits from weak dissipation to strong dissipation.

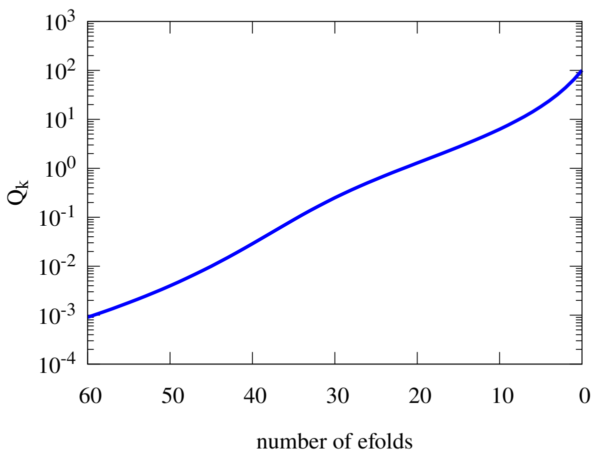

Figure 4.2: Plot showing how the dissipation parameter changes as a function of the number of efolds of inflation. For this plot, we have fixed $N_P = 50$ and considered the mean values for this model as $Q_P = 10^{-2.4}$, $\lambda = 1.68 \times 10^{-14}$, and $C_\phi = 8.8 \times 10^6$.

Dissipation parameter at the end of warm inflation

For our models, the end of warm inflation is governed by the violation of the slow-roll conditions, given in Eq. (3.9). As η_ϕ is the largest of all the slow-roll parameters, hence it is used to mark the end of warm inflation, as

$$\eta_e = \frac{12}{8\pi}\frac{M_{Pl}^2}{\phi_e^2} = 1 + Q_e. \tag{4.14}$$

For the cubic dissipation coefficient, we substitute ϕ_e from Eq. (4.8) and obtain the equation for Q_e as

$$Q_e^2 + Q_e = \left(\frac{64C_\phi^4\lambda}{9C_R^3}\right)\frac{1}{12^5}\,, \tag{4.15}$$

and for a linear dissipation coefficient, we substitute Eq. (4.10), and obtain

$$Q_e^3(1+Q_e)^{-1} = \frac{4C_T^4}{9A\lambda}\left(\frac{1}{12}\right)^3. \tag{4.16}$$

The solution to these equations are given in the Appendix B. We obtain Q_e as function of λ, C_ϕ (for cubic dissipation) or λ, C_T (for linear dissipation).

4.3.2 Calculation of dN/dx

The number of efolds when any perturbation scale k crosses the horizon ($k = aH$) is defined as,

$$N_k = \ln\frac{a_e}{a_k} = \ln\frac{a_e}{a_P} + \ln\frac{a_P}{a_k},$$

where a_e, a_P, and a_k are the scale factor at the end of inflation, and at the epoch when the pivot scale and the k^{th} scale cross the horizon, respectively. This can be written as

$$N_k = N_P + \ln\frac{k_P H_k}{k H_P} = N_P - \ln\frac{k}{k_P} + \ln\frac{H_k}{H_P}. \tag{4.17}$$

We define a quantity $x \equiv \ln(k/k_P)$, and then differentiate the above equation w.r.t x, which gives

$$\frac{dN_k}{dx} = -1 + \frac{\dot{H}_k}{H_k}\frac{dt}{dN}\frac{dN_k}{dx} = -1 - \frac{\dot{H}_k}{H_k^2}\frac{dN_k}{dx}. \tag{4.18}$$

Using the definition of slow roll parameter $\epsilon_H = -\dfrac{\dot{H}}{H^2}$, we thus obtain

$$\frac{dN_k}{dx} = -\frac{1}{1-\epsilon_H}\,. \tag{4.19}$$

Resulting expressions for dQ/dx

As a result of the calculations in the above two subsections, we finally obtain dQ/dx by substituting Eqs. (4.12) and (4.19) in Eq. (4.11) for the cubic dissipation as

$$\frac{dQ}{dx} = \frac{40}{1-\epsilon_H}\left(\frac{9A^3}{64C_\phi^4\lambda}\right)^{\frac{1}{5}} \frac{Q^{6/5}(1+Q)^{6/5}}{(1+7Q)}, \tag{4.20}$$

and from Eqs. (4.13) and (4.19) for the linear dissipation model as

$$\frac{dQ}{dx} = \frac{24}{1-\epsilon_H}\left(\frac{9A\lambda}{4C_T^4}\right)^{\frac{1}{3}} \frac{Q^{2}(1+Q)^{2/3}}{(3+5Q)}. \tag{4.21}$$

These expressions are then integrated from Q_P (at $x=0$) to Q_k (at any x) to obtain Q_k. On substituting Q_k in the parameterized power spectrum obtained in Section 4.2, we get $\Delta^2_{\mathcal{R}}(k)$.

4.4 Analysis

Here we plot and study the evolution of various quantities as a function of the number of efolds of inflation, using the calculations in the previous sections. We choose the cubic dissipation model for making the plots, however, the analysis done in this Section also applies to the other models considered in this thesis.

4.4.1 Evolution of the inflaton and the radiation

In Fig. 4.3 (*a*), we first plot the inflaton field evolution from Eq. (4.8) using the corresponding Q_k value calculated in Eq. (4.12). The inflaton energy density during inflation, $\rho_\phi \sim V(\phi) = \lambda\phi^4$, is also calculated and plotted in Fig. 4.3 (*b*). To plot these, we consider that at the pivot scale, $k_P = 0.05$ Mpc^{-1}, $N_P = 50$, and $Q_P = 10^{-2.4}$ (the mean value obtained for this model). It will be shown in Section 4.5, that for a fixed N_P and Q_P, the variables λ and C_ϕ (or C_T) are related, and the primordial power spectrum is a function of only λ and Q_P. Thus, if we fix the normalization of the power spectrum as $\Delta^2_{\mathcal{R}}(k_P) = A_s = 2.2\times10^{-9}$, we obtain λ and the corresponding C_ϕ. For $N_P = 50$, $Q_P = 10^{-2.4}$, we obtain $\lambda = 1.68\times10^{-14}$, and the corresponding $C_\phi = 8.8\times10^6$.

The temperature of the thermal bath of radiation, as calculated in Eq. (4.6) is plotted in Fig. 4.3 (c) using the Eqs. (4.8) and (4.12). Also, the radiation energy density, $\rho_r = (\pi^2/30)\, g_* T^4$ is calculated and plotted in Fig. 4.3 (b) for $Q_P = 10^{-2.4}$. We can see that ρ_ϕ is greater than ρ_r throughout the inflationary phase for this model of warm inflation. Therefore, the violation of slow roll conditions mark the end of warm inflation for our models. Also, a separate reheating phase will be needed at the end of inflation, so that the Universe becomes radiation dominated.

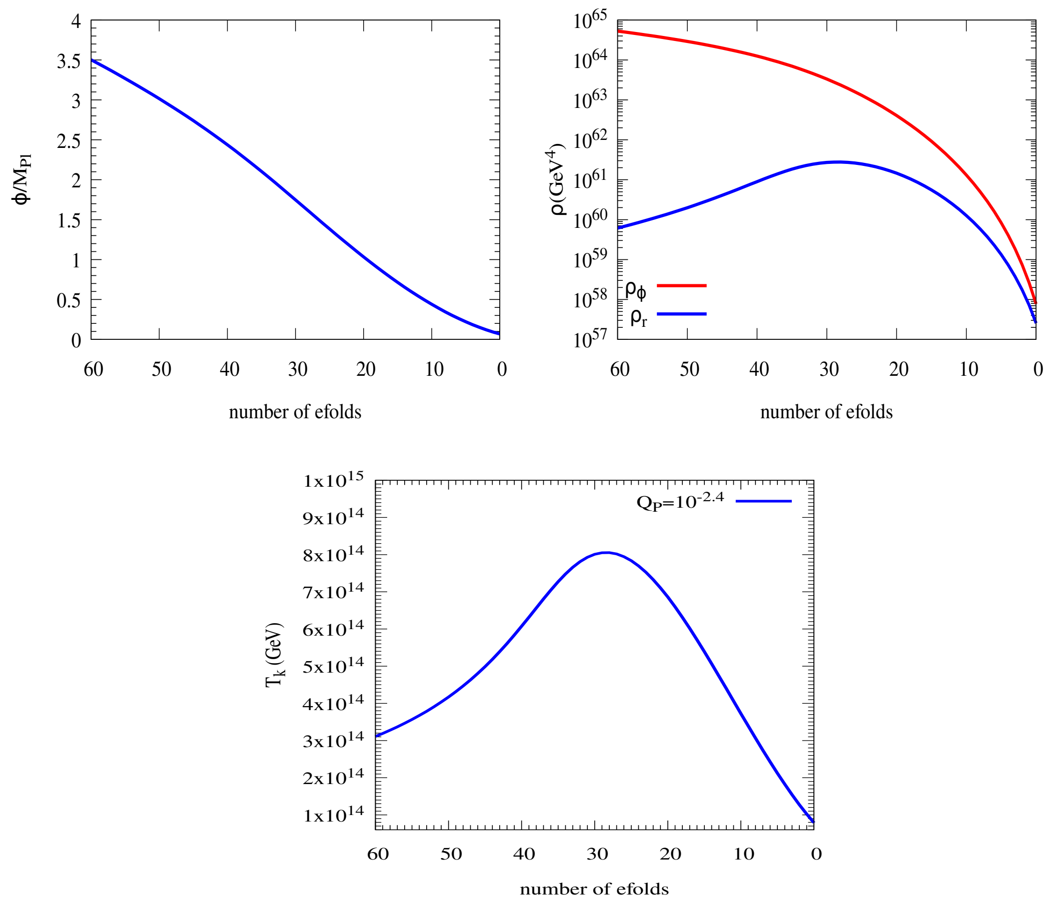

Figure 4.3: *(a)* The evolution of the inflaton field, *(b)* the energy density in inflaton and radiation, and *(c)* the temperature of the thermal bath of radiation, as a function of the number of efoldings. Here we have fixed $N_P = 50$ and chosen the mean values of parameters for this model as $Q_P = 10^{-2.4}$, $\lambda = 1.68 \times 10^{-14}$, and $C_\phi = 8.8 \times 10^6$.

4.4.2 Thermal equilibrium and a lower bound on Q_P

In the warm inflation description, we assume that the system is not far away from equilibrium and the radiation fields thermalize quickly over the time scale of Hubble expansion. The condition for warm inflation is that the temperature of the thermal bath of the radiation is greater than the Hubble rate of expansion. Here we ascertain the minimum value of the dissipation parameter for which the condition for warm inflation is satisfied.

We calculate T_k/H_k given in Eq. (4.7) as a function of the number of e-foldings using the Eqs. (4.8) and (4.12) and plot it for different values of Q_P in Fig. 4.4. We list the values of λ, and C_ϕ for different values of Q_P used for plotting in Table 4.1. For these plots, at the pivot scale, N_P is fixed to 50.

Q_P	λ	C_ϕ
10^{-1}	1.18×10^{-14}	1.45×10^{7}
$10^{-2.4}$	1.68×10^{-14}	8.82×10^{6}
$10^{-5.0}$	3.49×10^{-14}	2.73×10^{6}

Table 4.1: The values of λ, C_ϕ for various values of Q_P, used for plotting Fig. 4.4.

We find that $T_k > H_k$ holds for all $Q_P > 10^{-5.0}$. A similar behaviour is seen for all the other models with the condition being satisfied for $Q_P > 10^{-5.0}$. It is also seen that T_k/H_k increases as inflation proceeds till the end. Therefore, if $Q_P > 10^{-5.0}$ initially, it will ensure that throughout the inflation, the condition of warm inflation is satisfied.

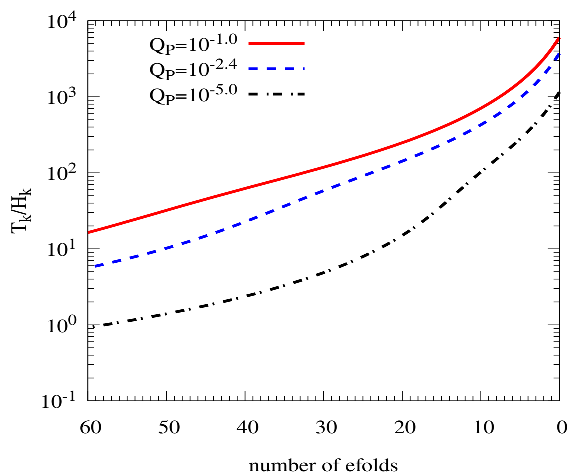

Figure 4.4: Plots showing the variation of T_k/H_k as a function of the number of efolds for different values of Q_P.

4.4.3 Primordial power spectrum

Now we plot the primordial power spectrum as a function of $x = \ln k/k_P$, by using the calculations carried out in Section 4.2.1, and the evolution of dissipation parameter from Eq. (4.20). The pivot scale k_P is chosen at 0.05 Mpc^{-1}, and the number of efold corresponding to it, N_P is fixed to 50. In Fig. 4.5, we plot $\log_{10} \Delta^2_{\mathcal{R}}(k)$ versus x for different values of Q_P, using the parameter values listed in Table 4.1. The range of x is chosen for the large scale CMB modes, corresponding to $k = 10^{-4}$ Mpc^{-1} ($x = -7$) to 1 Mpc^{-1} ($x = +3$). In the figure, we also plot the standard power law power spectrum, $\Delta^2_{\mathcal{R}} = A_s(k/k_P)^{n_s-1}$ with $n_s = 0.9645$ [223, 224] (Black line). For every Q_P, different values of λ are chosen to give the correct normalisation of the power spectrum, as given in Table 4.1.

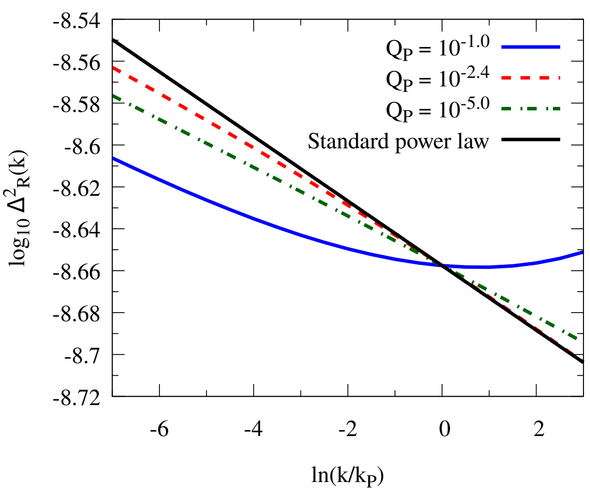

Figure 4.5: Plot of $\log_{10}\Delta^2_{\mathcal{R}}(k)$ vs $\ln(k/kp)$ for different values of Q_P for the model with cubic dissipation. Here $N_P = 50$ and A_s is fixed to obtain the corresponding λ for each Q_P. The standard power law with $n_s = 0.9645$ is also plotted as a solid (black) line.

It can be seen that for different value of the dissipation parameter, the amplitude of the power spectrum for the CMB modes varies, however the normalization is fixed at the pivot scale ($\ln(k/k_P) = 0$). The power spectrum for the mean value of Q_P for this model, resembles the standard power law spectrum for cold inflation.

4.4.4 Scalar Index

The slope of the primordial power spectrum at the pivot scale is determined by the spectral index, n_s. The scalar spectral index is defined as

$$n_s - 1 = \left.\frac{d\ln\Delta^2_{\mathcal{R}}(k)}{d\ln\left(\frac{k}{k_P}\right)}\right|_{k=k_P} = \left.\left(\frac{d\ln\Delta^2_{\mathcal{R}}}{dQ}\right)\left(\frac{dQ}{dx}\right)\right|_{k=k_P}.$$

We calculate the spectral index for our models using the calculations in the Section 4.2 and Eqs. (4.20), (4.21). The resulting expressions are given in the Appendix D.

It can be seen from the Appendix D, that the spectral index depends on the value of the dissipation parameter. Therefore, the observational bounds on n_s govern the range of dissipation values for any model of warm inflation. Depending on the slope of the primordial power spectrum, the spectral index can be red-tilted ($n_s - 1 < 0$) or blue-tilted ($n_s - 1 > 0$). We can see that for the Q_P values used in plotting Fig. 4.5, the spectrum is red-tilted for the CMB modes ($n_s < 1$).

4.5 Model Parameters

Till now, we have parameterized the primordial power spectrum in terms of λ, Q_k and C_T (or C_ϕ), and calculated Q_k. Now we reduce the number of independent variables by fixing the number of efolds corresponding to the pivot scale N_P. For this, we integrate dN/dQ by using the expressions for dQ/dN obtained in Section 4.3.1, from Q_P (at pivot where $N = N_P$) to Q_e (at the end of inflation where $N = 0$) for all the models (using the solution to Q_e from the Appendix B). The integration gives

$$N_P = F(Q_e) - F(Q_P) = F(\lambda, C_\phi \,\text{or}\, \lambda, C_T) - F(Q_P)\,, \tag{4.22}$$

where $F(Q)$ is the integral function, given in Appendix C. This equation implies that for a given Q_P, if we fix N_P, then λ and C_ϕ (or C_T) will be related. Therefore, the power spectrum will be effectively a function of only two variables, the inflaton self-coupling λ and the dissipation parameter value at the pivot scale Q_P, which will be our model parameters for running CosmoMC.

4.5.1 Choice of priors for model parameters

From Section 4.4.4, we see that the expressions for the spectral index depend on the dissipation parameter, and therefore the observational bounds on n_s restrict the range of Q_P values for any model.

Using the expressions for n_s given in the Appendix D, we generate the n_s versus Q_P plot in Fig. 4.6. To generate it, we take $N_P = 60$, and fix the normalisation of the power spectrum, thus for every Q_P value obtain the corresponding λ and C_ϕ (or C_T). In the plot, we also show the allowed values for n_s for a power-law power spectrum, from the *Planck* 2015 TT, TE, EE + low P results [223–225] given as

$$n_s = \begin{cases} 0.9645 \pm 0.0049 & (\,68\%\,\text{C.L.}\,) \\ 0.9645^{+0.0098}_{-0.0096} & (\,95\%\,\text{C.L.}\,) \end{cases}$$

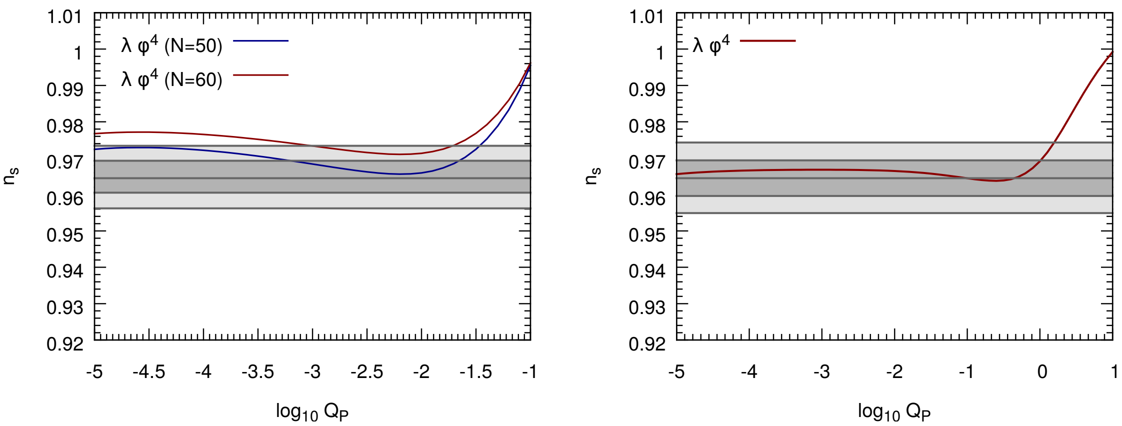

Figure 4.6: The spectral index, n_s as a function of the dissipation parameter, $\log_{10} Q_P$ are plotted for (*a*) the model with cubic dissipation coefficient on the left, and, (*b*) the model with a linear dissipation coefficient on the right. The colored band shows the allowed n_s values from *Planck* 2015 TT, TE, EE + low P results for a power law power spectrum with 68% and 95% C.L..

It can be seen from the figure that only a certain range of Q_P is consistent with the allowed n_s, as listed in the Table 5.1. Hence, we choose the prior for Q_P such that the n_s corresponding to it lies in the allowed band. In our study, we consider both the weak and strong dissipative regime for the linear dissipation coefficient. However, we see that for the cubic dissipation coefficient, none of the values of Q_P are consistent with the allowed n_s in the strong dissipative regime. Hence, we consider only the weak dissipative regime for the cubic dissipation model. Further, we estimate the priors for λ corresponding to the chosen priors for Q_P.

Model	Allowed Q_P range in weak dissipation regime	Allowed Q_P range in strong dissipation regime
cubic dissipation ($N_P = 50$)	$[10^{-5}, 0.032]$	–
cubic dissipation ($N_P = 60$)	$[6.31 \times 10^{-4}, 0.02]$	–
linear dissipation	$[10^{-5}, 1]$	$[1, 1.58]$

Table 4.2: The allowed values of Q_P from the n_s plots in Fig. 4.6. For the cubic dissipation ($\Upsilon \propto T^3$), only the weak dissipation regime is favored by the CMB *Planck* 2015 TT, TE, EE + low P observations.

4.6 CMB angular power spectrum

Now we generate the angular power spectrum for our warm inflation model and study the effects of varying the model parameters λ and Q_P on the angular power spectrum. For these plots, we consider the warm inflation model with the cubic dissipation.

4.6.1 When λ is fixed, and Q_P is variable

In Figure 4.7 we plot the TT angular power spectrum of CMB for our warm inflation model by fixing a value of λ while varying Q_P. In the same figure, we also plot the standard power law angular power spectrum, and show that for our mean values of parameters (for $N_P = 50$, $Q_P = 10^{-2.4}$ and $\lambda = 10^{-13.7746}$), the fit to the observational data points for our warm inflation model resembles the standard power law spectrum with $n_s = 0.96$. It can be seen in the plot that by increasing dissipation parameter, the angular power spectrum increases.

4.6.2 When Q_P is fixed, and λ is variable

Next we vary λ while keeping Q_P fixed to its mean value, and plot the angular power spectrum in Fig. 4.8 for our warm inflation model. We see that the angular power

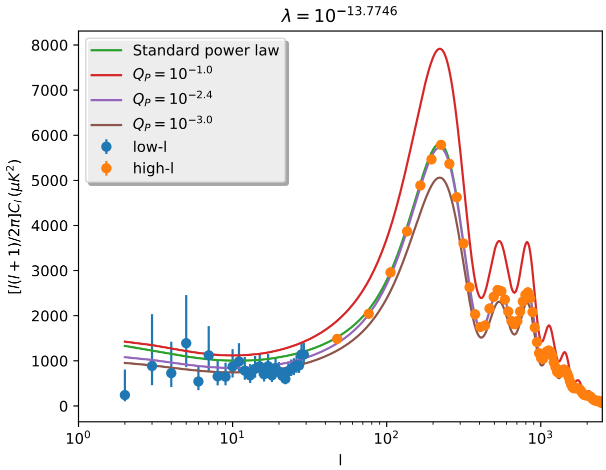

Figure 4.7: The TT angular power spectrum of the CMB for various values of Q_P, with $\lambda = 10^{-13.7746}$ and $N_P = 50$. In the plots, low ℓ refers to the range $\ell = 2 - 49$ while high ℓ refers to the range $\ell = 50 - 2500$.

spectrum is sensitive to even a slight variation in λ, and as the value of λ increases, the angular power spectrum increases.

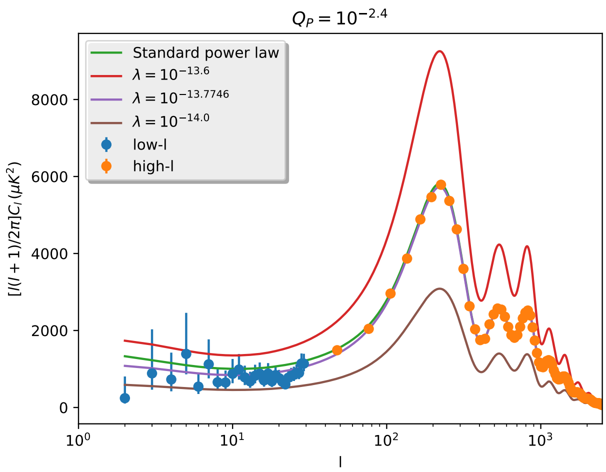

Figure 4.8: The TT angular power spectrum of the CMB for various values of λ, fixed $Q_P = 10^{-2.4}$ and $N_P = 50$.

4.6.3 Effect of the inflaton non-zero particle number distribution

In warm inflation, one considers a thermal distribution of inflaton particles excited from the zero momentum condensate state, due to the collisions with the thermal bath of radiation. This is quantified by a distribution function in the expression for the primordial power spectrum, as given in Eq. (3.26). Here we discuss the effects due to this non zero particle number distribution of the inflaton on the angular power spectrum of the CMB.

The inflaton particle distribution is taken as a Bose-Einstein distribution, which results in a *coth* term in the primordial power spectrum, as $1 + 2n_k = coth(H_k/2T_k)$. In the Fig. 4.9, we have plotted the angular power spectrum for our warm inflation model with the coth term retained ($n_k \neq 0$) and the coth term set to 1 ($n_k = 0$).

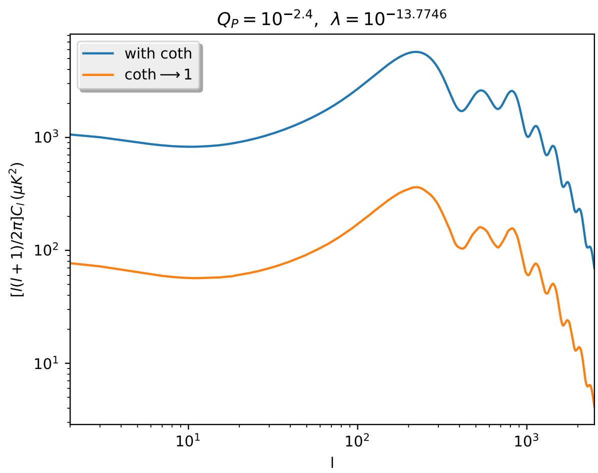

Figure 4.9: Angular power spectra for warm inflation with the coth term retained in the primordial power spectrum and with the coth term set to 1 ($n_k = 0$).

We see that the effect of the coth term is to enhance the angular power spectrum, and it is almost uniform across angular scales. It results in a lowering of the Hubble parameter so that the total primordial power is normalized at the pivot scale. In Table 4.3, we list the values for parameters λ, ϕ_P, and H_P for the three cases, when the coth term is retained in warm inflation ($n_k \neq 0$), when the coth term is set to 1 ($n_k = 0$), and also for comparison cold inflation.

We find that H_P for the warm inflation case with the coth term is the lowest. Lower H_P lowers the tensor power spectrum, given in Eq. (4.9) and hence the tensor to scalar ratio, r, thereby making the quartic potential warm inflation scenario with the coth term retained more compatible with Planck data.

	λ	ϕ_P	H_P
Warm inflation with $n_k \neq 0$	1.68×10^{-14}	$3.01\ M_{Pl}$	4.09×10^{13}GeV
Warm inflation with $n_k = 0$	3.09×10^{-13}	$3.01\ M_{Pl}$	1.76×10^{14}GeV
Cold inflation	6.14×10^{-14}	$4.03\ M_{Pl}$	1.40×10^{14}GeV

Table 4.3: The list of parameters λ, ϕ_P, and H_P for the cases when $n_k \neq 0$, $n_k = 0$ in warm inflation and for cold inflation. Here $Q_P = 10^{-2.4}$, $N_P = 50$ and A_s is fixed.

4.7 CosmoMC results

In this Section, we show the results for the Markov Chain Monte Carlo (MCMC) analysis of our models in the weak and strong dissipation regimes using CosmoMC. We run the CosmoMC chains over a six dimensional parameter space, listed in Table 4.4, with flat priors.

$\Omega_b h^2$	the baryon density
$\Omega_c h^2$	the cold dark matter density
$100\ \theta$	the observed angular size of the sound horizon at recombination
τ	the reionization optical depth
$-\log_{10}\lambda$	the inflaton self-coupling
$(\pm)\log_{10} Q_P$	the dissipation parameter ($+$ in the strong dissipation regime, $-$ in the weak dissipatve regime)

Table 4.4: The list of independent cosmological parameters over which the MCMC runs are carried out in this study.

CosmoMC configuration

We use the September 2017 version of the CAMB and the November 2016 version of CosmoMC and set the flags: compute tensor = T, CMB lensing = F, and use nonlinear lensing = F. The number of massless neutrino species is set to its value in the Standard Model, $n_\nu = 3.046$ and the Helium fraction $Y_{He} = 0.24$ in our analysis. The pivot scale is set at $k_P = 0.05\,\text{Mpc}^{-1}$, and the CosmoMC analysis is performed with the *Planck* 2015 TT, TE, EE + low P dataset.

4.7.1 Constraints on the parameters of the warm inflation model $V(\phi) = \lambda\phi^4$ with a cubic dissipation coefficient $\Upsilon = C_\phi T^3/\phi^2$

As was discussed in Section 4.5.1, for this model, none of the values of Q_P in the strong dissipative regime is allowed from the observed bounds on the spectral index. Therefore, only the weak dissipative regime of warm inflation is analysed for this model. We perform the MCMC analysis for this model for two cases, one by fixing $N_P = 50$, and two, when $N_P = 60$. The CosmoMC results for the mean and 68 % limits of the cosmological parameters are listed in Table 4.5 for the case when $N_P = 50$ and Table 4.6 for $N_P = 60$.

Parameter	Priors	68% C.L.
$\Omega_b h^2$	[0.005, 0.1]	0.02220 ± 0.00013
$\Omega_c h^2$	[0.001, 0.99]	0.1191 ± 0.0010
$100\,\theta$	[0.50, 10.0]	1.04089 ± 0.00029
τ	[0.1, 0.8]	0.065 ± 0.011
$-\log_{10}\lambda$	[13.0, 14.0]	13.783 ± 0.051
$-\log_{10} Q_P$	[1.0, 5.4]	2.4358 ± 0.5856

Table 4.5: The priors and the mean values of the parameters along with 68% C.L. for the model $V(\phi) = \lambda\phi^4$ with $\Upsilon = C_\phi T^3/\phi^2$ in the weak dissipative regime when $N_P = 50$. These values of the parameters are consistent with the *Planck* 2015 TT, TE, EE + low P dataset.

Analysis of n_s and r values

For $N_P = 50$, we obtain the mean values of $\lambda = 1.6 \times 10^{-14}$ and $Q_P = 3.7 \times 10^{-3}$. For these values, we get $n_s = 0.9660$ and $r = 0.0275$, which is within 68% C.L. of the allowed values from the Planck data. For $N_P = 60$, the mean values of $\lambda = 1.0 \times 10^{-14}$ and $Q_P = 4.4 \times 10^{-3}$. In Fig. 4.10, we plot the tensor-to-scalar ratio r vs $\log_{10} Q_P$ for fixed $N_P = 60$, and show that as the dissipation increases, the tensor-to-scalar ratio decreases. We also show the $n_s - r$ plot for different Q_P (and the corresponding λ) values in right plot of Fig. 4.10. Moving from left to right on the plot, the Q_P value

Parameter	Priors	68% C.L.
$\Omega_b h^2$	[0.005, 0.1]	0.02226 ± 0.00013
$\Omega_c h^2$	[0.001, 0.99]	0.1177 ± 0.0009
$100\ \theta$	[0.50, 10.0]	1.04105 ± 0.00029
τ	[0.1, 0.8]	0.075 ± 0.011
$-\log_{10}\lambda$	[13.5, 14.5]	13.998 ± 0.037
$-\log_{10} Q_P$	[1.0, 5.4]	2.3585 ± 0.4495

Table 4.6: The priors and the mean values of the parameters along with 68% C.L. for the model $V(\phi) = \lambda\phi^4$ with $\Upsilon = C_\phi T^3/\phi^2$ in the weak dissipative regime when $N_P = 60$. These values of the parameters are consistent with the *Planck* 2015 TT, TE, EE + low P dataset.

increases. For the mean value of $Q_P = 4.4 \times 10^{-3}$ for $N_P = 60$, we get $n_s = 0.9712$ and $r = 0.0222$, which is within 95% C.L. of the allowed values from the Planck data. Therefore, we infer that this potential of warm inflation is a viable model to describe inflation for some parameter space, given in Table 4.5 and 4.6. The value of the tensor-to-scalar ratio is within the sensitivity of next generation CMB experiments, therefore, this model of warm inflation can be tested in the near future.

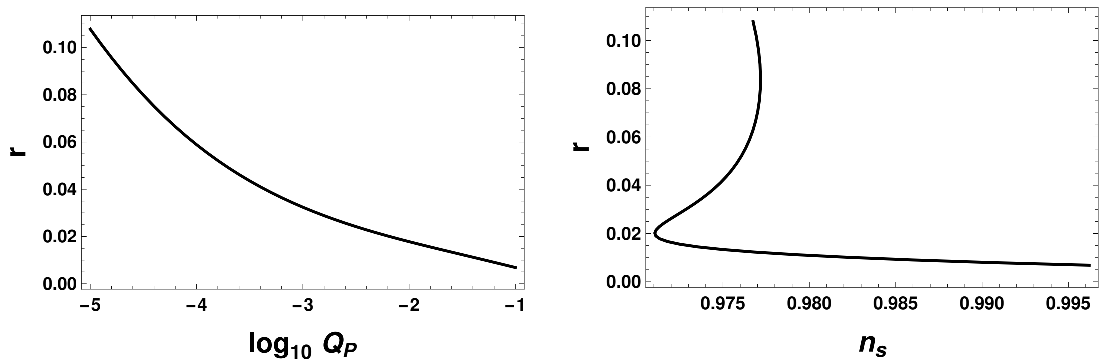

Figure 4.10: *Left:* Plot of the tensor-to-scalar ratio r vs $\log_{10} Q_P$ indicates that for larger dissipation (larger Q_P value), the r value is smaller. *Right:* Plot of $n_s - r$, where different points on the curve represent different Q_P values (and the corresponding λ). The Q_P value increases as we move from left to right on the plot, whereas as λ is inversely correlated to Q_P, it therefore decreases. Here we fix $N_P = 60$.

λ and Q_P correlation

We also plot the marginalized and the joint probability distributions of the cosmological parameters in Figures 4.11 and 4.13 when N_P is fixed to values 50 and 60, respectively. The slope of the joint probability distribution of $-\log_{10}\lambda$ and $-\log_{10}Q_P$ for this model gives $\lambda \sim Q_p^{-0.1}$.

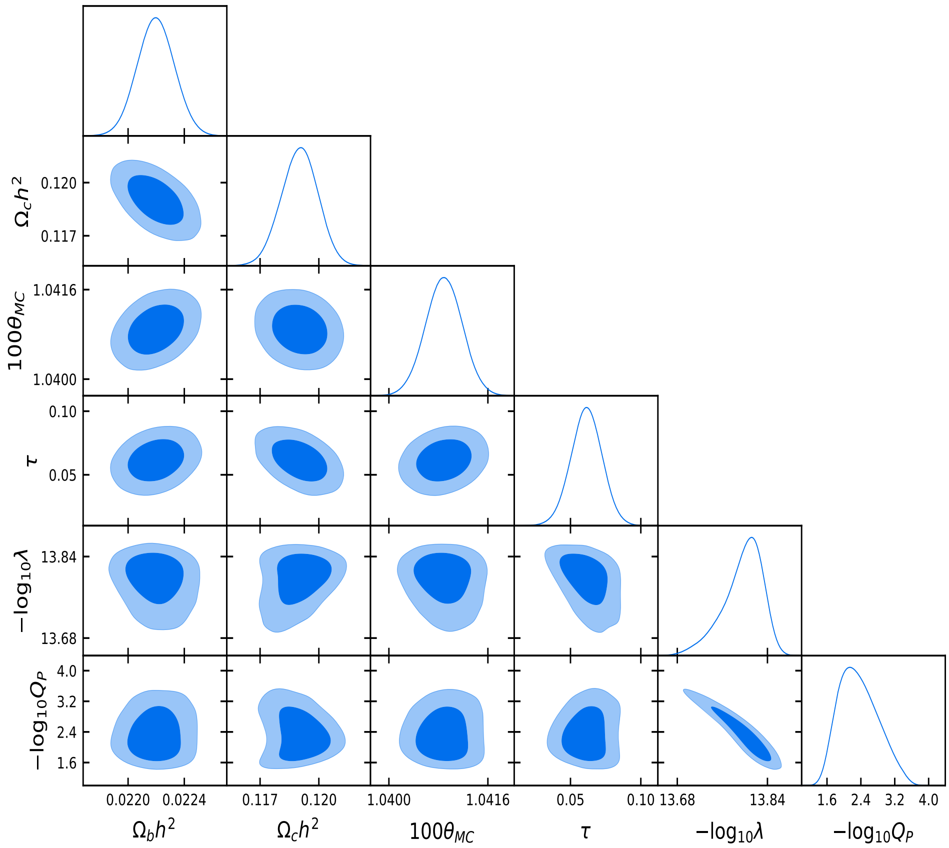

Figure 4.11: The joint probability distribution and the marginalized distributions of the cosmological parameters for the model $V(\phi) = \lambda\phi^4$ with $\Upsilon = C_\phi T^3/\phi^2$ in the weak dissipative regime for $N_P = 50$. The CosmoMC analysis is carried out with the *Planck* 2015 TT, TE, EE + low P dataset.

Analysis of C_ϕ values

In Fig. 4.12, we plot the behaviour of $\log_{10} C_\phi$ vs $\log_{10} Q_P$ for the weak dissipative regime of this model. We find that for a larger dissipation (indicated by a large Q_P value), the C_ϕ value is larger. By its formulation, C_ϕ is related to the couplings and multiplicities of the fields to which the inflaton couple. As described in Section 3.3.3, $C_\phi = \dfrac{1}{4}\alpha N_X$. We find that for the mean values of the model parameter $Q_P \sim 10^{-3}$, we have $C_\phi \sim \mathcal{O}(10^7)$. By assuming $\alpha \sim 0.1$, we find that for this model of warm inflation $N_X \sim 10^9$. Such a large multiplicity of fields is an unattractive feature of warm inflationary models. However, there are some string theory inspired mechanism [194] to generate large multiplicities of fields.

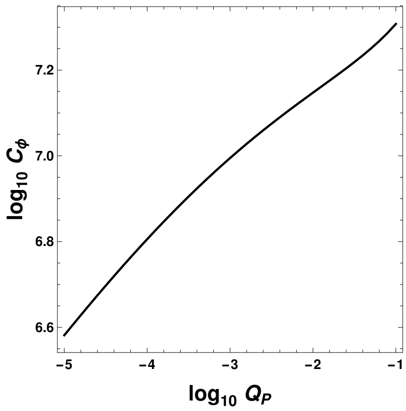

Figure 4.12: Plot of $\log_{10} C_\phi$ vs $\log_{10} Q_P$ for the weak dissipative regime shows that $C_\phi \sim \mathcal{O}(10^7)$ for this model of warm inflation. Here also $N_P = 60$.

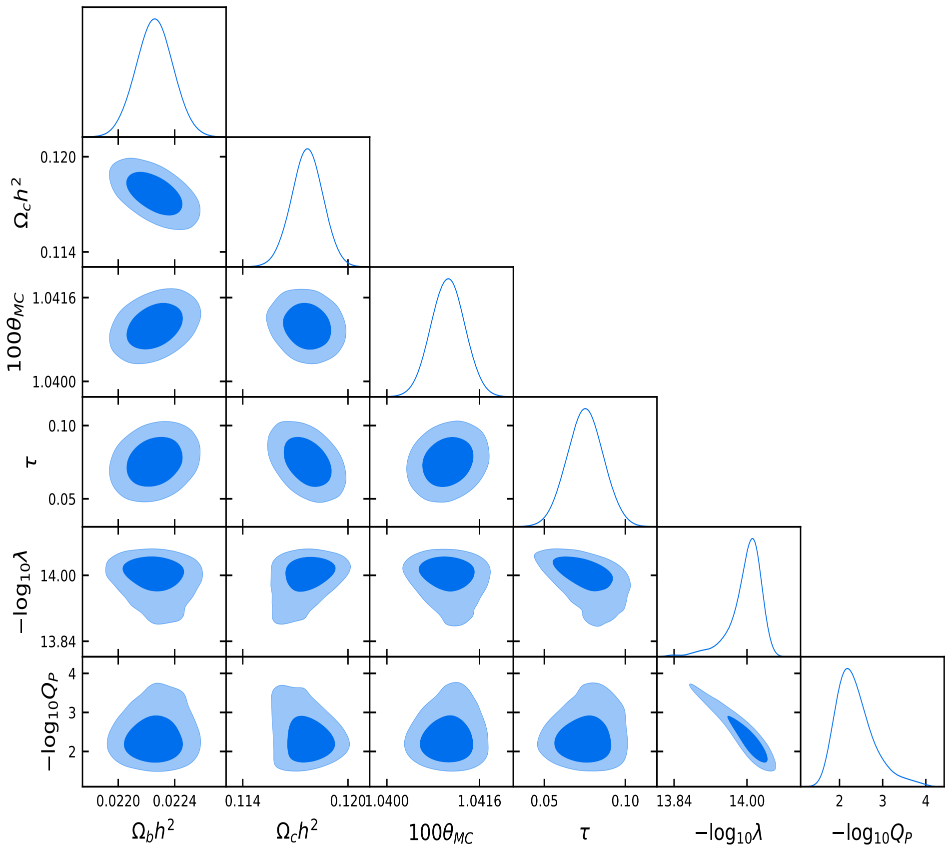

Figure 4.13: The joint probability distribution and the marginalized distributions of the cosmological parameters for the case $V(\phi) = \lambda\phi^4$ with $\Upsilon = C_\phi T^3/\phi^2$ in the weak dissipative regime for $N_P = 60$. To obtain this, we carry out the CosmoMC analysis using the *Planck* 2015 TT, TE, EE + low P dataset.

4.7.2 Constraints on the parameters of the warm inflation model $V(\phi) = \lambda\phi^4$ with a linear dissipation coefficient $\Upsilon = C_T T$

For this model, both the weak and strong regimes of dissipation are studied. We list the priors for the parameters and the mean values obtained in CosmoMC along with 68% confidence limits in the weak and the strong dissipative regimes in Tables 4.7 and 4.8, respectively.

Parameter	Priors	68% C.L.
$\Omega_b h^2$	[0.005, 0.1]	0.02168 ± 0.00014
$\Omega_c h^2$	[0.001, 0.99]	0.1217 ± 0.0010
$100\,\theta$	[0.50, 10.0]	$1.04027^{+0.00029}_{-0.00033}$
τ	[0.01, 0.8]	$0.048^{+0.016}_{-0.031}$
$-\log_{10}\lambda$	[13.7, 15.5]	$14.39^{+0.34}_{-0.24}$
$-\log_{10}Q_P$	[0.0, 5.4]	$3.64^{+0.76}_{-1.1}$

Table 4.7: The priors and the mean values of the parameters along with 68% C.L. for the model $V(\phi) = \lambda\phi^4$ with $\Upsilon = C_T T$ in the weak dissipative regime. These values of the parameters are consistent with the *Planck* 2015 TT, TE, EE + low P dataset.

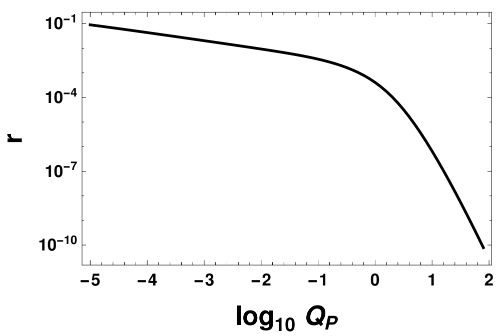

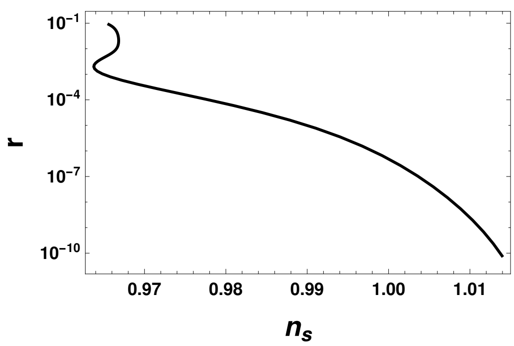

Figure 4.14: *Left*: Plot of r vs $\log_{10} Q_P$ indicates that the r value is smaller for the strong dissipation (large Q_P) case than the weak dissipation. *Right:* Plot of $n_s - r$, where different points on the curve represent different Q_P values (and the corresponding λ). The value of Q_P increases from left to right on the plot, whereas λ decreases. For the strong dissipation, r value is nearly 0.

Analysis of n_s and r values

In Fig. 4.14, we plot the tensor-to-scalar ratio $\log_{10} r$ vs $\log_{10} Q_P$ for both weak and strong dissipation, and show that as the dissipation increases (larger Q_P value), the tensor-to-scalar ratio decreases. We also show the $n_s - r$ plot for different Q_P (and the corresponding λ) values in right plot of Fig. 4.14. For the strong dissipation, r value is practically 0. In the weak dissipative regime, the mean values of $\lambda = 4.07 \times 10^{-15}$, and $Q_P = 2.29 \times 10^{-4}$. For these mean values, we obtain $n_s = 0.967$, and $r = 0.0330$, which are within the *Planck* 95% C.L. values. For the strong dissipative regime, the mean value of $\lambda = 6.82 \times 10^{-16}$ and the upper limit of $Q_P = 1.43$. For these, we obtain $n_s = 0.973$, and $r = 0.000214$, which are also consistent with the *Planck* bounds. Unlike in cold inflation, where this potential is ruled out from the $n_s - r$ constraints, in warm inflation this model predicts a tensor-to-scalar ratio which is within the observationally allowed range and hence it is a viable model for describing inflation. As inferred from Fig. 4.14, the value of r for the strong dissipation regime is much smaller than for the weak dissipative regime. Thus, warm inflation can only be tested in the weak dissipative regime with the upcoming CMB polarization experiments.

Parameter	Priors	68% C.L.
$\Omega_b h^2$	[0.005, 0.1]	0.02174 ± 0.00013
$\Omega_c h^2$	[0.001, 0.99]	0.1200 ± 0.0011
$100\ \theta$	[0.50, 10.0]	1.04044 ± 0.00029
τ	[0.01, 0.8]	0.061 ± 0.024
$-\log_{10}\lambda$	[15.0, 15.6]	$15.166^{+0.036}_{-0.056}$
$\log_{10} Q_P$	[0.0, 0.6]	< 0.156

Table 4.8: The priors and the marginalised values of the parameters along with 68% C.L. for the model $V(\phi) = \lambda\phi^4$ with $\Upsilon = C_T T$ in the strong dissipative regime. These parameter values are consistent with the *Planck* 2015 TT, TE, EE + low P dataset.

λ and Q_P correlation

The marginalized and the joint probability of the parameters obtained for this model are shown in Figs. 4.15 and 4.17 for the weak and strong dissipative regimes, respectively. Here N_P is fixed to 60. From the slope of the joint probability plots, we find that λ and Q_P are correlated in the weak dissipative regime as, $\lambda \propto Q_P^{-0.3}$ and for the strong dissipative regime, $\lambda \propto Q_P^{-0.6}$.

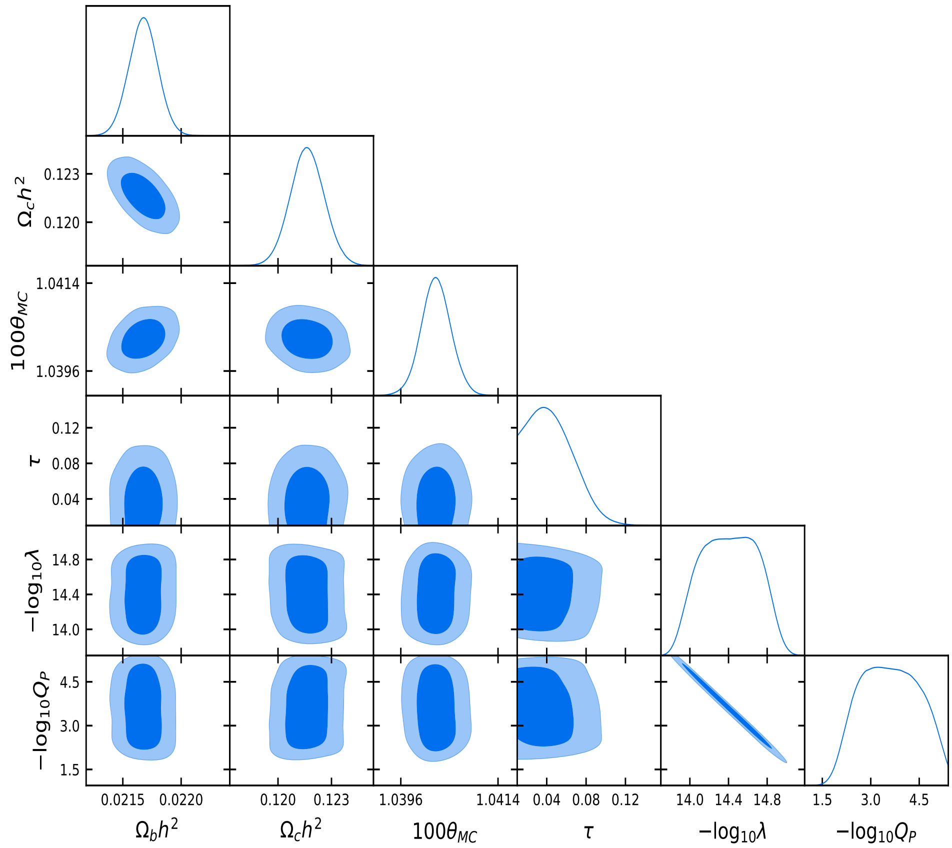

Figure 4.15: The joint probability distribution and the marginalized distributions of the cosmological parameters for the case $V(\phi) = \lambda\phi^4$, with $\Upsilon = C_T T$ in the weak dissipative regime, obtained using the *Planck* 2015 TT, TE, EE + low P dataset.

Analysis of C_T values

In Fig. 4.16, we plot the behaviour of $\log_{10} C_T$ vs $\log_{10} Q_P$ for both the weak and strong dissipative regime of this model. We find that the value of C_T is smaller in the weak dissipation case, and spans over many orders of magnitude from $\sim 10^{-4.6}$ to $10^{-1.5}$, whereas in the strong dissipation regime, the variation is less. By its definition in Section 3.3.3, the value of C_T depend on the ratio of couplings g^2/h^2. In the weak dissipative regime, for the mean values of λ and Q_P, we obtain $C_T = 1.75 \times 10^{-4}$ which signify that the ratio of couplings g/h is $\mathcal{O}(10^{-2})$. In the strong dissipative regime, for the upper limit value of Q_P, we have $C_T = 3.66 \times 10^{-2}$, which implies

$g/h \sim \mathcal{O}(10^{-1})$ in the strong dissipative regime. Thus, the inflaton couples strongly to the intermediate field in the strong dissipation case.

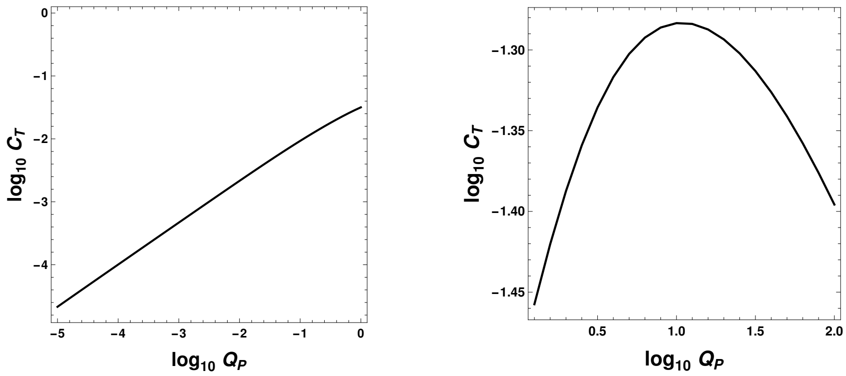

Figure 4.16: *Left*: Plot of $\log_{10} C_T$ vs $\log_{10} Q_P$ for the weak dissipative regime, and *Right*: for the strong dissipative regime is shown. The value of C_T is smaller in the weak dissipation regime than in the strong dissipation regime.

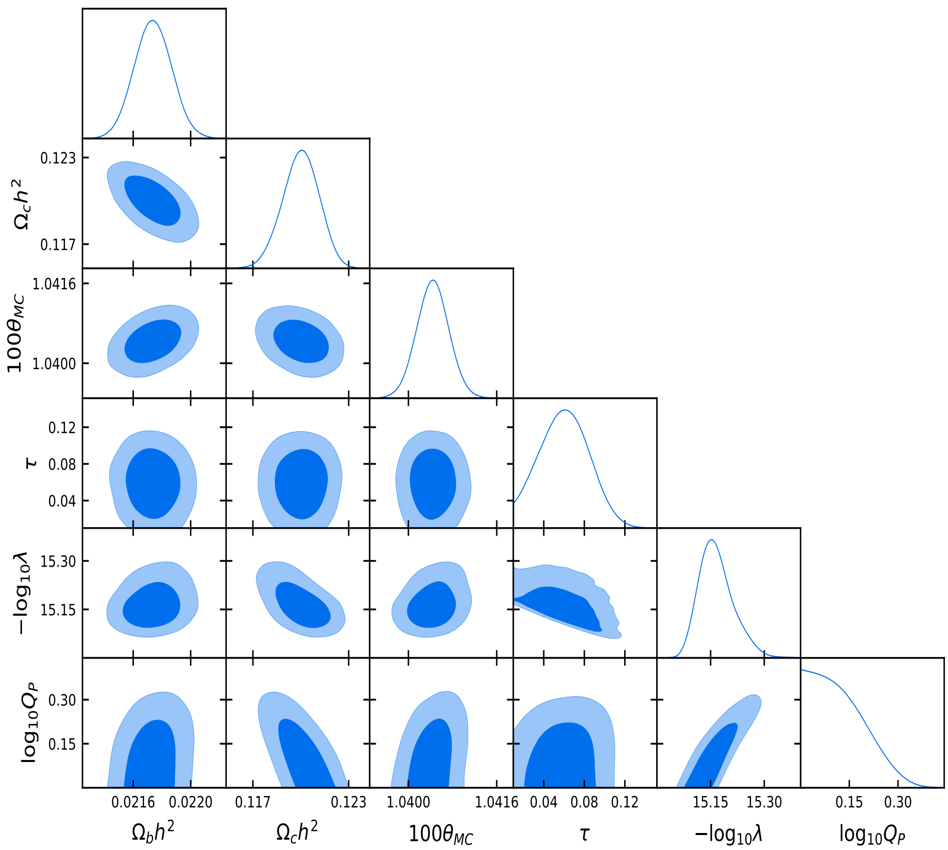

Figure 4.17: The joint probability distribution and the marginalized distributions of the cosmological parameters for the case $V(\phi) = \lambda\phi^4$, with $\Upsilon = C_T T$ in the strong dissipative regime. The CosmoMC analysis is carried out with the *Planck* 2015 TT, TE, EE + low P dataset.

Comparison with the literature

In Ref. [154], Panotopoulos et al. also estimated the bounds for C_T (denoted by a in their paper) and λ which satisfy the $n_s - r$ constraints from *Planck* data. However they do not carry out a CosmoMC analysis for their estimation. We performed a CosmoMC analysis to obtain the model parameters and find that our values of C_T are within their estimated range of values. Our results also agree with those in Ref. [156], where BOBYQA (Bound Optimization BY Quadratic Approximation) is carried out to estimate the best fit values of the parameters. We point out that we have adopted the full CosmoMC and our approach gives us the mean values and standard deviations of parameters, which carry more information than the best fit value obtained through BOBYQA.

4.8 Summary

Warm inflation predicts distinct signatures on the CMB radiation, compared to the standard cold inflation, and hence is very crucial to study. In light of this, here we consider warm inflation models with a monomial potential $V(\phi) = \lambda\phi^4$ and two forms of the dissipation coefficient ($\Upsilon \propto T^3$ and $\Upsilon \propto T$). The motivation to study monomial potentials is that they are simple one parameter models. For cold inflation, they predict a large amplitude of the tensor power spectrum and thus the tensor-to-scalar ratio, which is used as a test of these models. A non-detection of the B-mode polarization signal in the CMB observations rules out these potentials as feasible models in cold inflation. However, there is a possibility that these potentials may be viable in the context of the warm inflation description.

The different forms of dissipation coefficients arise when different channels of the inflaton dissipation are considered, and characterise the microphysics in terms of the coupling strengths and the multiplicities of the fields to which the inflaton is coupled. Therefore, by knowing these physical quantities, one can build a particle physics model of inflation. With this motivation, we carry out a MCMC analysis using a numerical code, CosmoMC, for estimating the parameters for these models which are consistent with the observations.

The primordial curvature power spectrum for warm inflation is parameterized in terms of the inflaton self coupling, λ, and the dissipation parameter at the pivot scale, Q_P. Using the CosmoMC code, we obtain the joint probability distribution and the marginalised values for these parameters. In our analysis, we find that for the model with cubic dissipation ($\Upsilon \propto T^3$), only the weak dissipation regime is allowed, whereas for the linear dissipation ($\Upsilon \propto T$), both weak and the strong dissipative regimes of warm inflation are favored. The n_s and r values for the mean values of the parameters are consistent with the *Planck* allowed values, from which we infer that for a range of parameters, our models of warm inflation are viable for describing inflation. We also obtain the quantities C_ϕ or C_T for the obtained mean values or limits of λ and Q_P, which provide us information about the couplings and multiplicities of fields in the warm inflation models.

The tensor-to-scalar ratio for the weak dissipative regime of our models is within the sensitivity of the next generation of ground-based and satellite-based CMB polarization experiments [72–74], which is an important observational test for these models. However, for the strong dissipative regime of our models, the tensor-to-scalar ratio is predicted to be very small. It has been argued that lensing of intensity fluctuations in the 21-cm signal from atomic hydrogen in the dark ages can in principle provide a probe of inflationary gravitational waves down to a sensitivity of 10^{-9} for the tensor-to-scalar ratio [226]. However such measurements would be challenging and require a futuristic experiment. Thus while the the weak dissipative regime of the warm inflation models studied here can be investigated by the upcoming CMB polarization experiments, it may only be possible to test the strong dissipative regime in the far future.

Chapter 5

Warm inflation models with $\lambda\phi^6/M_{Pl}^2$ potential

Now we consider another monomial potential of the form $V(\phi) = \lambda\phi^6/M_{Pl}^2$ in the context of warm inflation, and study its theoretical predictions on the CMB. In our study [227], the following models of warm inflation with the two forms of dissipation coefficient are considered in both the weak and the strong dissipation regimes.

- $V(\phi) = \lambda\phi^6/M_{Pl}^2$ with the dissipation coefficient $\Upsilon = C_\phi T^3/\phi^2$.
- $V(\phi) = \lambda\phi^6/M_{Pl}^2$ with the dissipation coefficient $\Upsilon = C_T T$.

This potential of inflation has also been ruled out in the cold inflation studies, as its theoretical predictions of n_s and r are inconsistent with the CMB observations. A large amplitude of the tensor perturbations is predicted according to this model, which is not supported in the CMB observations, as the primordial gravitational waves have not been detected yet. In this study, we are interested to know the status of the $\lambda\phi^6$ model of warm inflation from the observations, and the allowed parameter space for the model parameters which make it consistent with the CMB.

In the studies on model building, one is interested to estimate the parameter values of the theory, and to construct an embedding into the high energy theories. However, a first principle construction of this model of warm inflation is challenging and important, but is not addressed in this work. Instead, in this study, we do a phenomenological study of the warm inflation considering it as a toy model, and estimate its parameters consistent with the CMB observations. The information of the range of parameters then provides the foundation stone to build warm inflation from some high energy physics theory.

5.1 Parameterization of the primordial power spectrum

Following the similar approach as in the previous Chapter, we now parameterize the primordial power spectrum, given in Eq. (3.25) for the two models considered in this study.

5.1.1 When the dissipation coefficient $\Upsilon = C_\phi T^3/\phi^2$

- For this potential of warm inflation, from the Einstein equation, the Hubble parameter is given as

$$H^2 = \frac{8\pi}{3}\frac{\lambda\phi^6}{M_{Pl}^4}. \tag{5.1}$$

In the slow roll approximation, the inflaton evolution is given as

$$\dot{\phi} \approx \frac{-V'(\phi)}{3H(1+Q)} = -2\sqrt{\frac{3}{8\pi}}\sqrt{\lambda}\frac{\phi^2}{(1+Q)}. \tag{5.2}$$

Then on combining the above two equations, we obtain the prefactor of the primordial power spectrum as

$$\frac{H_k^2}{2\pi\dot{\phi}_k} = -\frac{2}{3}\sqrt{\frac{8\pi}{3}}\sqrt{\lambda}\left(\frac{\phi_k}{M_{Pl}}\right)^4(1+Q_k). \tag{5.3}$$

- Next we evaluate the terms in the square bracket of the primordial power spectrum. The temperature of the thermal bath is obtained from Eq. (3.11) to be,

$$T_k = \left(\frac{135}{4\pi^3 g_*}\frac{Q_k}{(1+Q_k)^2}\lambda\left(\frac{\phi_k}{M_{Pl}}\right)^4\right)^{\frac{1}{4}} M_{Pl}, \tag{5.4}$$

and then using Eq. (5.1), we get

$$\frac{T_k}{H_k} = \left(\frac{135}{4\pi^3 g_*}\right)^{\frac{1}{4}}\sqrt{\frac{3}{8\pi}}\lambda^{-\frac{1}{4}}\frac{Q_k^{\frac{1}{4}}}{(1+Q_k)^{\frac{1}{2}}}\left(\frac{\phi_k}{M_{Pl}}\right)^{-2}. \tag{5.5}$$

This factor has to be greater than 1 throughout the warm inflation phase.

- Now we evaluate the field value, ϕ_k. For the form of dissipation coefficient considered in this model, we can write $\phi = \left(\frac{C_\phi T^3}{3QH}\right)^{1/2}$. Then, on substituting Eq. (5.4) and (5.1) into it, we get

$$\left(\frac{\phi_k}{M_{Pl}}\right) = \sqrt{\frac{1}{8\pi}} \left(\frac{81\lambda C_\phi^4}{8\pi A^3} \frac{1}{Q_k(1+Q_k)^6}\right)^{\frac{1}{8}} . \tag{5.6}$$

Further, this is substituted in the prefactor and the T_k/H_k factor and the primordial power spectrum is expressed in terms of model parameters λ, Q_k and C_ϕ.

Similarly, we also parameterize the tensor power spectrum for this model as

$$\Delta_T^2(k) = \frac{128}{3}\lambda \left(\frac{\phi_k}{M_{Pl}}\right)^6 . \tag{5.7}$$

By substituting Eq. (5.6) into this, we express $P_T(k)$ in terms of λ, Q_k and C_ϕ.

5.1.2 When the dissipation coefficient $\Upsilon = C_T T$

In this model, the inflaton potential is the same as in the previous model, but the form of dissipation coefficient is different. The Eqs. (5.3), (5.5), and (5.7) hold for this model, but the field value evolves differently. For the form of dissipation coefficient considered in this model, we have $T/H = 3Q/C_T$. On equating this with Eq. (5.5), we obtain

$$\left(\frac{\phi_k}{M_{Pl}}\right) = \left(\frac{C_T^4}{\lambda A} \frac{1}{(8\pi)^3 Q_k^3 (1+Q_k)^2}\right)^{\frac{1}{8}} . \tag{5.8}$$

Then this is used to express the primordial scalar and tensor power spectrum in terms of variables λ, Q_k and C_T.

5.2 Dissipation parameter, Q_k

Following the approach of Section 4.3, here we obtain, for the model of warm inflation with the cubic dissipation,

$$\frac{dQ}{dx} = \frac{16}{1-\epsilon_H} \left(\frac{8\pi A^3}{\lambda C_\phi^4}\right)^{\frac{1}{4}} \frac{Q^{5/4}(1+Q)^{3/2}}{(1+7Q)} , \tag{5.9}$$

and for the linear dissipation case,

$$\frac{dQ}{dx} = \frac{6}{1-\epsilon_H} \left(\frac{512\pi^2 A\lambda}{C_T^4}\right)^{\frac{1}{4}} \frac{Q^{7/4}(1+Q)^{1/2}}{(3+5Q)} . \tag{5.10}$$

These expressions can then be integrated from Q_P (at $x = 0$) to Q_k (at any x) to obtain Q_k. On substituting Q_k in the parameterized power spectrum obtained in Section 5.1, we get $\Delta^2_{\mathcal{R}}(k)$.

Dissipation parameter at the end of warm inflation

For this potential of warm inflation also, the violation of slow roll parameters bring the inflationary phase to an end. Therefore, the condition at the end of inflation is given as

$$\eta_e = \frac{30}{8\pi}\frac{M_{Pl}^2}{\phi_e^2} = 1 + Q_e. \tag{5.11}$$

On substituting for ϕ_e from Eq. (5.6), for the case of cubic dissipation, we obtain

$$Q_e^3 + 2Q_e^2 + Q_e = \frac{\lambda C_\phi^4}{8\pi A^3}\left(\frac{1}{10}\right)^4. \tag{5.12}$$

For the case of linear dissipation, we substitute for ϕ_e from Eq. (5.8) and get

$$Q_e^3(1+Q_e)^{-2} = \frac{8\pi C_T^4}{A\lambda}\left(\frac{1}{30}\right)^4. \tag{5.13}$$

The solution to these equations are given in Appendix B. The dissipation parameter is a function of (λ, C_ϕ) for the cubic dissipation case and (λ, C_T) for the linear dissipation.

5.3 Model parameters and their priors

As discussed in Section 4.5 we choose the self coupling of inflaton λ and the dissipation parameter at the pivot scale Q_P as the model parameters for our CosmoMC analysis. The range of Q_P is determined from the spectral index plots. For this, we first calculate the expressions for the spectral index for our models, and using them generate the n_s versus Q_P plot in Fig. 5.1. The expressions for the spectral index are given in Appendix D. To generate the plot, we fix N_P and the normalisation of the power spectrum, and for every Q_P value obtain the corresponding λ and C_ϕ (or C_T). In Fig. 5.1, we also show the allowed values for n_s for a power-law power spectrum, from the *Planck* 2015 TT, TE, EE + low P results [223–225] in the shaded bands.

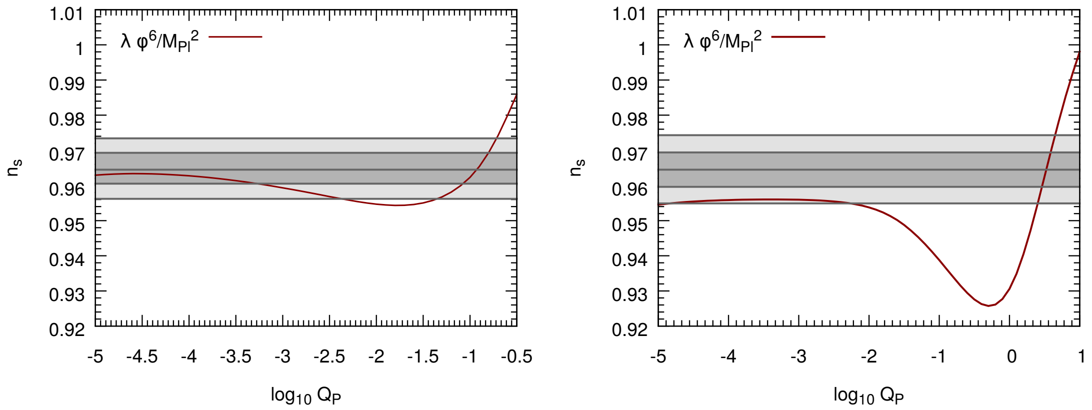

Figure 5.1: The spectral index, n_s as a function of the dissipation parameter, $\log_{10} Q_P$ are plotted for (*a*) the model with cubic dissipation coefficient, and, (*b*) the model with linear dissipation coefficient. The band shows the allowed n_s values from *Planck* 2015 TT, TE, EE + low P results for a power law power spectrum with 68% and 95% C.L..

Model	Allowed Q_P range in the weak dissipation regime	Allowed Q_P range in the strong dissipation regime
cubic dissipation	$[10^{-5}, 0.2]$	–
linear dissipation	$[10^{-5}, 5 \times 10^{-3}]$	$[2.51, 3.98]$

Table 5.1: The values of Q_P allowed from the n_s plots in Fig. 5.1. For the cubic dissipation, only the weak dissipation regime is favored by the CMB observations.

It can be seen from the figure that for these models, only a certain range of Q_P is consistent with the allowed values of n_s. Hence, we choose the prior for Q_P such that the n_s corresponding to it lies in the allowed band. We consider both the weak and strong dissipative regime for the model with linear dissipation coefficient. However, we see from Fig. 5.1 that for cubic dissipation coefficient, none of the values of Q_P are consistent with the allowed n_s in the strong dissipative regime. Hence, we consider only the weak dissipative regime for running CosmoMC for cubic dissipation models. We estimate the priors for λ corresponding to the chosen priors for Q_P. The estimated priors for each model are listed in their respective Section.

5.4 CosmoMC results

In this Section, we list the results of CosmoMC runs for the estimated parameter space. The triangle plots for the parameters are plotted using the GetDist GUI software.

5.4.1 Constraints on the parameters of the warm inflation model $V(\phi) = \lambda\phi^6/M_{Pl}^2$ with dissipation coefficient $\Upsilon = C_\phi T^3/\phi^2$

For this inflationary model, we consider only the weak dissipative regime for the CosmoMC analysis. In this case, we obtained two convergence regions, as shown in Fig. 5.2. However, it is inferred from the peak of the probability distribution that the region with $-\log Q_P$ near 0.8 has a higher probability. Therefore, we restrict the priors in such a way that we obtain the mean value of Q_P in the more probable region and redo the CosmoMC runs. We list the priors for the parameters and the mean values along with their 68% C.L. obtained in CosmoMC in Table 5.2.

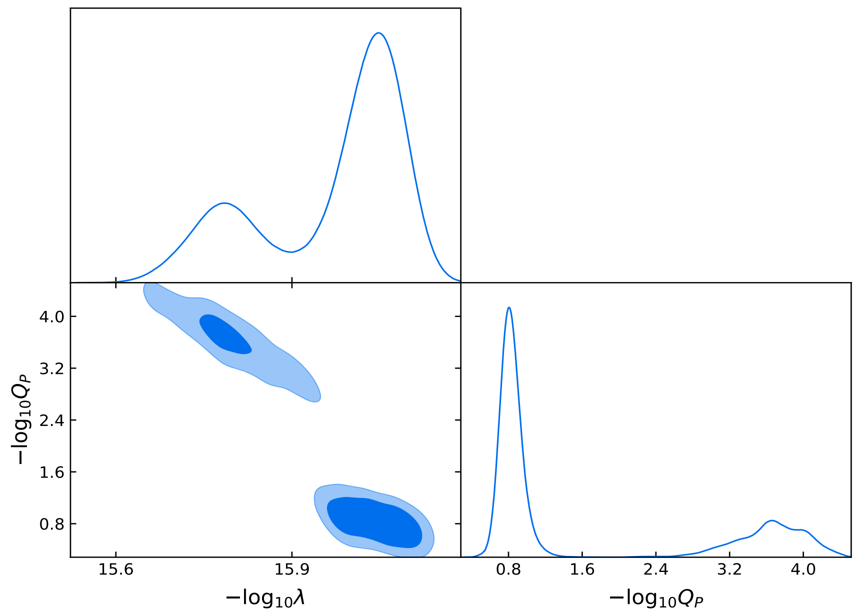

Figure 5.2: The joint probability distribution of $-\log_{10}\lambda$ and $-\log_{10}Q_P$ for the case $V(\phi) = \lambda\phi^6/M_{Pl}^2$, with $\Upsilon = C_\phi T^3/\phi^2$ in the weak dissipative regime. The plot shows that there are two convergence regions for the parameters.

Parameter	Priors	68% C.L.
$\Omega_b h^2$	[0.005, 0.1]	0.02170 ± 0.00013
$\Omega_c h^2$	[0.001, 0.99]	0.1207 ± 0.0014
$100\,\theta$	[0.50, 10.0]	1.04036 ± 0.00030
τ	[0.1, 0.8]	0.061 ± 0.023
$-\log_{10}\lambda$	[15.8, 17.0]	16.064 ± 0.38
$-\log_{10} Q_P$	[0, 1.5]	$0.799^{+0.068}_{-0.10}$

Table 5.2: The priors and the marginalised values of the parameters along with 68% C.L. for the model $V(\phi) = \lambda \dfrac{\phi^6}{M_{Pl}^2}$ with $\Upsilon = C_\phi \dfrac{T^3}{\phi^2}$ in the weak dissipative regime. These values are consistent with the *Planck* 2015 TT, TE, EE + low P dataset.

Analysis of n_s and r values

In Fig. 5.3, we plot the tensor-to-scalar ratio r vs $\log_{10} Q_P$ for fixed $N_P = 60$, and show that as the dissipation increases, the tensor-to-scalar ratio decreases. We also show the $n_s - r$ plot for different Q_P (and the corresponding λ) values in right plot of Fig. 5.3. Moving from left to right on the plot, the Q_P value increases. The mean values of the parameters $\lambda = 8.63 \times 10^{-17}$, and $Q_P = 0.1588$. For these values, we obtain $n_s = 0.969$, and $r = 0.00480$, which are consistent with the *Planck* bounds, thus implying that it is a viable model of inflation.

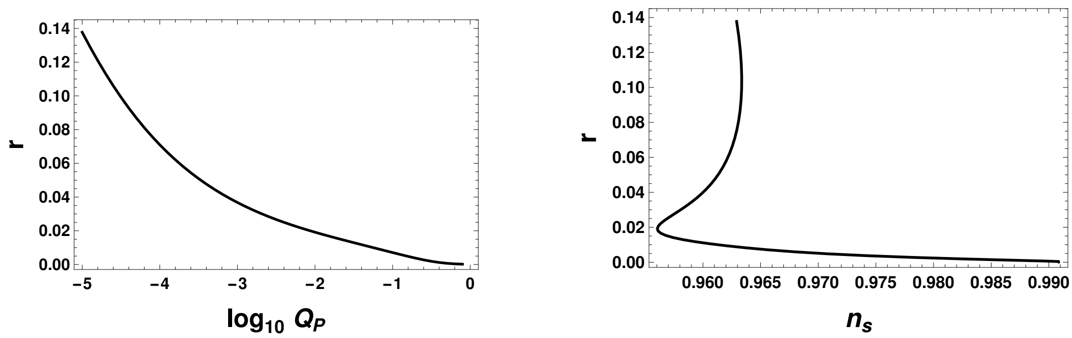

Figure 5.3: *Left:* Plot of the tensor-to-scalar ratio r vs $\log_{10} Q_P$ indicates that for larger dissipation (larger Q_P value), the r value is smaller. *Right:* Plot of $n_s - r$, where different points on the curve represent different Q_P values (and corresponding λ). Q_P increases from left to right on the plot, whereas λ decreases.

λ and Q_P correlation

In Fig. 5.4, we show the marginalized and joint probability distribution for the parameters, obtained for this warm inflation model. From the slope of $-\log\lambda$ versus $-\log Q_P$ plot, we find that the parameters λ and Q_P are correlated as $\lambda \propto Q_P^{-0.4}$ for this warm inflation model.

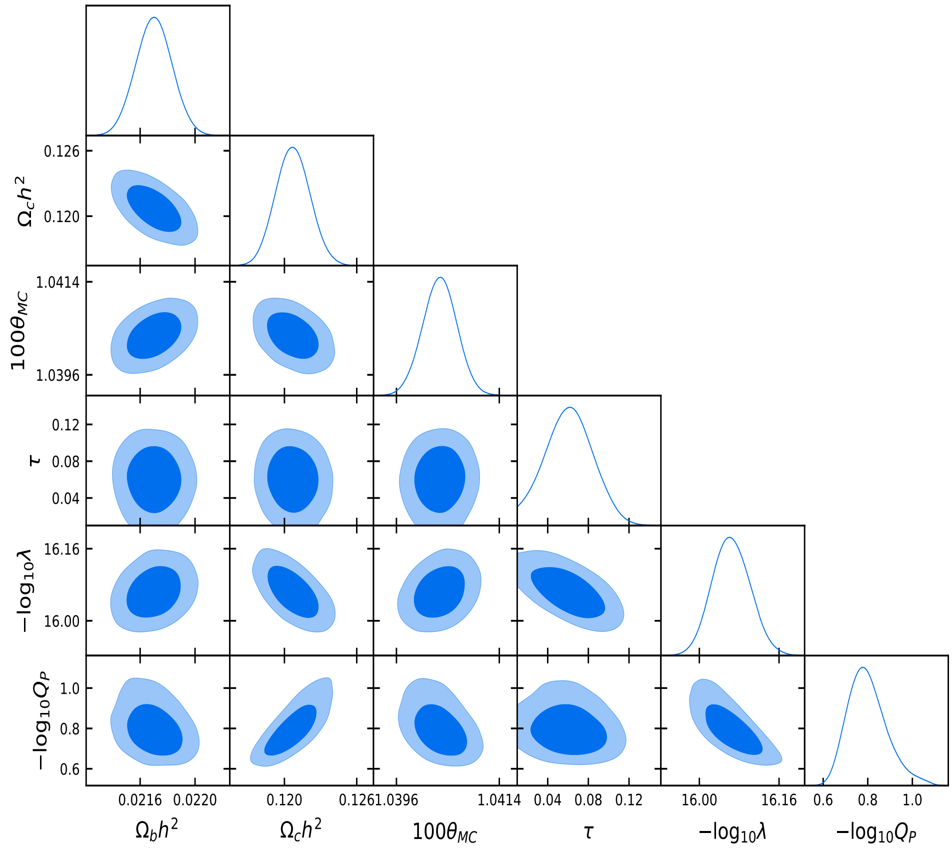

Figure 5.4: The joint probability distribution and the marginalized distributions of the cosmological parameters for the case $V(\phi) = \lambda\phi^6/M_{Pl}^2$, with $\Upsilon = C_\phi T^3/\phi^2$ in the weak dissipative regime, obtained using the *Planck* 2015 TT, TE, EE + low P dataset..

Analysis of C_ϕ values

In Fig. 5.5, we plot the behaviour of $\log_{10} C_\phi$ vs $\log_{10} Q_P$ for the weak dissipative regime of this model. We find that for a larger dissipation (indicated by a large Q_P value), the C_ϕ value is larger. For the mean values of λ and Q_P, we get $C_\phi = 4.87\times10^7$. As described in Section 3.3.3, C_ϕ is related to the couplings and multiplicities of the fields to which inflaton couple. By assuming $\alpha \sim 0.1$, we find that $N_X \sim 10^9$. Such a large multiplicity of fields is an unattractive feature of some warm inflationary models.

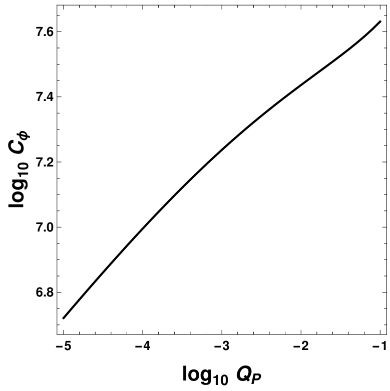

Figure 5.5: Plot of $\log_{10} C_\phi$ vs $\log_{10} Q_P$ for the weak dissipative regime shows that $C_\phi \sim \mathcal{O}(10^7 - 10^8)$ for this model of warm inflation.

5.4.2 Constraints on the parameters of the warm inflation model $V(\phi) = \lambda\phi^6/M_{Pl}^2$ with dissipation coefficient $\Upsilon = C_T T$

For this inflationary model, both the strong and weak dissipative regimes are allowed by the data. Therefore, we consider both the regimes in our MCMC analysis. The priors and the obtained mean values of the model parameters along with 68% confidence limits for the weak and the strong dissipative regimes are listed in Tables 5.3 and 5.4, respectively.

Parameter	Priors	68% C.L.
$\Omega_b h^2$	[0.005, 0.1]	0.02157 ± 0.00013
$\Omega_c h^2$	[0.001, 0.99]	0.12484 ± 0.00099
$100\,\theta$	[0.50, 10.0]	1.03989 ± 0.00029
τ	[0.01, 0.8]	0.056 ± 0.020
$-\log_{10}\lambda$	[15.4, 16.6]	$16.07^{+0.27}_{-0.19}$
$-\log_{10} Q_P$	[1.8, 5.4]	$3.54^{+0.68}_{-0.82}$

Table 5.3: The priors and the marginalised values of the parameters along with 68% C.L. for the model $V(\phi) = \lambda\phi^6/M_{Pl}^2$ with $\Upsilon = C_T T$ in the weak dissipative regime. These values are consistent with the *Planck* 2015 TT, TE, EE + low P dataset.

Parameter	Priors	68% C.L.
$\Omega_b h^2$	[0.005, 0.1]	0.02170 ± 0.00014
$\Omega_c h^2$	[0.001, 0.99]	0.1206 ± 0.0015
$100\,\theta$	[0.50, 10.0]	1.04037 ± 0.00030
τ	[0.01, 0.8]	0.066 ± 0.022
$-\log_{10}\lambda$	[14.8, 15.9]	15.253 ± 0.029
$\log_{10} Q_P$	[0, 1.5]	0.596 ± 0.048

Table 5.4: The priors and the marginalised values of the parameters along with 68% C.L. for the model $V(\phi) = \lambda\phi^6/M_{Pl}^2$ with $\Upsilon = C_T T$ in the strong dissipative regime. These values are consistent with the *Planck* 2015 TT, TE, EE + low P dataset.

Analysis of n_s and r values

We plot the tensor-to-scalar ratio $\log_{10} r$ vs $\log_{10} Q_P$ for both weak and strong dissipation in Fig. 5.6, and show that for larger Q_P value, the tensor-to-scalar ratio is smaller. We also show the $n_s - r$ plot for different Q_P (and the corresponding λ) values in right plot of Fig. 5.6. As we move from left to right on the plot, the Q_P value increases. For the strong dissipation, r value is practically 0. In the weak dissipative regime, the mean values of model parameters $\lambda = 8.51 \times 10^{-17}$, and $Q_P = 2.88 \times 10^{-4}$. For these mean values, we obtain $n_s = 0.956$, and $r = 0.0451$, which are within the observationally allowed band.

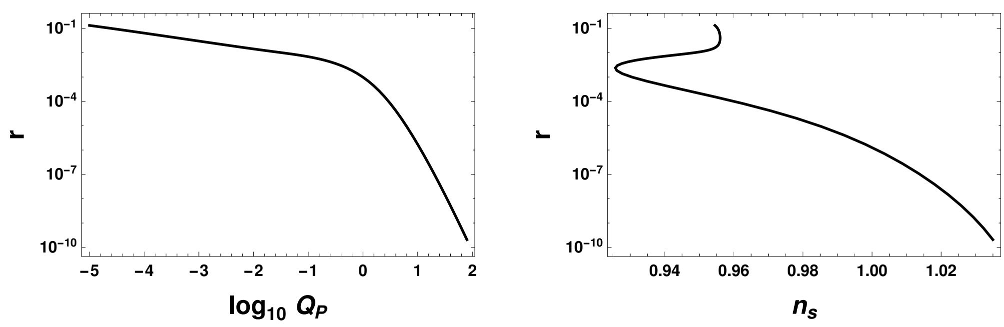

Figure 5.6: *Left*: Plot of r vs $\log_{10} Q_P$ indicates that the r value is smaller for the strong dissipation (large Q_P) case than the weak dissipation. *Right:* Plot of $n_s - r$, where different points on the curve represent different Q_P values (and λ). The Q_P value increases from left to right on the plot, while λ decreases. For the strong dissipation, r value is nearly 0.

For the strong dissipative regime, the mean values of $\lambda = 5.59 \times 10^{-16}$, and Q_P = 3.94. For these values, we obtain $n_s = 0.970$, and $r = 0.0000426$, which are also consistent with the observations. Thus, we argue that this warm inflationary model is viable for describing inflation. Here also, it should be noted that the tensor-to-scalar ratio for the mean parameters of the strong dissipative regime is much smaller than for the weak dissipative regime. Hence, a detection or non-detection of the B-mode polarization in the upcoming CMB experiments can either validate or rule out the weak dissipation regime of warm inflation, while the strong dissipation regime is far more difficult to test.

λ and Q_P correlation

The marginalized and the joint probability of the parameters obtained for this model are shown in Figs. 5.7 and 5.8 for the weak and strong dissipative regimes, respectively. From the slope of the joint distribution plots, we find that $\lambda \propto Q_P^{-0.3}$ in the weak dissipative regime, and $\lambda \propto Q_P^{-0.4}$ in the strong dissipative regime.

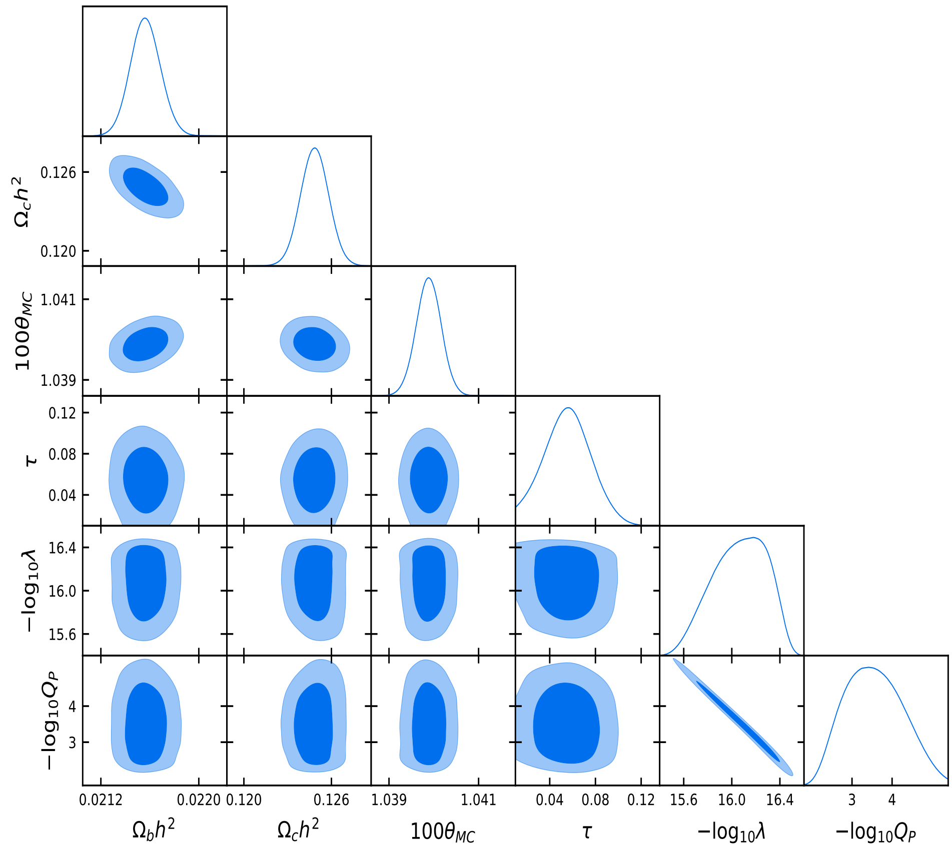

Figure 5.7: The joint probability distribution and the marginalized distributions of the cosmological parameters for the case $V(\phi) = \lambda\phi^6/M_{Pl}^2$, with $\Upsilon = C_T T$ in the weak dissipative regime, obtained using the *Planck* 2015 TT, TE, EE + low P dataset.

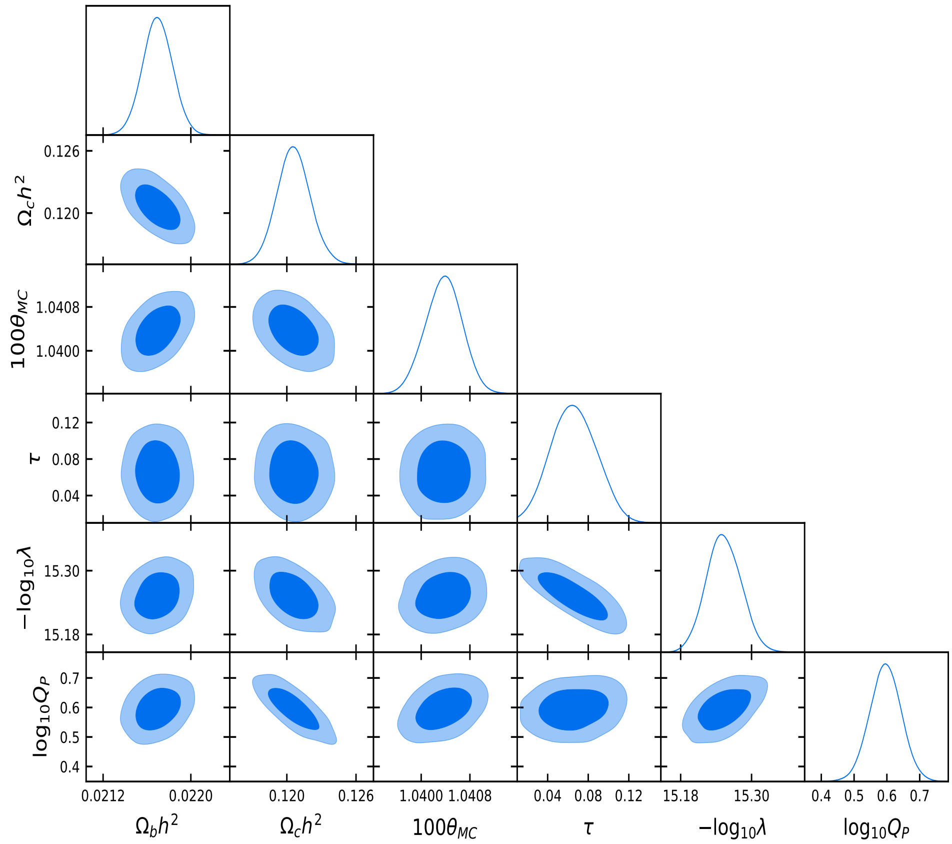

Figure 5.8: The joint probability distribution and the marginalized distributions of the cosmological parameters for the case $V(\phi) = \lambda\phi^6/M_{Pl}^2$, with $\Upsilon = C_T T$ in the strong dissipative regime, obtained using the *Planck* 2015 TT, TE, EE + low P dataset.

Analysis of C_T values

In Fig. 5.9, we plot the behaviour of $\log_{10} C_T$ vs $\log_{10} Q_P$ for both the weak and strong dissipative regime of this model. For the linear dissipation ($\Upsilon \propto T$), the value of C_T is independent of the potential of inflation. Thus, we get the same plots in this case, as for the quartic potential. The value of C_T is smaller in the weak dissipation case, and spans over many orders of magnitude $\sim 10^{-4.6}$ to $10^{-1.5}$, whereas in the strong dissipation regime, the variation is less. By its definition in Section 3.3.3, the value of C_T depend on the ratio of couplings g^2/h^2. Further, we obtain for the mean values of λ and Q_P, $C_T = 2.04 \times 10^{-4}$ in the weak dissipative regime, and a value equal to 4.81×10^{-2} in the strong dissipative regime. These values signify that the ratio of couplings g/h is $\mathcal{O}(10^{-2})$ in the weak dissipative regime and $\mathcal{O}(10^{-1})$ in the strong dissipative regime of warm inflation, respectively.

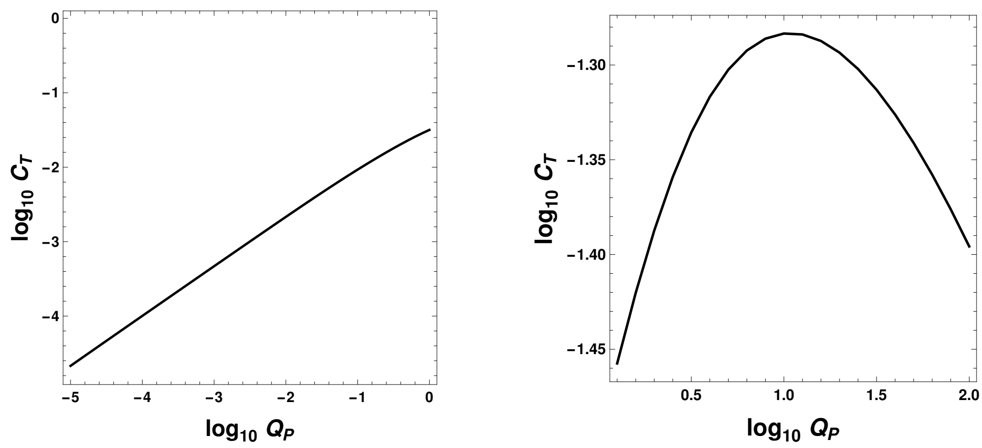

Figure 5.9: *Left*: Plot of $\log_{10} C_T$ vs $\log_{10} Q_P$ for the weak dissipative regime, and *Right*: for the strong dissipative regime is shown here. The value of C_T is smaller in the weak dissipation than in the strong dissipation.

5.5 Comparison of results with the $\lambda\phi^4$ model

Here we compare our findings of our study of both the ϕ^4 and ϕ^6 potentials of warm inflation with the dissipation coefficients $\Upsilon = C_\phi T^3/\phi^2$ and $\Upsilon = C_T T$.

In our analysis, we find that when the dissipation is weak $Q_P \ll 1$, then for the ϕ^6 potential, the inflaton self-coupling is smaller ($\lambda \sim \mathcal{O}(10^{-16})$) than for the ϕ^4 potential ($\lambda \sim \mathcal{O}(10^{-14})$). This is obtained in both the situations, when the dissipation is cubic ($\Upsilon \propto T^3$) and when it is linear ($\Upsilon \propto T$). However, when the dissipation is strong, as favored when $\Upsilon \propto T$, the inflaton self-coupling is of the same order ($\lambda \sim \mathcal{O}(10^{-15})$) for both the potentials.

The value of C_ϕ for T^3 dissipation is $\mathcal{O}(10^7 - 10^8)$ for both the potentials, which implies a similar requirement for high multiplicities of the intermediate X fields. The value of C_T is independent of the potential of inflation. Depending on the Q_P value, it is of the order $\mathcal{O}(10^{-4})$ in the weak dissipative regime, and $\mathcal{O}(10^{-2})$ in the strong dissipative regime. By its definition, this gives a ratio of couplings $g/h \sim 10^{-2}$ and 10^{-1} in the weak and strong dissipative regimes, respectively, for both the potentials.

A common trend for both the potentials is observed, which is related with the tensor-to-scalar ratio. The r value decreases as the dissipation increases (i.e. Q_P increases), and is very negligible for the strong dissipation.

5.6 Summary

In this study, we analyze warm inflation models with a $\lambda\phi^6/M_{Pl}^2$ potential and cubic ($\propto T^3$) and linear ($\propto T$) dissipation coefficients. Being a large field model, this potential predicts a large value of the tensor-to-scalar ratio for cold inflation, and a non-detection of the B-mode polarization signal, rules out this model as viable to describe inflation. Here, we do a phenomenological study of this potential in the context of warm inflation, and estimate the parameters for these models which are consistent with the CMB observations.

For the cubic dissipation case, only the weak dissipation regime is favored by the CMB observations, while for the linear dissipation, both weak and strong dissipation are allowed. We carry out a MCMC analysis to estimate the parameters for our models using CosmoMC. For the mean value of the parameters, we also calculate C_ϕ or C_T, and discuss its interpretation in terms of the coupling strengths and multiplicities of the fields. In our analysis, we find that for the mean values of λ and Q_P, the n_s and r values are consistent with the CMB, suggesting that these models are viable models of inflation. For weak dissipation, the predicted tensor-to-scalar ratio is within the sensitivity of the next decade CMB polarization experiments, while for strong dissipation, the tensor-to-scalar ratio is too small for detection in the near future.

Chapter 6

Primordial Black Hole formation from warm inflation

In the previous part of the thesis, I discussed the large scale perturbations generated during inflation and their observational imprints on the cosmic microwave background radiation. I now discuss the growth of small scale perturbations generated during inflation, in the context of the formation of compact objects called primordial black holes.

6.1 Introduction

Primordial Black Holes (PBHs) [163–166] refers to the black holes with a primordial origin, i.e., they are produced in the very early Universe. They are very crucial to study as they provide us a unique probe to the rich physics of the Universe at all epochs of its evolution. While the cosmic microwave background radiation and large scale structure observations measure only the modes ranging from $10^{-4} - 1$ Mpc^{-1}, PBHs can be formed over a range of fluctuation modes varying from $10^{-2} - 10^{23}$ Mpc^{-1} and thus provide a probe for a huge range of small scales. Some good reviews on PBHs can be found in Refs. [228–234].

The mass of a PBH at the time of its formation (t after the Big-Bang) is of the order of the particle horizon mass at that epoch, and is given by

$$M_{PBH}(t) \approx \frac{c^3 t}{G_N} \simeq 10^{15} \left(\frac{t}{10^{-23} s}\right) g. \tag{6.1}$$

Therefore, PBHs span over a wide range of masses, with the lightest PBH corresponding to the Planck time ($t = 10^{-43}s$) with mass $M_P = 10^{-5}$ g [165]. For different mass ranges of PBHs, different observational effects are associated, as given below.

- **PBHs with masses $M_{PBH} < 10^{15}$ g :**
  Such PBHs have a short lifetime, and would have evaporated into Hawking radiation by the present time [235, 236]. Therefore, the consequences of PBH evaporation on the nucleosynthesis (BBN) [237–239], or the constraints on the relic abundance of stable (eg. lightest supersymmetric particle) and long-lived decaying particles (eg. gravitino, modulii) produced from PBH evaporation [240–242] can provide constraints on their abundance (for review, see Ref. [243]). The upper limit on PBH abundance further gives bounds on the amplitude of the primordial curvature power spectrum and hence various inflationary models [10, 244–247]. In this way, PBHs can serve as a powerful and unique probe to the inflationary epoch, and various models of inflation.

- **PBHs with $M_{PBH} \sim 10^{15}$ g :**
  They would be evaporating into radiation at the present epoch and have interesting astrophysical consequences. Such PBHs can contribute to the diffuse gamma-ray background [248], or positrons and antiprotons in the cosmic rays [249], and therefore can provide useful information about the high energy physics of PBH evaporation [228].

- **PBHs with $M_{PBH} > 10^{15}$ g :**
  Such PBHs would have survived till today, and interestingly they can contribute as some or all of the Dark Matter (DM) present in the Universe. (For a review, see Refs. [250, 251] and [252, 253]). If they are present, the signatures of such PBHs can be seen in different lensing experiments [254–256], or from their dynamical effects on astrophysical systems. (For a review, see Ref. [233].) Massive PBHs of a few solar masses can accrete its surrounding gas and emit X-rays, which can change the ionization history of the Universe [257] and cause spectral distortions in the CMB radiation [258, 259]. Also, there could be stochastic gravitational

waves generated from the binary PBH mergers [260–263]. (For a review, see Refs. [233, 264].)

- **PBHs with $M_{PBH} \sim 10^{-5}$ g :**
  These PBHs are interesting to study, as they are also the probes to the quantum gravity epochs. The string theory studies show that at the Planck energy scale 10^{19} GeV, the extra dimensions influence the PBH evaporation resulting in stable remnants of Planck mass [265]. These Planck mass relics are also the candidates for dark matter [266]. For a review, see Ref. [229, 230].

6.2 Formation of Primordial Black Holes

A number of phenomena could lead to PBH formation, such as the collapse of large overdensities generated in the early Universe [164, 165], or the collision of bubbles [267–269], or the collapse of strings [270, 271] and domain walls [272, 273], or during some phase transitions in which the equation of state becomes soft (reduction in pressure) for a period [274–279]. In this study, we consider the formation of primordial black holes by the collapse of overdense inhomogeneities generated during inflation. As mentioned in Chapter 2, the density fluctuations generated during the inflationary phase exit the horizon during inflation and then reenter at some later epoch in the Universe evolution. Here it is assumed that the reentry takes place in the radiation era and the collapse of perturbations into PBHs is studied.

6.2.1 Mass of the generated primordial black holes

When an overdense fluctuation with a comoving wavenumber k reenters the horizon at a later epoch (i.e. physical wavelength equals the horizon size, $H^{-1} = (k/a)^{-1}$) with an overdensity δ greater than a critical density δ_c, it collapses through gravitational instability into a primordial black hole. The mass of the generated PBH, M_{PBH} depends on the epoch of its formation and is taken to be a fixed fraction, γ of the horizon mass at that time [246],

$$M_{PBH}(k) = \gamma \, \frac{4\pi}{3} \rho \, H^{-3}\big|_{k=aH} \, , \tag{6.2}$$

where H is the Hubble expansion rate and ρ is the energy density of the Universe at the epoch of PBH formation. Here we take $\gamma = 0.2$.

It is assumed that the PBH formation takes place during the radiation dominated era. Therefore ρ is the energy density of the radiation, i.e., $\rho = \rho_r = \frac{\pi^2}{30} g_* T^4$, where g_* is the number of relativistic degrees of freedom, and T represents the temperature of the Universe in the radiation dominated era. If we assume that no out-of-equilibrium processes occur in the Universe, then from the principle of conservation of entropy, we have

$$S = g_{*s} a^3 T^3 = \text{constant},$$

where S is the entropy, a is the scale factor of the Universe, and g_{*s} represent the number of relativistic degrees of freedom contributing to the entropy. Here it is assumed that the number of relativistic degrees of freedom contributing to the radiation equals to the ones contributing to the entropy i.e. $g_* \approx g_{*s}$ (also see Ref. [280] for comments on massive neutrinos and relativistic degrees of freedom), and thus

$$T \propto g_*^{-1/3} a^{-1}, \quad \text{and} \quad \rho_r \propto g_*^{-1/3} a^{-4}.$$

With this relation, the radiation energy density at the initial time of PBH formation ρ_{ri} can be related to the present radiation energy density ρ_{r0} as

$$\rho_{ri} = \left(\frac{g_{*i}}{g_{*0}}\right)^{-1/3} \left(\frac{a_i}{a_0}\right)^{-4} \rho_{r0}. \tag{6.3}$$

The subscript '0' and 'i' to any quantity represent its value at the present epoch and at the initial time when the PBH formed, respectively. The present radiation density can be written as $\rho_{r0} = \rho_{crit}\,\Omega_{r0}$, where the critical energy density $\rho_{crit} = 3H_0^2/8\pi G_N = 1.054 \times 10^{-5} h^2$ GeV cm^{-3}, $H_0 = 100\ h$ is the present Hubble expansion rate with $h = 0.678$, and $\Omega_{r0} \approx 5.38 \times 10^{-5}$ is the radiation density parameter today [31]. Thus we can write Eq. (6.3) as

$$\rho_{ri} = \left(\frac{g_{*i}}{g_{*0}}\right)^{-1/3} a_i^{-4} \rho_{crit}\,\Omega_{r0}\ , \tag{6.4}$$

and substitute it in Eq. (6.2) to obtain the mass of the generated PBH as

$$M_{PBH}(k) = \gamma\,\frac{4\pi}{3}\left(\frac{g_{*i}}{g_{*0}}\right)^{-1/3} a_i^{-4} \rho_{crit}\,\Omega_{r0}\left(\frac{k}{a_i}\right)^{-3}$$

$$= \gamma \frac{4\pi}{3} \left(\frac{g_{*i}}{g_{*0}}\right)^{-1/3} a_i^{-1} \rho_{crit}\, \Omega_{r0}\, k^{-3}. \tag{6.5}$$

Now we will determine the scale factor a_i at the time of PBH formation, as shown in Ref. [262]. Using the Friedmann equation, the Hubble rate of expansion at the time of PBH formation, when the k^{th} fluctuation mode re-enters the horizon can be written as,

$$H_i^2 = \left(\frac{k}{a_i}\right)^2 = \frac{8\pi G_N}{3}\, \rho_{ri}. \tag{6.6}$$

By substituting the expression for the initial radiation energy density from Eq. (6.4) into this, we get

$$\left(\frac{k}{a_i}\right)^2 = \frac{8\pi G_N}{3} \rho_{crit} \left(\frac{g_{*i}}{g_{*0}}\right)^{-1/3} a_i^{-4} \Omega_{r0} \tag{6.7}$$

which gives

$$a_i^{-1} = \left(k^2 H_0^{-2} \left(\frac{g_{*i}}{g_{*0}}\right)^{1/3} \Omega_{r0}^{-1}\right)^{1/2}. \tag{6.8}$$

Finally, we substitute Eq. (6.8) in Eq. (6.5) and obtain

$$M_{PBH}(k) = \gamma \frac{4\pi}{3} \rho_{crit} \left(\frac{g_{*i}}{g_{*0}}\right)^{-1/6} \Omega_{r0}^{1/2}\, k^{-2} H_0^{-1}. \tag{6.9}$$

This relation implies that the mass of the generated PBH is proportional to the inverse square of the k^{th} mode of fluctuation that creates it, $M_{PBH} \propto k^{-2}$. Therefore, more massive PBHs form when small k modes re-enter the horizon, whereas the lighter PBHs form when large k modes re-enter the horizon, with the amplitude of power spectrum large enough to generate them. As large k mode leaves the horizon late during inflation and re-enters in the horizon first, this implies that lighter PBHs form early in the radiation era, and the small k modes corresponding to the more massive PBHs enter late and form later in the radiation era.

Further, we can express Eq. (6.9) in terms of the present horizon mass which is given as $M_0 = \frac{4\pi}{3} \rho_{crit}\, H_0^{-3} \approx 4.62 \times 10^{22} M_\odot$, where $M_\odot$ is the solar mass. This is as follows

$$M_{PBH}(k) = \gamma\, M_0 \left(\frac{g_{*0}}{g_{*i}}\right)^{1/6} \Omega_{r0}^{1/2} \left(\frac{H_0}{k}\right)^2 \tag{6.10}$$

$$\approx 5 \times 10^{15} \mathrm{g} \left(\frac{g_{*0}}{g_{*i}}\right)^{1/6} \left(\frac{10^{15}\mathrm{Mpc}^{-1}}{k}\right)^2. \tag{6.11}$$

This relation implies that for an overdense fluctuation mode with $k \sim 10^{15}$ Mpc^{-1}, PBHs of mass $M_{PBH} \sim 5 \times 10^{15}$ g are formed.

6.2.2 Initial mass fraction of PBHs

As discussed above, various mass ranges of the PBHs have different astrophysical signatures and significance. Therefore, a non-detection of PBHs in observations gives an upper limit on their present abundance, which can be further translated into constraints on the initial mass fraction of PBHs defined as

$$\beta(M_{PBH}) \equiv \frac{\rho_{PBH,i}}{\rho_{\text{total},i}} \,. \tag{6.12}$$

For any PBH of mass M_{PBH}, the initial mass fraction is the ratio of its energy density at the time of its formation, $\rho_{PBH,i}$ to the total energy density of the Universe at that epoch, $\rho_{\text{total},i}$.

As the PBH formation is assumed to take place in the radiation dominated era, the total energy density at that epoch is in the radiation, i.e. $\rho_{\text{total},i} = \rho_{ri}$, given in Eq. (6.4), while the energy density of PBHs evolve as $\rho_{PBH,i} = \rho_{PBH,0}\ a_i^{-3}$. Thus we obtain

$$\beta(M_{PBH}) = \frac{\Omega_{PBH0}(M_{PBH})}{\Omega_{r0}} \left(\frac{g_{*i}}{g_{*0}}\right)^{1/3} a_i, \tag{6.13}$$

where $\Omega_{PBH0}(M_{PBH}) = \rho_{PBH0}/\rho_{crit}$ is the density parameter for PBH of mass M_{PBH}. On substituting Eq. (6.8) in Eq. (6.13) and then using Eq. (6.11), we obtain

$$\beta(M_{PBH}) = \frac{\Omega_{PBH0}(M_{PBH})}{\Omega_{r0}^{3/4}} \left(\frac{g_{*i}}{g_{*0}}\right)^{1/4} \left(\frac{M_{PBH}}{M_0}\right)^{1/2} \gamma^{-1/2}. \tag{6.14}$$

With this relation, the observational constraints on Ω_{PBH0} for a PBH of mass M_{PBH}, can be used to calculate the upper bound on its initial mass fraction $\beta(M_{PBH})$ (see Refs. [243, 246, 247]).

Observational constraints on the initial mass fraction of PBHs

The constraints on the initial mass fraction of various mass ranges of PBHs from numerous observations are given in detail in Refs. [9, 233, 243, 247, 250, 252, 253] (Refs. [9, 252, 253] are the recent) and summarised in Fig. 6.1. Here is a brief status of the present constraints on the initial mass fraction for various mass ranges of PBHs.

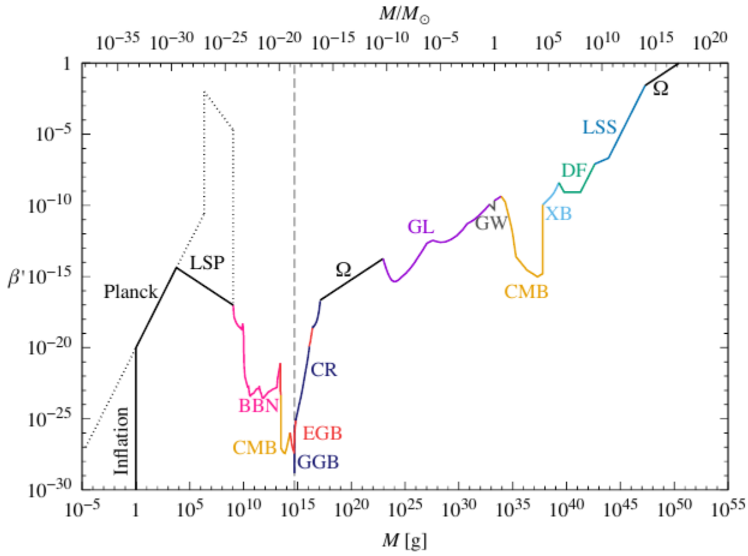

Figure 6.1: Constraints on the initial mass fraction $\beta(M_{PBH})$ versus the mass of PBH is shown here [9]. The acronyms stand for: the lightest supersymmetric paricle (LSP), big-bang nucleosynthesis (BBN), galactic gamma-ray background (GGB), extagalactic gamma-ray background (EGB), cosmic ray (CR), gravitational lensing (GL), gravitational waves (GW), X-ray binary (XB), dynamical friction (DF), large scale structure (LSS).

- The bounds on PBHs with $M_{PBH} < 10^9$g are not very stringent and are theoretically motivated. The products of the evaporation of such PBHs (stable LSP or long-lived particles) could be the signature of these PBHs. Also, these PBHs can evaporate and leave Planck mass remnants, which constrain their abundance. The lowest mass PBHs correspond to the smallest scale leaving the horizon during inflation.

- For the mass ranges 10^9g$< M_{PBH} < 10^{13}$g, the bounds are well constrained from the observations of the BBN abundances [237–239].

- PBHs in the mass ranges 10^{13}g$< M_{PBH} < 10^{14}$g are constrained from the damping of CMB anisotropies due to the modification of recombination and reionization by the evaporation of such PBHs.

- For the mass range 10^{14}g$< M_{PBH} < 10^{15}$g, the bounds are from the observations of the extragalactic and galactic gamma-ray searches.

- The constraints on PBHs with mass 10^{15}g$< M_{PBH} < 10^{17}$g are obtained from the galactic electron-positron emissions from these PBHs in the cosmic ray (CR) detectors such as Voyager 1 [281].

- PBHs with mass 10^{17}g$< M_{PBH} < 10^{19}$g are constrained from the femtolensing of the gamma-ray bursts. Such PBHs can contribute a fraction (less than 0.1) to the dark matter energy density defined as $f(M_{PBH}) \equiv \Omega_{PBH}/\Omega_{DM}$. However, also see Ref. [282] for the revised constraints. The fraction of PBH energy density contributing as the present dark matter for different mass ranges is shown in Fig. 6.2.

- The PBHs in the mass window 10^{19}g$< M_{PBH} < 10^{22}$g are interesting as they could constitute the entire dark matter. Hence, the only constraint on such PBHs is that their abundance should not overclose the energy density of the Universe ($\Omega_{PBH} \leq \Omega_{DM}$).

- Recent observations of microlensing of the stars in the Andromeda galaxy by Subaru Hyper Suprime-Cam (HSC) suggest that PBHs in the mass range 10^{22}g$< M_{PBH} < 10^{27}$g can constitute only a small fraction $< 0.1\%$ of the dark matter energy density [283].

- There are other microlensing observations of stars in the Magellanic clouds like by OGLE, EROS, MACHO, which probe the PBHs over the mass range $10^{-7}M_{\odot} < M_{PBH} < 10M_{\odot}$. (For reference, $M_{\odot} \sim 10^{33}$ g.)

- The abundance of PBHs of mass $10M_{\odot} < M_{PBH} < 100M_{\odot}$ is also constrained from the lensing of Fast Radio Bursts (FRB) and pulsars. The observations with Square Kilometer Array (SKA) has put a constraint on the fraction of such PBHs as dark matter to be < 0.01.

- Apart from lensing, the dynamical effects of PBHs can also constrain its abundance. PBHs with mass 10^{19}g$< M_{PBH} < 10^{20}$g can trigger a white dwarf (WD) to explode as they pass nearby. Other constraint for PBHs with mass 10^{18}g$< M_{PBH} < 10^{24}$g arise from capture by a neutron star [284].

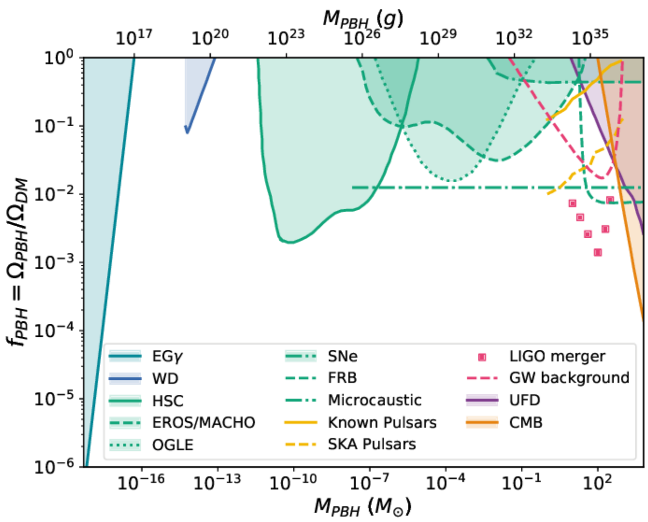

Figure 6.2: The fraction of PBH energy density contributing as the dark matter, as constrained from various observations [10].

- A crucial point about PBHs is that they can be of subsolar mass, unlike the black holes produced from stellar evolution, which are always heavier than a solar mass. A non-detection of binary PBH merger ($0.2M_\odot < M_{PBH} < 1M_\odot$) by LIGO gives the constraints on the fraction as DM. Further, PBHs with mass $0.5M_\odot < M_{PBH} < 30M_\odot$ are also constrained from the gravitational wave background observations.

- Massive PBHs $10M_\odot < M_{PBH} < 10^4M_\odot$ are constrained from their accretion effects on the ionization history and its observations in the CMB spectral distortions. Also, PBHs can capture a nearby star and form an accretion disk while emitting X-rays. The searches for these high mass X-ray binaries are used to constraint the abundance of such PBHs with $10M_\odot < M_{PBH} < 10^7M_\odot$.

- The effects of dynamical friction and disk heating are important for the supermassive PBHs $10^6M_\odot < M_{PBH} < 10^9M_\odot$ and thus constraints their abundance.

- It is also proposed that PBHs can become the seeds for structure formation. Thus, observations of Lyman-α forest, dwarf galaxies, galaxy clusters give upper limits on the abundance of PBHs over a mass range of $10^4M_\odot < M_{PBH} < 10^{14}M_\odot$.

6.2.3 Press-Schechter theory for the PBH formation

Now we discuss the Press-Schechter theory for the formation of a primordial black hole. We assume that the initial gaussian seeds of density perturbations re-enter the horizon during the radiation dominated epoch and the PBH formation takes place in the regions with overdensity above a critical value, $\delta > \delta_c$ where $\delta_c \sim \mathcal{O}(1)$ [166] (see Refs. [285], [286] for more details).

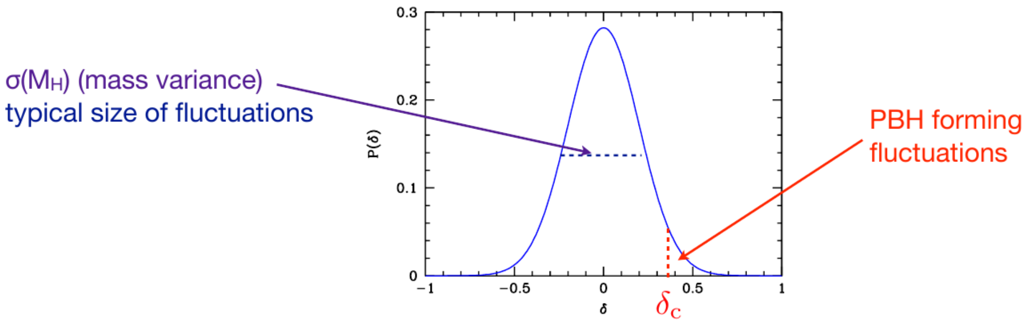

Figure 6.3: Gaussian probability distribution $p(\delta)$ of the density fluctuation δ is plotted here [11]. The width of the distribution shown here $\sigma(M_H)$ can be related to $\sigma(R)$ in the text, as M_H and R are related.

On smoothening the density perturbations using a Gaussian window function, the probability distribution for a smoothed density contrast over a radius $R = (aH)^{-1}$ is given as [287],

$$p(\delta(R)) = \frac{1}{\sqrt{2\pi}\sigma(R)} \exp\left(\frac{-\delta^2(R)}{2\sigma^2(R)}\right). \tag{6.15}$$

This is shown in Fig. 6.3. Here $\sigma(R)$ is the mass variance evaluated at the horizon crossing, and is defined as,

$$\sigma^2(R) = \int_0^\infty \tilde{W}^2(kR)\Delta_\delta^2(k)\frac{dk}{k}, \tag{6.16}$$

where $\Delta_\delta^2(k) = \dfrac{k^3}{2\pi^2}\langle|\delta_k|^2\rangle$ is the dimensionless matter power spectrum, and $\tilde{W}(kR)$ is the Fourier transform of the window function

$$\tilde{W}(kR) = \exp(-k^2R^2/2). \tag{6.17}$$

The dimensionless primordial curvature power spectrum $\Delta_{\mathcal{R}}^2(k)$ for the fluctuations generated during the inflation can be related to the dimensionless density power spectrum $\Delta^2_\delta(k)$ as [288],

$$\Delta^2_\delta(k) = \frac{4(1+w)^2}{(5+3w)^2}\left(\frac{k}{aH}\right)^4 \Delta^2_{\mathcal{R}}(k), \tag{6.18}$$

where w is the equation of state of the fluid and is equal to 1/3 for radiation.

Theoretical calculation of initial mass fraction of PBHs

Using the Press-Schechter theory, the initial mass fraction of a PBH with mass $M_{\rm PBH}$ is obtained as [289],

$$\begin{aligned}\beta(M_{PBH}) &= 2\int_{\delta_c}^{1} p(\delta(R))\, d\delta(R) = \frac{2}{\sqrt{2\pi}\sigma(R)}\int_{\delta_c}^{1} \exp\left(\frac{-\delta^2(R)}{2\sigma^2(R)}\right) d\delta(R) \\ &= \mathrm{erfc}\left(\frac{\delta_c}{\sqrt{2}\sigma(R)}\right), \end{aligned} \tag{6.19}$$

where erfc is the complimentary error function, and we consider $\delta_c = 0.5$ in this study. For any parameterization of the primordial power spectrum, we carry out the integration in Eq. (6.20) by using Eq. (6.18), and then substitute the obtained mass variance into Eq. (6.19).

The expression thus obtained for $\beta(M_{PBH})$ using Press-Schechter theory is equated to Eq. (6.14), and constrained using the observational bounds on $\Omega_{PBH0}(M_{PBH})$, as argued in the previous subsection. In this way, the primordial power spectrum, and hence inflationary models are constrained from the bounds on abundance of PBHs [244–247]. For the various mass of PBHs, the upper bound on the amplitude of the primordial power spectrum is obtained to be, $\Delta^2_{\mathcal{R}}(k_{PBH}) \sim \mathcal{O}(10^{-2} - 10^{-1})$ [232, 233], as shown in Fig. 6.4.

6.3 PBH formation from various models of inflation

PBHs are a unique probe to inflation, and the observational bounds on the abundance of PBHs provide an upper limit on the amplitude of the primordial power spectrum. Therefore, a study of PBHs is crucial to test various inflationary models.

In the literature, there are a lot of studies which discuss the PBH production from the collapse of large inhomogeneties generated from various inflationary scenarios.

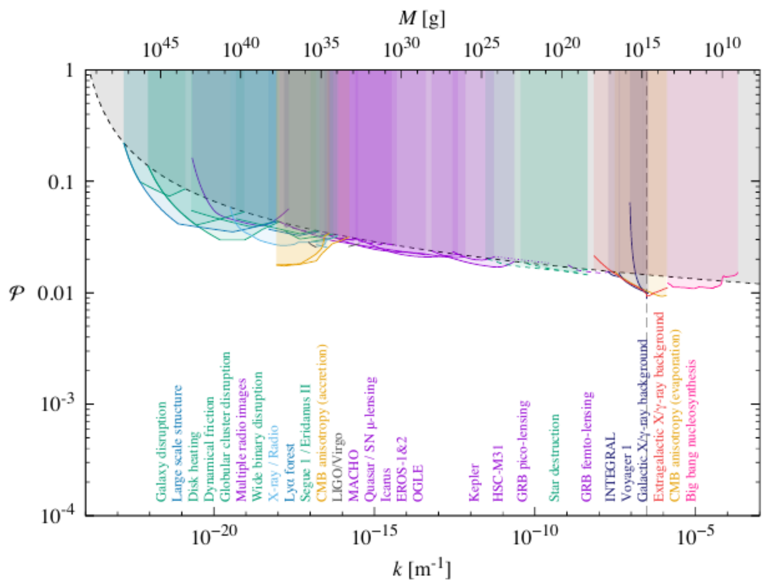

Figure 6.4: Upper bound on the primordial power spectrum obtained from observations for various mass of PBHs corresponding to comoving wavenumber k. *Source*: [9].

Some examples are the hybrid inflation models [290–292], running-mass inflation models [293–296], hilltop inflation model [297], inflating curvaton model [298], axion curvaton inflation model [299, 300], double inflation model [301, 302], thermal inflation [303], single field inflation with a broken scale invariance [304], or by introducing a inflection point (plateau) in the potential [251, 305], running of the spectral index [306, 307], etc. It is shown in Ref. [308] that for a power-law form of the primordial power spectrum, $\Delta^2_{\mathcal{R}}(k) = A_s(k/k_P)^{n_s-1}$, the spectral index has to be blue-tilted ($n_s > 1$) at the small scales for a significant formation of PBHs. But from the CMB observations, the spectral index of the power spectrum is precisely measured to be red-tilted ($n_s < 1$) at the large scales. If the running of the spectral index, α_s, and running of the running, β_s are also considered in the primordial power spectrum, $\Delta^2_{\mathcal{R}}(k) = A_s(k/k_P)^{n_s(k)-1}$, where $n_s(k) = n_s(k_P) + \alpha_s \ln(k/k_P) + \beta_s \ln^2(k/k_P)$, then the amplitude of the power spectrum can become $\Delta^2_{\mathcal{R}}(k) \sim \mathcal{O}(10^{-2})$ for some values of n_s, α_s, β_s allowed from the CMB observations. However, Ref. [309] shows that such a Taylor series expansion of $n_s(k)$ in the parameterization of $\Delta^2_{\mathcal{R}}(k)$ can lead to large errors in the amplitude of primordial power spectrum at the small scales and hence PBH formation.

6.4 Formation of PBHs from warm inflation

Now I discuss the formation of primordial black holes from warm inflation. In this study, we consider a quartic potential of warm inflation $V(\phi) = \lambda\phi^4$ with a cubic dissipation coefficient $\Upsilon = C_\phi T^3/\phi^2$. As discussed in Chapter 3, this kind of dissipation coefficient is calculated for supersymmetric models of warm inflation with a two-stage decay mechanism, in which the inflaton couples to intermediate X superfields, which then decay into Y superfields which thermalize to form a radiation bath. The primordial power spectrum in warm inflation is sourced dominantly by the thermal fluctuations of the fields and is characterized in terms of the inflaton self-coupling and a dissipation parameter, which is a measure of inflaton couplings to the other fields.

The motivation for considering this warm inflation model is that it is the simplest renormalizable potential, and in our study [310], we found that it is consistent with the CMB observations for some parameter space of the model parameters. Also, the tensor-to-scalar ratio prediction for this model is within the sensitivity of the next generation CMB polarisation experiments and therefore, can be tested in the near future. Furthermore, we shall see that the primordial power spectrum for this model of warm inflation has the amplitude required for PBH generation. These features arise due to the intrinsic properties of the inflaton-radiation system and therefore are interesting to study.

As discussed in Section 3.3.4, that there is a growth factor in the power spectrum due to the coupling of radiation fluctuations to the inflaton fluctuations. This factor plays an important role in the enhancement of power at the small scales, as we show next. Thus, the choice of the dissipation coeffient in this study determines whether the enhancement of power as required for the formation of primordial black holes can be achieved.

For a dissipation coefficient with a cubic dependence on the temperature of the thermal bath $\Upsilon \propto T^3$, the numerically obtained growth factor is given as [156, 190]

$$G(Q_k)_{cubic} = 1 + 4.981\, Q_k^{1.946} + 0.127\, Q_k^{4.330}.$$

We also list the growth factor for $\Upsilon \propto T$ and $\Upsilon \propto 1/T$, as given in Refs. [156, 171, 190]

$$\text{For } \Upsilon \propto T, \quad G(Q_k)_{linear} = 1 + 0.0185\, Q_k^{2.315} + 0.335\, Q_k^{1.364}.$$

$$\text{For } \Upsilon \propto 1/T, \quad G(Q_k)_{inverse} = \frac{1 + 0.4\, Q_k^{0.77}}{(1 + 0.15 Q_k^{0.1.09})^2}.$$

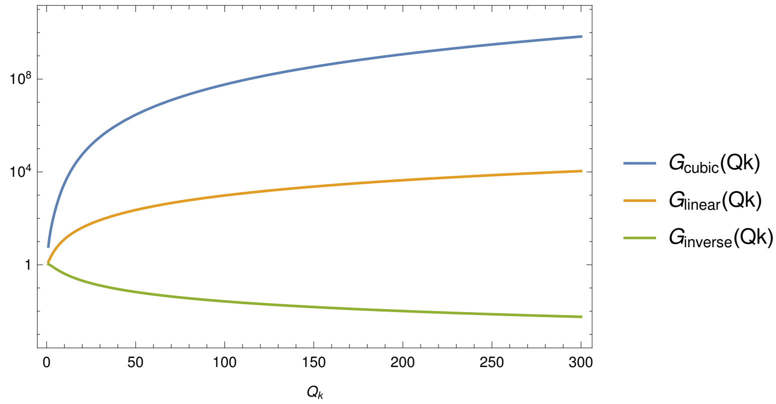

Figure 6.5: Plot of the growth functions in the primordial power spectrum for $\Upsilon \propto T^3, T$ and $1/T$.

In Fig. 6.5, we plot the different growth functions for some forms of dissipation coefficients considered in warm inflation studies. We can see in this plot that for a cubic dissipation, the growth is huge for large value of the dissipation parameter, whereas for a linear dissipation, there is not that large enhancement in the growth factor. For a dissipation coefficient inversely dependent on the temperature, there is rather a suppression in the power for large Q_k values, and it also not very large. As we discussed in the previous Chapters, the dissipation coefficient increases as inflation proceeds in the case of $\Upsilon \propto T^3$, T and near the end of inflation, it can have a large value ($\mathcal{O}(100)$). Thus, we argue that a cubic dissipation coeffiecient is the most suitable for PBH studies, as the primordial power spectrum is hugely enhanced in this case.

6.4.1 Features in the primordial power spectrum

In our earlier study [310], we parameterized the primordial power spectrum in terms of two model parameters - the inflaton self-coupling, λ, and the dissipation parameter at the pivot scale, Q_P, and estimated them using CMB observations. By using the same parameterization, we study the formation of small scale PBHs for our warm

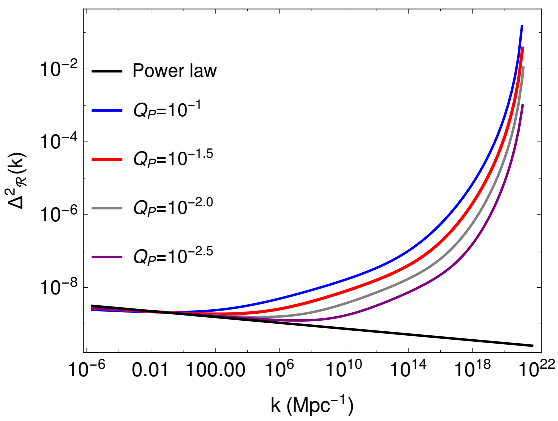

Figure 6.6: Plot of the primordial power spectrum $\Delta^2_{\mathcal{R}}(k)$ versus k for our warm inflation model with different values of Q_P. Here the black line represents the standard power law parameterization considered in cold inflation.

inflationary model considering different values of Q_P in this work. For each Q_P value, we consider λ such that the primordial power spectrum is normalized at the pivot scale as $\Delta^2_{\mathcal{R}}(k_P) = 2.1 \times 10^{-9}$.

We first plot the primordial curvature power spectrum for our warm inflation model as a function of the comoving wavenumber k in Fig. 6.6. For that, we fix the number of efolds when the pivot scale leaves the horizon, $N_P = 60$ (in our notation, $N_e = 0$ at the end of inflation). As already mentioned, PBHs provide a probe for a vast range of small scale modes. Here we consider only those k modes that leave the horizon near the end of inflation and form PBHs when they reenter in the radiation era. In order to produce a significant number of PBHs that can have measurable observational consequences, the amplitude of $\Delta^2_{\mathcal{R}}(k)$ needs to be $\mathcal{O}(10^{-2})$. We consider various cases of inflation with different values of the dissipation parameter at the pivot scale, $Q_P = 10^{-1}, 10^{-1.5}$, 10^{-2}, and $10^{-2.5}$ (weak dissipation regime when the CMB scales exit the horizon) to plot Fig. 6.6.

We also plot the power-law power spectrum parameterization, considered in cold inflation (without running of n_s) (black line) in Fig. 6.6 for comparison. It can be seen that for a power-law power spectrum, as the spectrum is red-tilted ($n_s < 1$), the amplitude of $\Delta^2_{\mathcal{R}}(k)$ can never reach the value $\mathcal{O}(10^{-2})$, and therefore a negligible abundance of PBHs can be produced for such a form of $\Delta^2_{\mathcal{R}}(k)$. But for our model of warm inflation, we find that the power spectrum changes to blue-tilted ($n_s > 1$) at the PBH scales and therefore PBH formation can take place for some range of model parameters.

As can be seen, for some Q_P values in the weak dissipation range, a large amplitude of $\Delta^2_{\mathcal{R}}(k)$ is achieved near the end of inflation at $k \sim 10^{21}$ Mpc^{-1}. These small scale modes leave the horizon when inflation is near its end, and then reenter in the horizon during radiation dominated era. When they reenter, these overdense perturbations collapse to form the primordial black holes, as discussed in Section 6.2. For the strong dissipation regime of warm inflation also, the amplitude of $\Delta^2_{\mathcal{R}}(k)$ at small scales is $\mathcal{O}(10^{-2})$ and higher, but those cases are not of interest, for the reason discussed in Section 6.4.2.

Now we discuss the effects of the inflaton dissipation during warm inflation to the primordial power spectrum. It can be seen from Fig. 6.6 that at the PBH scales (large k), for a large dissipation parameter Q_P, the amplitude of the primordial power spectrum $\Delta^2_{\mathcal{R}}(k)$ is larger as compared to the smaller dissipation case. This implies that for a large Q_P, the amplitude of $\Delta^2_{\mathcal{R}}(k)$ is enhanced to $\mathcal{O}(10^{-2})$ at a comparatively smaller k, and all the larger k modes leaving the horizon further are sufficiently overdense to form PBHs. From the plot, it is also seen that for $Q_P < 10^{-2.0}$, the amplitude of the primordial power spectrum is not sufficient to generate a significant abundance of PBHs. Therefore, we limit our study of PBH formation till $Q_P = 10^{-2}$.

6.4.2 Relevant range of the dissipation parameter

In Chapter 4, we plotted the spectral index plot for this model in Fig. 4.6, and listed the values of the dissipation parameter consistent with the CMB in Table 4.2. In our analysis here, we use this information in the study of PBHs. We see that only a range of Q_P values in the weak dissipation regime ($10^{-3.2}$ to $10^{-1.7}$) are consistent with the CMB observations. Therefore we do not consider $Q_P > 10^{-1.7}$, despite the fact that the amplitude of the primordial power spectrum at PBH scales is large.

6.5 Results and Discussion

Till now, we have found that for a certain range of Q_P values for our warm inflation model, the amplitude of the primordial power spectrum at the PBH scales, $\sim \mathcal{O}(10^{-2})$, required to generate a significant abundance of PBHs, which can have measurable observational consequences. Now, I discuss the results obtained for the mass and the mass fraction of the PBHs generated from our model. Further, I also discuss the constraints and implications of these PBHs.

6.5.1 Mass and the Initial mass fraction of the PBHs formed

For each scenario of our warm inflation model, represented by the different values of Q_P, we plot the primordial power spectrum $\Delta^2_{\mathcal{R}}(k)$ as a function of k, as shown in Section 6.4.1. Then we fit an approximate function $f(k)$ to $\Delta^2_{\mathcal{R}}(k)$ numerically for all our models. By substituting them in Eq. (6.18), we carry out the integration in Eq. (6.20) to obtain the mass variance $\sigma(R)$ as

$$\sigma^2(R) = \int_0^\infty \exp(-k^2R^2)\frac{16}{81}\left(\frac{k}{aH}\right)^4 f(k)\frac{dk}{k}. \tag{6.20}$$

Here $R = (aH)^{-1} = k^{-1}$ at the horizon crossing, which is related to M_{PBH} through Eq. (6.11) as

$$R = \left[\frac{M_{PBH}}{5\times 10^{15}\mathrm{g}}\left(\frac{g_{*i}}{g_{*0}}\right)^{1/6}\right]^{1/2}\frac{1}{10^{15}}\mathrm{Mpc}. \tag{6.21}$$

The obtained mass variance is then substituted in the expression for the initial mass fraction for the PBHs in Eq. (6.19), $\beta(M_{PBH}) = \mathrm{erfc}\left(\frac{\delta_c}{\sqrt{2}\sigma(R)}\right)$ and calculated numerically. δ_c is taken to be 0.5.

Here we plot the obtained inital mass fraction $\beta(M_{PBH})$ of the generated PBH versus the mass of the PBH in Fig. 6.7 for the cases when $Q_P = 10^{-1.7}, 10^{-1.8}, 10^{-1.9}$, and 10^{-2}.

From Fig. 6.7, we can see that the mass of PBHs generated from our warm inflation model is of the order $M_{PBH} \sim 10^3$ g. From the plots, we infer that a large dissipation during inflation leads to a comparatively more massive PBH formation, whereas small dissipation produces small mass PBHs. The reason for this is that, as shown in Fig. 6.6, for a larger dissipation, the desired amplitude of the primordial power spectrum

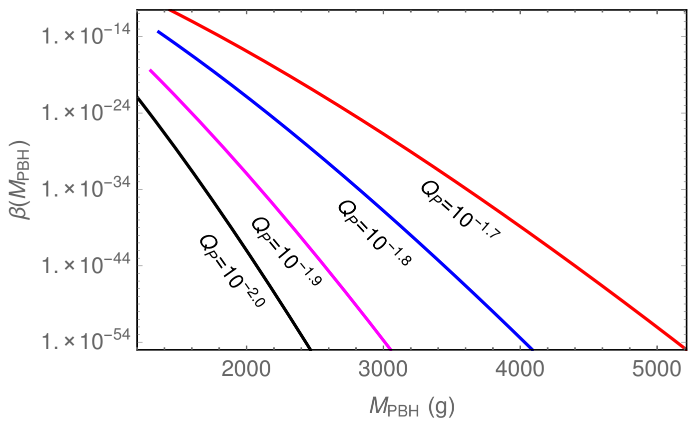

Figure 6.7: Plot of the initial mass fraction of the generated PBH, $\beta(M_{PBH})$, versus its mass $M_{PBH}(g)$.

$\Delta^2_{\mathcal{R}}(k_{PBH}) \sim \mathcal{O}(10^{-2})$, is achieved at a comparatively smaller k, and as the mass of the generated PBH is proportional to k^{-2}, this implies that larger dissipation leads to more massive PBH formation.

6.5.2 Constraints on the abundance of generated PBHs

As discussed in Section 6.4, the range of Q_P values of our model, relevant for our study is very small, and a significant PBH formation takes place only near the end of inflation at $k \sim 10^{21}$ Mpc^{-1}. Thus, as a consequence, a small mass range of the generated PBHs is generated from our warm inflation model. The order of the mass of the PBHs formed, $M_{PBH} \sim 10^3$ g. There is a minimum mass of PBH that is formed, corresponding to the maximum k mode that exits the horizon ($M_{PBH} \propto k^{-2}$), as shown in Eq. (6.11). These PBHs emit Hawking radiation [235, 236] with temperature

$$T_{BH} = \frac{1}{8\pi G_N M_{PBH}} \approx \frac{10^{13}\text{g}}{M_{PBH}}\text{GeV} \tag{6.22}$$

and evaporate into all elementary particles with rest mass less than the black hole temperature on timescale given by [311]

$$\tau(M_{PBH}) = \frac{5120\pi G_N^2 M_{PBH}^3}{\hbar c^4} \sim 10^{10}\text{yr}\left(\frac{M_{PBH}}{10^{14}g}\right)^3, \tag{6.23}$$

Thus, the tiny mass (10^3g) PBHs formed from our warm inflation model would have fully evaporated in a short lifetime of $\sim 10^{-16}$ sec. Interestingly, there are studies which discuss a mechanism to stabilize the light PBHs against evaporation so that it comprises the present dark matter density [266, 312–315].

The abundance of tiny mass PBHs is not strictly bounded; it depends on the physics beyond the Standard Model of particle physics. There are certain bounds from the PBH evaporation leading to the generation of stable massive particles (Supersymmetric LSP) [240] or long-lived decaying particles (eg. gravitino, modulii) [241, 242], and their relic abundance, which can be used to put constraints on PBH initial abundance [232, 243, 247]. Stable supersymmetric particles may contribute as the present dark matter; therefore, their abundance should be constrained so that they do not overclose the Universe. The initial mass fraction of PBH depends on the mass of the LSP emitted and the upper bound on it is given as [243, 247]

$$\beta(M_{PBH}) \leq 10^{-18}\left(\frac{M_{PBH}}{10^{11}\text{g}}\right)^{-1/2}\left(\frac{m_{LSP}}{100\text{ GeV}}\right)^{-1}. \tag{6.24}$$

For a PBH with mass $\sim 10^3$g evaporating into LSP of mass $m_{LSP} = 100$ GeV, the upper bound on the abundance $\beta(M_{PBH})$ is 10^{-14}. For various scenarios (different Q_P) of our warm inflation model, we find that the calculated initial abundance of PBHs (of all masses) is in accordance with this limit for $Q_P = 10^{-1.8}, 10^{-1.9}$, and $10^{-2.0}$. But for the case with $Q_P = 10^{-1.7}$, the theoretical estimate of the initial mass fraction for PBHs with masses $M_{PBH} < 1800$ g is higher than the above mentioned constraint. This implies that for $Q_P = 10^{-1.7}$, there is an overproduction of PBHs above mass 1800g and therefore the abundance of PBHs for this masses is inconsistent with the observations.

Additionally, PBH evaporation can lead to a large abundance of gravitinos and modulii which has important cosmological consequences. These quasi-stable massive particles decay into energetic particles, which destroy the nuclei of the light elements created in the era of nucleosynthesis. Thus, the abundance of PBHs evaporating into such species should be controlled so that these problems can be avoided, which gives another bound on their initial mass fraction as [243, 247]

$$\beta(M_{PBH}) \leq 5\times 10^{-19}\left(\frac{M_{PBH}}{10^{9}\text{g}}\right)^{-1/2}\left(\frac{Y_\phi}{10^{-14}}\right)\left(\frac{x_\phi}{0.006}\right)^{-1}, \tag{6.25}$$

where Y_ϕ is the ratio of number density to entropy density and x_ϕ is the fraction of the luminosity in quasi-stable massive particles. To an order of magnitude, for $M_{PBH} \sim$

10^3 g, the upper bound on $\beta(M_{PBH}) < 10^{-16}$. This is a stronger bound than from the LSP. We find that for our warm inflation model, the calculated initial abundance of PBHs is in accordance with the observational limit for $Q_P = 10^{-1.9}$ and $10^{-2.0}$. But for the cases with $Q_P = 10^{-1.7}$ and $10^{-1.8}$ of our model, the theoretical estimate of the abundance is higher than the upper limit on the initial mass fraction for certain PBH masses, which implies that in these models, PBHs of certain masses are overproduced and thus inconsistent with the observations.

6.5.3 PBH relics as a constituent of dark matter

Here we explore the possibilty that the evaporation of PBHs cease when the black hole mass reaches the Planck scale M_{Pl}, resulting in stable relics of Planck mass [316], which can contribute to the dark matter as proposed in Refs. [266, 314]. In the literature, there are many studies which lead to the formation of remnants. Some examples include Refs. [317–319], where it is shown that by invoking a generalized uncertainty principle (GUP), the Hawking temperature can be modified and the evaporation of a black hole can be stopped, thus leading to a Planck mass remnant. Some other examples are based on modified gravity and string theories, like including higher curvature terms of the dilaton field or gravity theories derived from Lovelock form of gravitational Lagrangian, in which the black hole solutions are modified, and thus remnants could be produced [312]. There are also primordial extremal black hole solutions, like in Ref. [315], which lead to stable black hole remnants. For a comprehensive review on the challenges for the existence and stability of Planck mass remnants and its current status, see Ref. [320, 321].

The black hole remnants can be possible candidates of the dark matter in the Universe. In order that the Planck mass relics do not overclose the Universe today, the present density of Planck mass relics should be less than the present cold dark matter density $\Omega_{CDM} \approx 0.25$, which gives an upper bound on the initial mass fraction of the PBH as [313]

$$\beta(M_{PBH}) < 8 \times 10^{-28} \kappa^{-1} \left(\frac{M_{PBH}}{M_{Pl}} \right)^{3/2}, \tag{6.26}$$

where the remnant mass equals κM_{Pl}. To an order of magnitude, the constraints on the initial mass fraction of PBH of mass $M_{PBH} \sim 10^3$ g, is given to be $\beta(10^3 g) < 10^{-16}$

to avoid overclosure of the Planck mass ($\kappa \sim 1$) remnants of their evaporation. We find that in our warm inflation models with $Q_P = 10^{-1.9}$, and $Q_P = 10^{-2}$, the initial mass fraction lies within the above estimated limits, and therefore the possibility that PBH remnants form DM, remains valid for these cases. But as the Planck mass relics are tiny, it is extremely difficult or nearly impossible to observationally detect them non-gravitationally. However, in Ref. [322], it is argued that if such relics carry an electric charge, then they can be explored in the direct detection experiments in the near future. A detection of such events would be crucial to deepen our understanding of the dark matter and black holes physics.

6.6 Summary

Primordial Black Holes are a remarkable probe to the physics of the early Universe. They provide us an opportunity to investigate a huge range of small scales perturbations generated during the inflationary phase. In this study, we consider one model of warm inflation and discuss the PBH formation by the collapse of large inhomogeneities generated during it. The inflaton dissipation during warm inflation enhances the amplitude of the primordial power spectrum at the small scales to $\mathcal{O}(10^{-2})$, as required to generate a significant abundance of PBHs.

We find that for some parameter range of our model, PBHs can be generated with a significant abundance. We consider those cases with values of the dissipation parameter at the pivot scale as, $Q_P = 10^{-1.7}, 10^{-1.8}, 10^{-9}, 10^{-2}$. We calculate the initial mass fraction and the mass of the generated PBHs for these values of the dissipation parameter. We obtain that our model of warm inflation can produce a significant abundance of PBHs with mass, $M_{PBH} \sim 10^3$ g. Such tiny mass PBHs have a very short lifetime of 10^{-16} sec and would have evaporated into Hawking radiation. Our analysis shows that for the cases with $Q_P = 10^{-1.9}, 10^{-2.0}$, the obtained initial mass fraction is in accordance with the upper limit obtained from the abundance of stable and long-lived decaying particles produced by evaporating PBHs. But the cases with $Q_P = 10^{-1.7}, 10^{-1.8}$ overproduce PBHs of certain masses, which is inconsistent with the upper bounds on β.

Furthermore, it is also argued that PBH evaporation ceases when PBH mass gets close to the Planck mass, and such Planck mass relics can thus constitute the present dark matter. The present density of the Planck mass relics should be less than the cold dark matter density so that it does not overclose the Universe today. This gives a rough upper bound on the PBH initial mass fraction for a PBH of mass 10^3 g of $\mathcal{O}(10^{-16})$. For our warm inflation models with $Q_P = 10^{-1.9}$, and $Q_P = 10^{-2}$, we find that the calculated initial mass fraction lies within the limits, and hence the possibility to form DM remains valid. The Planck mass relics are extremely tiny and almost impossible to detect by non-gravitational measures. But if they carry an electric charge, then they may be possibly detected in the dark matter direct detection experiments, which will have a lot of implications for the black hole physics and dark matter.

Chapter 7

Summary and Conclusions

The inflationary paradigm of the early Universe has been extraordinarily successful and consistent with the observations of the cosmic microwave background radiation. However, the microphysics governing inflation is not well understood and tested. There are two approaches to describe the dynamics of inflation, one is the standard cold inflation, in which it is assumed that the Universe attains a supercooled state because of an enormous dilution of the number densities of particles during the inflationary phase. The second is a more general description, known as *Warm Inflation*, in which the inflaton interactions and dissipation to other fields during inflation are not neglected. Thus, as a consequence of particle production, the Universe has a finite temperature during warm inflation. The description of warm inflation arises from the fundamental principles of a coupled inflaton-radiation system, which makes it interesting. In this thesis, we focus on warm inflation and investigate its implications on cosmological (large scale) and astrophysical (small scale) observations.

In Chapter 1, I discussed the shortcomings of the Standard Model of cosmology in explaining the uniformity of the cosmic microwave background radiation temperature and the extreme fine-tuning needed to address the spatial flatness of the present Universe. By introducing a phase of inflation in the early Universe, these problems can be resolved.

In Chapter 2, I discussed the dynamics of standard cold inflation in terms of a scalar inflaton field. Using linear perturbation theory, all the physical quantities (metric and matter fields) are separated into their classical background values and perturbations. A gauge-invariant quantity, known as comoving curvature perturbation, $\mathcal{R}$ is constructed from the inflaton and metric scalar perturbations. The two-point correlation of this quantity gives the primordial curvature power spectrum, $\Delta^2_{\mathcal{R}}(k)$ characterized by amplitude, A_s, and tilt n_s at the pivot scale. The anisotropies in the CMB temperature are sourced by the primordial curvature power spectrum generated during inflation. Thus, various inflationary models are tested by comparing their theoretically predicted values with the measured observables. Similar to scalar perturbations, tensor fluctuations are also generated during inflation, with an amplitude of A_T. The signatures of these tensor fluctuations are looked for in the B-mode polarization of the CMB. As no successful observation has been made to date for the detection of B-modes, we have an upper bound on the amplitude A_T. The ratio of the tensor to the scalar amplitudes is known as the tensor-to-scalar ratio r. With the precision measurements of CMB, stringent bounds have been put on the parameters n_s and r, which gives constraints on the various inflationary models.

In Chapter 3, I discussed the warm inflation scenario and its associated dynamics. The kinematics of inflaton during warm inflation is modified due to an extra friction term arising from the inflaton couplings with other fields. This term is quantified by a dissipation parameter, which can play a dominant (for strong dissipation $Q \gg 1$) or a subdominant role (for weak dissipation $Q < 1$) during warm inflation. The primordial power spectrum during warm inflation is sourced by both the thermal and quantum fluctuations, unlike in cold inflation where only quantum fluctuations play a role. Also, the value of the tensor-to-scalar ratio is lowered in warm inflation, allowing for the viability of some models which are ruled out in cold inflation.

In Chapters 4 and 5, we considered models of warm inflation with monomial potentials ($V(\phi) = \lambda\phi^4$ and $\lambda\phi^6/M_{Pl}^2$) and two forms of the dissipation coefficient ($\Upsilon \propto T^3$ and $\Upsilon \propto T$). These potentials of cold inflation have been ruled out from the current allowed $n_s - r$ bounds. In our study, we determined the parameter space for which these potentials could be viable models of inflation. The information of the range of parameters then provides the foundation stone to build warm inflation from some high energy physics theory. The primordial curvature power spectrum for these models is parameterized in terms of the inflaton self-coupling λ and the dissipation parameter at the pivot scale Q_P, arising due to the inflaton's dissipation into the other fields. After choosing suitable priors, a Markov Chain Monte Carlo was performed for both strong and weak dissipation regimes of these models using CosmoMC, and the joint and marginalized values of these parameters were obtained. We obtain the quantities C_ϕ or C_T for the obtained mean values or limits of λ and Q_P, which provide us information about the couplings and multiplicities of fields in the warm inflation models. Further, we also calculated the n_s and r values for the mean values of the parameters and found that for the weak dissipative regime, the tensor-to-scalar ratio is within the sensitivity of the next generation CMB polarization experiments, which is an important observational test for these models.

During inflation, scalar fluctuations of a wide range of comoving wavenumbers is generated. The physical wavelengths of these perturbation modes stretch during inflation with the scale factor and leave the horizon when their wavelength exceeds the horizon size. These fluctuation modes then reenter the horizon at some later epochs of the Universe evolution and then grow in amplitude to become the structures at late time. Small scale fluctuations, if sufficiently overdense, can collapse by gravitational instability into compact objects, called Primordial Black Holes (PBHs). PBHs are a remarkable probe to the physics of the early Universe and the inflationary epoch. The observational constraints on the abundance of various mass ranges of PBHs provide a limit on the amplitude of the primordial curvature power spectrum at the small scales. In Chapter 6, I discussed the formation of primordial black holes during warm inflation. I considered a model of warm inflation with a potential $V(\phi) = \lambda\phi^4$ and dissipation coefficient $\Upsilon = C_\phi T^3/\phi^2$. The primordial curvature power spectrum for this model is consistent with the CMB observations for some range of parameters, and also has a large amplitude at the small scales, as required to form a significant abundance of primordial black holes. This feature arises naturally in this model of warm inflation, which makes it interesting. It is found that PBHs with mass, $M_{PBH} \sim 10^3$g can be generated in this model for cases with Q_P values between $10^{-2.0}$ and $10^{-1.7}$. Such tiny mass PBHs have a very short lifetime of 10^{-16} sec and would have evaporated into Hawking radiation. Further, I discussed the observational and theoretical bounds on the abundance of such PBHs. It is seen that for the cases with $Q_P = 10^{-1.9}, 10^{-2.0}$, the initial mass fraction of PBHs is in accordance with the upper limit on black hole abundances, but the cases with $Q_P = 10^{-1.7}, 10^{-1.8}$ overproduce PBHs of certain masses, which is inconsistent with the upper bounds on β. Furthermore, I also discuss the possibilty that Planck mass remnants of the evaporating PBHs can constitute the present dark matter. The initial mass fraction of these PBHs is constrained so that the remnants do not overclose the Universe. It is seen that for the cases $Q_P = 10^{-1.9}$, and 10^{-2}, the calculated initial mass fraction satisfy the constraints, and hence the possibility for PBHs to form dark matter remains valid. The Planck mass relics are extremely tiny and almost impossible to detect by non-gravitational measures. But if they carry an electric charge, then they may be possibly detected in the dark matter direct detection experiments, which will have a lot of implications for the physics of black holes and dark matter.

To conclude, warm inflation is a well-motivated and interesting description of inflation, in which one accounts for the dissipation processes and non-equilibrium effects during inflation. The present demand of inflation model building is to construct models with a physical motivation that can be successfully embedded in a UV complete theory. Recent warm inflation studies are progressing in this aspect. The upcoming CMB experiments will hunt for the B-mode polarization and non-Gaussianities, and warm inflation offers a promising subject of research in this direction.

Appendix A

Thermal Field Theory

An ensemble of interacting particles in a thermodynamical or near thermodynamical equilibrium setup is described using a framework of thermal field theory (TFT) [187, 188]. This formalism is applied in the study of hot plasmas - such as the quark gluon plasma (QGP) in heavy ion colliders and the early hot and dense Universe [186].

For systems which are slighly away from equilibrium, the real time formalism (RTF) of thermal field theory is used to study the field dynamics. This formalism was developed by Schwinger, Mills, and Keldysh, in which a Closed Time Path (CTP) contour is considered in a complex plane, as shown in Fig. A.1. Starting from some initial time t_i on the negative real axis, the contour C_1 runs to some positive real time t_f, then it moves vertically down on C_3 to $t_f - i\sigma$. Then, it moves backward on the real time axis along C_2 to $t_i - i\sigma$, and finally vertically along C_4 to $t_i - i\beta$. Taking $t_i \to -\infty, t_f \to \infty$, the contour spans the full real time axis. The contributions to the generating functional from C_3, C_4 are some multiplicative constants and can be neglected [188]. Thus, for computing the Green's function, the time arguments can lie only on C_1 or C_2. This involves both time ordering and anti-time ordering and leads to an effective doubling of the degrees of freedom (For a detailed review, see Refs. [12, 184–187]).

The propagator at finite temperature in the RTF is a 2×2 matrix given by

$$G_{ab}(x, x') = \begin{bmatrix} \langle T\hat{\phi}(x)\hat{\phi}(x')\rangle_C & \langle \hat{\phi}(x')\hat{\phi}(x)\rangle_C \\ \langle \hat{\phi}(x)\hat{\phi}(x')\rangle_C & \langle T^*\hat{\phi}(x)\hat{\phi}(x')\rangle_C \end{bmatrix} \tag{A.1}$$

Here C denotes the CTP contour, T stands for normal time ordering along C_1 and T^*

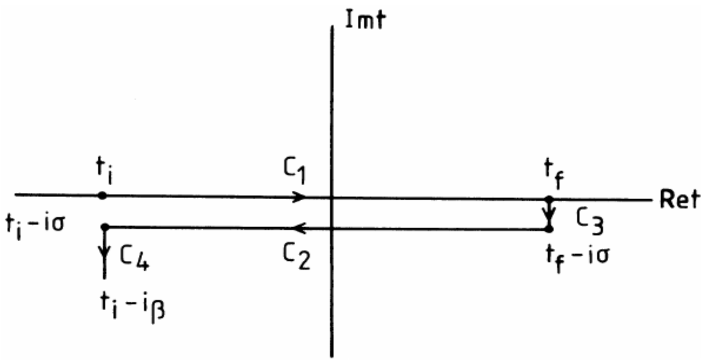

Figure A.1: Schwinger-Keldysh contour in the complex time plane. Figure taken from Ref. [12].

denotes anti-time ordering along C_2. Here the $\langle ....\rangle$ denote a thermal average of any quantity. The individual components are

$$\begin{aligned}
G_{12}(x,x') &= G^{<}(x,x') = \langle \hat{\phi}(x')\hat{\phi}(x)\rangle \\
G_{21}(x,x') &= G^{>}(x,x') = \langle \hat{\phi}(x)\hat{\phi}(x')\rangle \\
G_{11}(x,x') &= \theta(t-t')G^{>}(x,x') + \theta(t'-t)G^{<}(x,x') \\
G_{22}(x,x') &= \theta(t-t')G^{<}(x,x') + \theta(t'-t)G^{>}(x,x')
\end{aligned} \tag{A.2}$$

The indices $a, b = 1, 2$ represent whether the time coordinates t, t' lie on C_1 or C_2. On the contour, the time coordinate on C_2 come after the time on C_1. The component G_{11} is recognized as the standard Feynman propagator, whereas for a system in thermal equilibrium, G_{21} is the thermal Wightman function, G_{12} is its transpose, and G_{22} is the thermal Dyson function.

We can also express the propagator matrix for the ϕ field in momentum space as

$$G_{ab}(P) = \int d^4x \, G_{ab}(x,x')e^{-iP.(x-x')} \tag{A.3}$$

where the 4-momentum $P = (\omega, \boldsymbol{p})$. The components of thermal Green's function for a free boson are given as [188]

$$\begin{aligned}
G_{11}(P) &= \frac{1}{p^2 - m^2 + i\epsilon} - 2i\,\pi n(\omega)\delta(p^2 - m^2) \\
G_{12}(P) &= -2i\,\pi\,(\theta(-\omega) + n(\omega))\,\delta(p^2 - m^2) \\
G_{21}(P) &= -2i\,\pi\,(\theta(\omega) + n(\omega))\,\delta(p^2 - m^2)
\end{aligned}$$

$$G_{22}(P) = \frac{-1}{p^2 - m^2 - i\epsilon} - 2i\,\pi n(\omega)\delta(p^2 - m^2) \tag{A.4}$$

where $n(\omega)$ is the thermal distribution function, $n(\omega) = \dfrac{1}{e^{\beta\omega} - 1}$. In these expressions, the first part corresponds to the zero temperature Green's function and the second part with $n(\omega)$ is the thermal contribution.

We next define the spectral function as

$$\rho(x, x') = i\langle[\hat{\phi}(x), \hat{\phi}(x')]\rangle = i(G_{21} - G_{12}) \tag{A.5}$$

and the anti-commutator function as

$$F(x, x') = \frac{1}{2}\langle\{\hat{\phi}(x), \hat{\phi}(x')\}\rangle = \frac{1}{2}(G_{12} + G_{21}). \tag{A.6}$$

In terms of these, the propagator matrix is written as

$$G_{ab}(x, x') = \begin{bmatrix} F(x, x') - \frac{i}{2}\sigma(x, x') & F(x, x') + \frac{i}{2}\rho(x, x') \\ F(x, x') - \frac{i}{2}\rho(x, x') & F(x, x') + \frac{i}{2}\sigma(x, x') \end{bmatrix} \tag{A.7}$$

Here $\sigma(x, x') = \mathrm{sgn}(t - t')\rho(x, x')$ is the Wheeler-Feynman propagator (where $\mathrm{sgn(t - t')} = +$ if $t > t'$ and $-$ if $t < t'$ is the sign function). This shows that $-\rho(x, x')/2$ and $F(x, x')$ are the imaginary and real components of the Wightman function $G_{21}(x, x')$. The propagators depend on the combination $x - x'$, thus it is convenient to take the Fourier transform over time and space into $(\omega, \boldsymbol{p})$. By the Kubo-Martin-Schwinger (KMS) relation, the spectral function and the anti-commutator function are related as

$$F(\omega, \boldsymbol{p}) = -\frac{i}{2}[1 + 2n(\omega)]\rho(\omega, \boldsymbol{p}). \tag{A.8}$$

Thus, the propagator matrix (A.7) can be completely described in terms of the spectral function.

The propagator, and thus the spectral function for an interacting theory are obtained as a solution to the Schwinger-Dyson equation

$$(\omega^2 - \boldsymbol{p}^2 - m^2)G_{ab} - \Sigma_a^c G_{cb} = ic_{ab}. \tag{A.9}$$

Here Σ_{ab} is the self energy matrix which accounts for the loop corrections to the free 2-point correlation function, and c_{ab} is a diagonal matrix $(1, -1)$. Similar to the Green's function matrix, the self energy matrix is separated into real and imaginary functions [126]

$$\Sigma_{12} = (i\Sigma_F) + i\left(\frac{i\Sigma_\rho}{2}\right)$$

and

$$\Sigma_{21} = (i\Sigma_F) - i\left(\frac{i\Sigma_\rho}{2}\right),$$

by defining

$$i\Sigma_F = \frac{1}{2}(\Sigma_{21} + \Sigma_{12}) \qquad\qquad i\Sigma_\rho = i(\Sigma_{21} - \Sigma_{12}).$$

By the KMS relation, the functions satisfy the relation

$$\Sigma_F(\omega, \boldsymbol{p}) = -\frac{i}{2}[1 + 2n(\omega)]\Sigma_\rho(\omega, \boldsymbol{p}).$$

The imaginary part of the self energy represent the dissipative part and yields the decay width of the field as

$$\Gamma(\omega, \boldsymbol{p}) = \frac{i\Sigma_\rho(\omega, \boldsymbol{p})}{4\omega_p}, \tag{A.10}$$

where $\omega_p = \sqrt{\boldsymbol{p}^2 + m_R^2}$ is the energy of any on-shell particle.

Appendix B

Dissipation parameter at the end of inflation, Q_e

Here we provide the solutions to the algebraic equations obtained in the calculation of the dissipation parameter at the end of inflation, Q_e, as given in Sections 4.3.1 and 5.2. In these expressions $A = (\pi^2/30)g_*$.

For $V(\phi) = \lambda\phi^4$ with $\Upsilon = C_\phi \dfrac{T^3}{\phi^2}$

The positive real solution to Eq. (4.15) is given by

$$Q_e(\lambda, C_\phi) = \frac{-1}{2} + \frac{1}{2}\sqrt{1 + 4\left(\frac{64 C_\phi^4 \lambda}{9A^3}\right)\frac{1}{12^5}}\,. \tag{B.1}$$

For $V(\phi) = \lambda\phi^4$ with $\Upsilon = C_T T$

The positive real solution to Eq. (4.16) is given by

$$Q_e(\lambda, C_T) = \frac{2^{1/3} Y}{3^{1/3}(9Y + \sqrt{3}\sqrt{27Y^2 - 4Y^3})^{1/3}} + \frac{(9Y + \sqrt{3}\sqrt{27Y^2 - 4Y^3})^{1/3}}{2^{1/3}3^{2/3}}, \tag{B.2}$$

where $Y = \dfrac{1}{12^3}\dfrac{4C_T^4}{9A\lambda}$.

For $V(\phi) = \lambda \dfrac{\phi^6}{M_{Pl}^2}$ with $\Upsilon = C_\phi \dfrac{T^3}{\phi^2}$

The positive real solution to Eq. (5.12) is given by

$$Q_e(\lambda, C_\phi) = \frac{1}{3}\left[-2 + \frac{2^{1/3}}{(2+27Y+3\sqrt{3}\sqrt{4Y+27Y^2})^{1/3}} + \frac{(2+27Y+3\sqrt{3}\sqrt{4Y+27Y^2})^{1/3}}{2^{1/3}}\right], \tag{B.3}$$

where $Y = \dfrac{1}{10^4}\dfrac{\lambda C_\phi^4}{8\pi A^3}$.

For $V(\phi) = \lambda \dfrac{\phi^6}{M_{Pl}^2}$ with $\Upsilon = C_T T$

The positive real solution to Eq. (5.13) is given by

$$\begin{aligned} Q_e(\lambda, C_T) = \frac{Y}{3} &+ \frac{2^{1/3}(6Y+Y^2)}{3(27Y+18Y^2+2Y^3+3\sqrt{3}\sqrt{(27Y^2+4Y^3})^{1/3}} \\ &+ \frac{(27Y+18Y^2+2Y^3+3\sqrt{3}\sqrt{(27Y^2+4Y^3})^{1/3}}{2^{1/3}\,3}, \end{aligned} \tag{B.4}$$

where $Y = \dfrac{1}{30^4}\dfrac{8\pi C_T^4}{A\lambda}$.

Appendix C

Integral Function of dN/dQ

We give the integral function $F(Q)$ in Eq. (4.22) obtained while integrating dN/dQ in Section 4.3.1. In these expressions, ${}_2F_1(a, b; c; z)$ is the hypergeometric function, the expressions for which can be found in Ref. [323].

For $V(\phi) = \lambda\phi^4$ with $\Upsilon = C_\phi \dfrac{T^3}{\phi^2}$

For this model, using Eq. (4.12) we get

$$F(Q) = \frac{5}{4Z} Q^{-1/5}(1+Q)^{-1}\left[4(1+Q)^{\frac{4}{5}}(-1+5Q) - 15Q(1+Q)\,{}_2F_1\left(\frac{1}{5}, \frac{4}{5}, \frac{9}{5}, -Q\right)\right], \tag{C.1}$$

where $Z = 40\left(\dfrac{9A^3}{64\lambda C_\phi^4}\right)^{1/5}$.

For $V(\phi) = \lambda\phi^4$ with $\Upsilon = C_T T$

For this model, using Eq. (4.13) the integral function is calculated to be

$$F(Q) = -\frac{3}{2Z} Q^{-1}(1+Q)^{\frac{1}{3}}\left[2 + 3\,{}_2F_1\left(1, 1; \frac{5}{3}; \frac{-1}{Q}\right)\right], \tag{C.2}$$

where $Z = \dfrac{1}{24}\left(\dfrac{4C_T^4}{9A\lambda}\right)^{1/3}$.

For $V(\phi) = \lambda \frac{\phi^6}{M_{Pl}^2}$ with $\Upsilon = C_\phi \frac{T^3}{\phi^2}$

Using Eq. (5.9) the integral function for this model is calculated to be

$$F(Q) = \frac{1}{Z} Q^{-1/4} (1+Q)^{-1/2} \left[-4 + 8Q - \frac{8}{3} Q (1+Q) \, {}_2F_1 \left(1, \frac{5}{4}; \frac{7}{4}; -Q \right) \right], \tag{C.3}$$

where $Z = \frac{1}{16} \left(\frac{\lambda C_\phi^4}{8\pi A^3} \right)^{1/4}$.

For $V(\phi) = \lambda \frac{\phi^6}{M_{Pl}^2}$ with $\Upsilon = C_T T$

Using Eq. (5.10) the integral function for this model is calculated to be

$$F(Q) = \frac{1}{Z} Q^{-3/4} 4 \left[(1+Q)^{\frac{1}{2}} - 4Q \, {}_2F_1 \left(\frac{1}{4}, \frac{1}{2}; \frac{5}{4}; -Q \right) \right], \tag{C.4}$$

where $Z = \frac{\pi}{6} \left(\frac{C_T^4}{(8\pi)^3 A \lambda} \right)^{1/4}$.

Appendix D

Spectral index

Here we give the expressions for the spectral index, n_s for all the warm inflation models we have studied. In these expressions, ϵ_H is the horizon slow roll parameter defined in Eq. (3.8) and n_P is the inflaton distribution function given in Eq. (3.26), both evaluated at $k = k_P$. Here we have defined $x = 1 + 2n_P + \dfrac{T_P}{H_P}\dfrac{2\sqrt{3}\pi Q_P}{\sqrt{3+4\pi Q_P}}$.

For $V(\phi) = \lambda\phi^4$ with $\Upsilon = C_\phi \dfrac{T^3}{\phi^2}$

$$
\begin{aligned}
n_s = 1 &- \frac{\epsilon_H}{(1-\epsilon_H)}\frac{(3+11Q_P)}{(1+7Q_P)} + y\left(\frac{9.69\,Q_P^{0.946} + 0.550\,Q_P^{3.330}}{1+4.98\,Q_P^{1.946} + 0.127\,Q_P^{4.330}}\right) \\
&+ \frac{y}{x\,Q_P}\left[\frac{4H_P}{5T_P}\exp\left(\frac{H_P}{T_P}\right)n_P^2\frac{(1+2Q_P)}{(1+Q_P)} + \frac{T_P}{H_P}\frac{2\sqrt{3}\pi Q_P}{\sqrt{3+4\pi Q_P}}\left(1+\frac{2(1+2Q_P)}{5(1+Q_P)} - \frac{2\pi Q_P}{3+4\pi Q_P}\right)\right],
\end{aligned}
\tag{D.1}
$$

where $y = \dfrac{5\epsilon_H}{(1-\epsilon_H)}\dfrac{Q_P(1+Q_P)}{(1+7Q_P)}$.

For $V(\phi) = \lambda\phi^4$ with $\Upsilon = C_T T$

$$
\begin{aligned}
n_s = 1 &- \frac{\epsilon_H}{(1-\epsilon_H)}\frac{9(1+Q_P)}{(3+5\,Q_P)} + y\left(\frac{0.0428\,Q_P^{1.315} + 0.457\,Q_P^{0.364}}{1+0.0185\,Q_P^{2.315} + 0.335\,Q_P^{1.364}}\right) \\
&+ \frac{y}{x\,Q_P}\left[\frac{2H_P}{T_P}\exp\left(\frac{H_P}{T_P}\right)n_P^2 + \frac{T_P}{H_P}\frac{2\sqrt{3}\pi Q_P}{\sqrt{3+4\pi Q_P}}\frac{(6+6\pi Q_P)}{(3+4\pi Q_P)}\right].
\end{aligned}
\tag{D.2}
$$

Here $y = \dfrac{3\epsilon_H}{(1-\epsilon_H)}\dfrac{Q_P(1+Q_P)}{3+5\,Q_P}$.

For $V(\phi) = \lambda \dfrac{\phi^6}{M_{Pl}^2}$ with $\Upsilon = C_\phi \dfrac{T^3}{\phi^2}$

$$n_s = 1 - \frac{8\epsilon_H}{3(1-\epsilon_H)} \frac{(1+5\,Q_P)}{(1+7\,Q_P)} + y\left(\frac{9.69\,Q_P^{0.946} + 0.550\,Q_P^{3.330}}{1+4.98\,Q_P^{1.946} + 0.127\,Q_P^{4.330}}\right)$$
$$+ \frac{y}{x\,Q_P}\left[\frac{H_P}{T_P}\exp\left(\frac{H_P}{T_P}\right) n_P^2 \frac{(1+3Q_P)}{(1+7Q_P)} + \frac{T_P}{H_P}\frac{2\sqrt{3}\pi Q_P}{\sqrt{3+4\pi Q_P}}\left(1 + \frac{2(1+Q_P)(3+2\pi Q_P)}{(1+3\,Q_P)(3+4\pi Q_P)}\right)\right], \tag{D.3}$$

where $y = \dfrac{8\epsilon_H}{3(1-\epsilon_H)} \dfrac{Q_P(1+Q_P)}{(1+7\,Q_P)}$.

For $V(\phi) = \lambda \dfrac{\phi^6}{M_{Pl}^2}$ with $\Upsilon = C_T T$

$$n_s = 1 - \frac{8\epsilon_H}{(1-\epsilon_H)} \frac{(1+Q_P)}{(3+5\,Q_P)} + y\left(\frac{0.0428\,Q_P^{1.315} + 0.457\,Q_P^{0.364}}{1+0.0185\,Q_P^{2.315} + 0.335\,Q_P^{1.364}}\right)$$
$$+ \frac{y}{x\,Q_P}\left[\frac{2H_P}{T_P}\exp\left(\frac{H_P}{T_P}\right) n_P^2 + \frac{T_P}{H_P}\frac{2\sqrt{3}\pi Q_P}{\sqrt{3+4\pi Q_P}}\frac{6+6\pi Q_P}{3+4\pi Q_P}\right], \tag{D.4}$$

where $y = \dfrac{8\epsilon_H}{3(1-\epsilon_H)} \dfrac{Q_P(1+Q_P)}{(3+5\,Q_P)}$.

Bibliography

[1] D. Baumann, *Inflation,* in "Physics of the large and the small, TASI 09, 1-26 June 2009," (2011), pp. 523–686.

[2] K. Belotsky and M. Khlopov, *Cosmoparticle physics as a physically selfconsistent basis of modern cosmology,* Grav. Cosmol. **7**, 183–188 (2001).

[3] A. Albrecht, *Cosmic inflation and the arrow of time,* pp. 363–401 (2002). Astro-ph/0210527.

[4] A. H. Guth, *Inflation and eternal inflation,* Physics Reports **333-334**, 555 – 574 (2000).

[5] D. Baumann *et al.*, *CMBPol Mission Concept Study: Probing Inflation with CMB Polarization,* AIP Conf. Proc. **1141**, 10–120 (2009).

[6] L. Sriramkumar, *An introduction to inflation and cosmological perturbation theory,* (2009). ArXiv:0904.4584.

[7] Y. Akrami *et al.*, *Planck 2018 results. X. Constraints on inflation,* (2018). ArXiv:1807.06211.

[8] E. Komatsu *et al.*, *Seven-year Wilkinson Microwave Anisotropy Probe (WMAP) Observations: Cosmological Interpretation,* The Astrophysical Journal Supplement **192**, 18 (2011).

[9] B. Carr, K. Kohri, Y. Sendouda, and J. Yokoyama, *Constraints on Primordial Black Holes,* (2020). ArXiv:2002.12778.

[10] G. Sato-Polito, E. D. Kovetz, and M. Kamionkowski, *Constraints on the primordial curvature power spectrum from primordial black holes,* Phys. Rev. **D100**, 063521 (2019).

[11] https://conferences.pa.ucla.edu/ATI-2018/talks/green.pdf.

[12] M. Quiros, *Finite temperature field theory and phase transitions,* in "ICTP Summer School in High-Energy Physics and Cosmology," (1999), pp. 187–259.

[13] S. Weinberg, *Gravitation and Cosmology: Principles and Applications of the General Theory of Relativity* (John Wiley and Sons, New York, 1972).

[14] E. W. Kolb and M. S. Turner, *The Early Universe*, vol. 69 (1990).

[15] J. Peacock, *Cosmological physics* (1999).

[16] S. Dodelson, *Modern Cosmology* (Academic Press, Amsterdam, 2003).

[17] B. Ryden, *Introduction to cosmology* (Cambridge University Press, 2016).

[18] V. Mukhanov, *Physical Foundations of Cosmology* (Cambridge University Press, Oxford, 2005).

[19] P. Peter and J.-P. Uzan, *Primordial Cosmology* (Oxford University Press, Oxford, UK, 2005).

[20] S. Weinberg, *Cosmology* (2008).

[21] D. H. Lyth and A. R. Liddle, *The Primordial Density Perturbation: Cosmology, Inflation and the Origin of Structure* (Cambridge University Press, 2009).

[22] V. A. Rubakov and D. S. Gorbunov, *Introduction to the Theory of the Early Universe: Hot big bang theory* (World Scientific, Singapore, 2017).

[23] W. M. Samuel J. Ling, Jeff Sanny, *University Physics Volume 3* (OpenStax, 2016).

[24] J. Garcia-Bellido, *Astrophysics and cosmology,* in "1999 European School of High-Energy Physics," (1999), pp. 109–186.

[25] R. H. Brandenberger, *Cosmology of the Very Early Universe,* AIP Conf. Proc. **1268**, 3–70 (2010).

[26] A. Riotto, *Particle cosmology,* in "5th CERN - Latin American School of High-Energy Physics," (2010).

[27] R. H. Brandenberger, *Introduction to Early Universe Cosmology,* PoS **ICFI2010**, 001 (2010).

[28] V. Rubakov, *Cosmology,* in "2011 European School of High-Energy Physics," (2014), pp. 151–195.

[29] D. Baumann, *Primordial Cosmology,* PoS **TASI2017**, 009 (2018).

[30] J. M. Cline, *TASI Lectures on Early Universe Cosmology: Inflation, Baryogenesis and Dark Matter,* PoS **TASI2018**, 001 (2019).

[31] M. Tanabashi *et al.*, *Review of Particle Physics,* Phys. Rev. **D98**, 030001 (2018).

[32] E. Hubble, *A relation between distance and radial velocity among extra-galactic nebulae,* Proceedings of the National Academy of Sciences **15**, 168–173 (1929).

[33] A. A. Starobinsky, *A New Type of Isotropic Cosmological Models Without Singularity,* Phys. Lett. **91B**, 99–102 (1980). [,771(1980)].

[34] D. Kazanas, *Dynamics of the Universe and Spontaneous Symmetry Breaking,* Astrophys. J. **241**, L59–L63 (1980).

[35] K. Sato, *First Order Phase Transition of a Vacuum and Expansion of the Universe,* Mon. Not. Roy. Astron. Soc. **195**, 467–479 (1981).

[36] A. H. Guth, *The Inflationary Universe: A Possible Solution to the Horizon and Flatness Problems,* Phys. Rev. **D23**, 347–356 (1981). [Adv. Ser. Astrophys. Cosmol.3,139(1987)].

[37] A. D. Linde, *A New Inflationary Universe Scenario: A Possible Solution of the Horizon, Flatness, Homogeneity, Isotropy and Primordial Monopole Problems,* Phys. Lett. **108B**, 389–393 (1982). [Adv. Ser. Astrophys. Cosmol.3,149(1987)].

[38] A. Albrecht and P. J. Steinhardt, *Cosmology for Grand Unified Theories with Radiatively Induced Symmetry Breaking,* Phys. Rev. Lett. **48**, 1220–1223 (1982). [Adv. Ser. Astrophys. Cosmol.3,158(1987)].

[39] A. D. Linde, *Chaotic Inflation,* Phys. Lett. **129B**, 177–181 (1983).

[40] S. Weinberg, *The first three minutes : a modern view of the origin of the universe* (1993).

[41] A. A. Penzias and R. W. Wilson, *A Measurement of Excess Antenna Temperature at 4080 Mc/s.* The Astrophysical Journal **142**, 419–421 (1965).

[42] D. Fixsen, E. Cheng, J. Gales, J. C. Mather, R. Shafer, and E. Wright, *The Cosmic Microwave Background spectrum from the full COBE FIRAS data set,* Astrophys. J. **473**, 576 (1996).

[43] G. F. Smoot *et al.*, *Structure in the COBE differential microwave radiometer first year maps,* Astrophys. J. Lett. **396**, L1–L5 (1992).

[44] C. L. Bennett *et al.*, *Nine-year Wilkinson Microwave Anisotropy Probe (WMAP) Observations: Final Maps and Results,* The Astrophysical Journal Supplement **208**, 20 (2013).

[45] https://pla.esac.esa.int/.

[46] M. White, D. Scott, and J. Silk, *Anisotropies in the cosmic microwave background,* Annual Review of Astronomy and Astrophysics **32**, 319–370 (1994).

[47] W. Hu and S. Dodelson, *Cosmic microwave background anisotropies,* Annual Review of Astronomy and Astrophysics **40**, 171–216 (2002).

[48] A. Riotto, *Inflation and the theory of cosmological perturbations,* ICTP Lect. Notes Ser. **14**, 317–413 (2003).

[49] D. Langlois, *Lectures on inflation and cosmological perturbations* (2010), vol. 800, pp. 1–57.

[50] Y. Wang, *Inflation, Cosmic Perturbations and Non-Gaussianities,* Commun. Theor. Phys. **62**, 109–166 (2014).

[51] L. Senatore, *Lectures on Inflation,* in “Theoretical Advanced Study Institute in Elementary Particle Physics: New Frontiers in Fields and Strings,” (2017), pp. 447–543.

[52] S. Tsujikawa, *Introductory review of cosmic inflation,* in “2nd Tah Poe School on Cosmology: Modern Cosmology,” (2003).

[53] D. Baumann and H. V. Peiris, *Cosmological Inflation: Theory and Observations,* Adv. Sci. Lett. **2**, 105–120 (2009).

[54] A. D. Linde, *Coleman-Weinberg Theory and a New Inflationary Universe Scenario,* Phys. Lett. B **114**, 431–435 (1982).

[55] L. Kofman, A. D. Linde, and A. A. Starobinsky, *Reheating after inflation,* Phys. Rev. Lett. **73**, 3195–3198 (1994).

[56] R. H. Brandenberger, *Quantum field theory methods and inflationary universe models,* Rev. Mod. Phys. **57**, 1–60 (1985).

[57] K. A. Olive, *Inflation,* Phys. Rept. **190**, 307–403 (1990).

[58] J. E. Lidsey, A. R. Liddle, E. W. Kolb, E. J. Copeland, T. Barreiro, and M. Abney, *Reconstructing the inflation potential : An overview,* Rev. Mod. Phys. **69**, 373–410 (1997).

[59] D. H. Lyth and A. Riotto, *Particle physics models of inflation and the cosmological density perturbation,* Phys. Rept. **314**, 1–146 (1999).

[60] A. R. Liddle and D. Lyth, *Cosmological inflation and large scale structure* (2000).

[61] B. A. Bassett, S. Tsujikawa, and D. Wands, *Inflation dynamics and reheating,* Rev. Mod. Phys. **78**, 537–589 (2006).

[62] A. D. Linde, *Particle physics and inflationary cosmology*, vol. 5 (1990).

[63] A. D. Linde, *Inflationary Cosmology,* Lect. Notes Phys. **738**, 1–54 (2008).

[64] H. Kodama and M. Sasaki, *Cosmological Perturbation Theory,* Prog. Theor. Phys. Suppl. **78**, 1–166 (1984).

[65] V. Mukhanov, H. Feldman, and R. Brandenberger, *Theory of cosmological perturbations,* Physics Reports **215**, 203 – 333 (1992).

[66] K. A. Malik and D. Wands, *Cosmological perturbations,* Phys. Rept. **475**, 1–51 (2009).

[67] P. Peter, *Cosmological Perturbation Theory,* in "15th Brazilian School of Cosmology and Gravitation," (2013).

[68] https://en.wikipedia.org/wiki/List_of_cosmic_microwave_background_experiments.

[69] J. Martin, C. Ringeval, and V. Vennin, *Encyclopdia Inflationaris,* Phys. Dark Univ. **5-6**, 75–235 (2014).

[70] A. Linde, *Inflationary Cosmology after Planck 2013,* in "100e Ecole d'Ete de Physique: Post-Planck Cosmology," (2015), pp. 231–316.

[71] S. Clesse, *An introduction to inflation after Planck: from theory to observations,* in "10th Modave Summer School in Mathematical Physics," (2015).

[72] P. Creminelli, D. L. Lpez Nacir, M. Simonovi, G. Trevisan, and M. Zaldarriaga, *Detecting Primordial B-Modes after Planck,* JCAP **1511**, 031 (2015).

[73] K. N. Abazajian *et al.*, *CMB-S4 Science Book, First Edition,* (2016).

[74] H. Ishino *et al.*, *LiteBIRD: lite satellite for the study of B-mode polarization and inflation from cosmic microwave background radiation detection,* Proc. SPIE Int. Soc. Opt. Eng. **9904**, 99040X (2016).

[75] F. Finelli *et al.*, *Exploring cosmic origins with CORE: Inflation,* JCAP **04**, 016 (2018).

[76] R. A. Battye *et al.*, *H I intensity mapping: a single dish approach,* MNRAS **434**, 1239–1256 (2013).

[77] R. Nan *et al.*, *The Five-Hundred Aperture Spherical Radio Telescope (fast) Project,* International Journal of Modern Physics D **20**, 989–1024 (2011).

[78] P. E. Dewdney *et al.*, *The Square Kilometre Array,* IEEE Proceedings **97**, 1482–1496 (2009).

[79] Y.-C. Li and Y.-Z. Ma, *Constraints on Primordial non-Gaussianity from Future HI Intensity Mapping Experiments,* Phys. Rev. D **96**, 063525 (2017).

[80] E. M. Leitch, J. Kovac, C. Pryke, B. Reddall, E. Sandberg, M. Dragovan, J. Carlstrom, N. Halverson, and W. Holzapfel, *Measuring polarization with DASI,* Nature **420**, 763–771 (2002).

[81] S. Das *et al.*, *The Atacama Cosmology Telescope: temperature and gravitational lensing power spectrum measurements from three seasons of data,* JCAP **04**, 014 (2014).

[82] R. Keisler *et al.*, *A Measurement of the Damping Tail of the Cosmic Microwave Background Power Spectrum with the South Pole Telescope,* The Astrophysical Journal **743**, 28 (2011).

[83] P. Ade *et al.*, *BICEP2 II: Experiment and Three-Year Data Set,* Astrophys. J. **792**, 62 (2014).

[84] S. Cole *et al.*, *The 2dF Galaxy Redshift Survey: Power-spectrum analysis of the final dataset and cosmological implications,* Mon. Not. Roy. Astron. Soc. **362**, 505–534 (2005).

[85] D. J. Eisenstein *et al.*, *Detection of the Baryon Acoustic Peak in the Large-Scale Correlation Function of SDSS Luminous Red Galaxies,* Astrophys. J. **633**, 560–574 (2005).

[86] F. Beutler *et al.*, *The 6dF Galaxy Survey: baryon acoustic oscillations and the local Hubble constant,* MNRAS **416**, 3017–3032 (2011).

[87] S. Alam *et al.*, *The clustering of galaxies in the completed SDSS-III Baryon Oscillation Spectroscopic Survey: cosmological analysis of the DR12 galaxy sample,* Mon. Not. Roy. Astron. Soc. **470**, 2617–2652 (2017).

[88] P. Ade *et al.*, *Planck 2015 results. XXIV. Cosmology from Sunyaev-Zeldovich cluster counts,* Astron. Astrophys. **594**, A24 (2016).

[89] J. D. Bowman, A. E. E. Rogers, R. A. Monsalve, T. J. Mozdzen, and N. Mahesh, *An absorption profile centred at 78 megahertz in the sky-averaged spectrum,* Nature **555**, 67–70 (2018).

[90] P. McDonald *et al.*, *The Lyman-alpha forest power spectrum from the Sloan Digital Sky Survey,* Astrophys. J. Suppl. **163**, 80–109 (2006).

[91] C. Heymans *et al.*, *CFHTLenS: the Canada-France-Hawaii Telescope Lensing Survey,* MNRAS **427**, 146–166 (2012).

[92] T. Abbott *et al.*, *Dark Energy Survey year 1 results: Cosmological constraints from galaxy clustering and weak lensing,* Phys. Rev. D **98**, 043526 (2018).

[93] M. Betoule *et al.*, *Improved cosmological constraints from a joint analysis of the SDSS-II and SNLS supernova samples,* Astron. Astrophys. **568**, A22 (2014).

[94] A. G. Riess *et al.*, *A 3% Solution: Determination of the Hubble Constant with the Hubble Space Telescope and Wide Field Camera 3,* Astrophys. J. **730**, 119 (2011).

[95] N. Suzuki *et al.*, *The Hubble Space Telescope Cluster Supernova Survey. V. Improving the Dark-energy Constraints above z > 1 and Building an Early-type-hosted Supernova Sample,* Astrophys. J. **746**, 85 (2012).

[96] https://en.wikipedia.org/wiki/List_of_cosmological_computation_software.

[97] https://camb.info/.

[98] A. Lewis, A. Challinor, and A. Lasenby, *Efficient computation of CMB anisotropies in closed FRW models,* Astrophysics Journal **538**, 473–476 (2000).

[99] A. Lewis and A. Challinor, *CAMB: Code for Anisotropies in the Microwave Background,* (2011).

[100] A. Lewis, *CAMB Notes,* https://cosmologist.info/notes/CAMB.pdf.

[101] C.-P. Ma and E. Bertschinger, *Cosmological perturbation theory in the synchronous and conformal Newtonian gauges,* Astrophysics Journal **455**, 7–25 (1995).

[102] A. Lewis and A. Challinor, *Evolution of cosmological dark matter perturbations,* Phys. Rev. D **66**, 023531 (2002).

[103] https://cosmologist.info/cosmomc/.

[104] A. Lewis and S. Bridle, *Cosmological parameters from CMB and other data: A Monte Carlo approach,* Phys. Rev. **D66**, 103511 (2002).

[105] M.-H. Li, P. Wang, Z. Chang, and D. Zhao, *CosmoMC Installation and Running Guidelines,* (2014). ArXiv:1409.1354.

[106] H. Moshafi and M. Bahraminasr, *A Guide for CosmoMC Installation and Running,* (2018). ArXiv:1808.05080.

[107] R. Trotta, *Bayes in the sky: Bayesian inference and model selection in cosmology,* Contemp. Phys. **49**, 71–104 (2008).

[108] A. Heavens, *Statistical techniques in cosmology,* arXiv:0906.0664 (2009).

[109] L. Verde, *Statistical Methods in Cosmology* (2010), vol. 800, pp. 147–177.

[110] R. Trotta, *Bayesian Methods in Cosmology,* (2017).

[111] A. Lewis, *GetDist: a Python package for analysing Monte Carlo samples,* (2019).

[112] https://getdist.readthedocs.io/.

[113] https://cosmologist.info/cosmomc/readme_gui.html.

[114] A. Berera, *Warm inflation,* Phys. Rev. Lett. **75**, 3218–3221 (1995).

[115] A. Berera, *Thermal properties of an inflationary universe,* Phys. Rev. D **54**, 2519–2534 (1996).

[116] A. Berera, *Interpolating the stage of exponential expansion in the early universe: A Possible alternative with no reheating,* Phys. Rev. D **55**, 3346–3357 (1997).

[117] A. Berera and L.-Z. Fang, *Thermally induced density perturbations in the inflation era,* Phys. Rev. Lett. **74**, 1912–1915 (1995).

[118] M. Morikawa and M. Sasaki, *Entropy Production in the Inflationary Universe,* Progress of Theoretical Physics **72**, 782–798 (1984).

[119] A. Berera and R. O. Ramos, *Absence of isentropic expansion in various inflation models,* Phys. Lett. **B607**, 1–7 (2005).

[120] G. Aarts and A. Tranberg, *Particle creation and warm inflation,* Phys. Lett. B **650**, 65–71 (2007).

[121] I. G. Moss and C. M. Graham, *Particle production and reheating in the inflationary universe,* Phys. Rev. D **78**, 123526 (2008).

[122] L. Kofman, A. D. Linde, and A. A. Starobinsky, *Towards the theory of reheating after inflation,* Phys. Rev. D **56**, 3258–3295 (1997).

[123] K. D. Lozanov, *Lectures on Reheating after Inflation,* (2019).

[124] A. Berera, *Warm inflation dissipative dynamics,* in “5th International Conference on Particle Physics and the Early Universe,” (2001).

[125] A. Berera, *The warm inflationary universe,* Contemp. Phys. **47**, 33–49 (2006).

[126] A. Berera, I. G. Moss, and R. O. Ramos, *Warm Inflation and its Microphysical Basis,* Rept. Prog. Phys. **72**, 026901 (2009).

[127] S. del Campo, *Warm inflationary universe models,* in “Aspects of Today’s Cosmology,” , A. Alfonso-Faus, ed. (IntechOpen, Rijeka, 2011), chap. 1.

[128] R. O. Ramos, *Warm Inflation, Cosmological Fluctuations and Constraints from Planck,* Astrophys. Space Sci. Proc. **45**, 283–297 (2016).

[129] O. Grøn, *Warm Inflation,* Universe **2**, 20 (2016).

[130] R. Rangarajan, *Current Status of Warm Inflation,* in "Proceedings, 18th Lomonosov Conference on Elementary Particle Physics: Moscow, Russia, August 24-30, 2017," (2019), pp. 339–345.

[131] A. Berera and R. O. Ramos, *Construction of a robust warm inflation mechanism,* Phys. Lett. **B567**, 294–304 (2003).

[132] A. Berera, M. Gleiser, and R. O. Ramos, *Strong dissipative behavior in quantum field theory,* Phys. Rev. D **58**, 123508 (1998).

[133] A. Berera, M. Gleiser, and R. O. Ramos, *A First principles warm inflation model that solves the cosmological horizon / flatness problems,* Phys. Rev. Lett. **83**, 264–267 (1999).

[134] A. Berera, *Warm inflation at arbitrary adiabaticity: A Model, an existence proof for inflationary dynamics in quantum field theory,* Nucl. Phys. **B585**, 666–714 (2000).

[135] A. Berera and R. O. Ramos, *The Affinity for scalar fields to dissipate,* Phys. Rev. **D63**, 103509 (2001).

[136] M. Bastero-Gil and A. Berera, *Warm inflation model building,* Int. J. Mod. Phys. **A24**, 2207–2240 (2009).

[137] M. Bastero-Gil, A. Berera, R. Hernndez-Jimnez, and J. G. Rosa, *Warm inflation within a supersymmetric distributed mass model,* Phys. Rev. **D99**, 103520 (2019).

[138] H. de Oliveira and R. O. Ramos, *Dynamical system analysis for inflation with dissipation,* Phys. Rev. D **57**, 741–749 (1998).

[139] A. Berera and R. O. Ramos, *Dynamics of interacting scalar fields in expanding space-time,* Phys. Rev. **D71**, 023513 (2005).

[140] M. Bastero-Gil and A. Berera, *Warm inflation dynamics in the low temperature regime,* Phys. Rev. D **76**, 043515 (2007).

[141] A. Berera, I. G. Moss, and R. O. Ramos, *Local Approximations for Effective Scalar Field Equations of Motion,* Phys. Rev. D **76**, 083520 (2007).

[142] I. G. Moss and C. Xiong, *Dissipation coefficients for supersymmetric inflatonary models,* (2006).

[143] Y. Zhang, *Warm Inflation With A General Form Of The Dissipative Coefficient,* JCAP **03**, 023 (2009).

[144] M. Bastero-Gil, A. Berera, and R. O. Ramos, *Dissipation coefficients from scalar and fermion quantum field interactions,* JCAP **1109**, 033 (2011).

[145] M. Bastero-Gil, A. Berera, R. O. Ramos, and J. G. Rosa, *General dissipation coefficient in low-temperature warm inflation,* JCAP **1301**, 016 (2013).

[146] W. Lee and L.-Z. Fang, *Mass density perturbations from inflation with thermal dissipation,* Phys. Rev. D **59**, 083503 (1999).

[147] A. Taylor and A. Berera, *Perturbation spectra in the warm inflationary scenario,* Phys. Rev. D **62**, 083517 (2000).

[148] L. M. H. Hall, I. G. Moss, and A. Berera, *Scalar perturbation spectra from warm inflation,* Phys. Rev. **D69**, 083525 (2004).

[149] C. Graham and I. G. Moss, *Density fluctuations from warm inflation,* JCAP **0907**, 013 (2009).

[150] R. O. Ramos and L. A. da Silva, *Power spectrum for inflation models with quantum and thermal noises,* JCAP **1303**, 032 (2013).

[151] L. Visinelli, *Cosmological perturbations for an inflaton field coupled to radiation,* JCAP **01**, 005 (2015).

[152] L. M. Hall, I. G. Moss, and A. Berera, *Constraining warm inflation with the Cosmic Microwave Background,* Phys. Lett. B **589**, 1–6 (2004).

[153] L. M. Hall and H. V. Peiris, *Cosmological Constraints on Dissipative Models of Inflation,* JCAP **01**, 027 (2008).

[154] G. Panotopoulos and N. Videla, *Warm* $\frac{\lambda}{4}\phi^4$ *inflationary universe model in light of Planck 2015 results,* Eur. Phys. J. **C75**, 525 (2015).

[155] L. Visinelli, *Observational Constraints on Monomial Warm Inflation,* JCAP **1607**, 054 (2016).

[156] M. Benetti and R. O. Ramos, *Warm inflation dissipative effects: predictions and constraints from the Planck data,* Phys. Rev. **D95**, 023517 (2017).

[157] S. Gupta, A. Berera, A. F. Heavens, and S. Matarrese, *Non-Gaussian signatures in the cosmic background radiation from warm inflation,* Phys. Rev. **D66**, 043510 (2002).

[158] I. G. Moss and C. Xiong, *Non-Gaussianity in fluctuations from warm inflation,* JCAP **0704**, 007 (2007).

[159] I. Moss and C. Graham, *Testing models of inflation with CMB non-gaussianity,* JCAP **11**, 004 (2007).

[160] I. G. Moss and T. Yeomans, *Non-gaussianity in the strong regime of warm inflation,* JCAP **1108**, 009 (2011).

[161] M. Bastero-Gil, A. Berera, I. G. Moss, and R. O. Ramos, *Theory of non-Gaussianity in warm inflation,* JCAP **1412**, 008 (2014).

[162] R. Arya, *Formation of Primordial Black Holes from Warm Inflation,* JCAP **09**, 042 (2020).

[163] Y. B. Zel'dovich and I. D. Novikov, *The Hypothesis of Cores Retarded During Expansion and the Hot Cosmological Model,* Soviet Astronomy **10**, 602 (1967).

[164] S. Hawking, *Gravitationally collapsed objects of very low mass,* Mon. Not. Roy. Astron. Soc. **152**, 75 (1971).

[165] B. J. Carr and S. W. Hawking, *Black holes in the early Universe,* Mon. Not. Roy. Astron. Soc. **168**, 399–415 (1974).

[166] B. J. Carr, *The Primordial black hole mass spectrum,* Astrophys. J. **201**, 1–19 (1975).

[167] A. Berera, *Warm inflation solution to the eta problem,* p. AHEP2003/069 (2004). [PoSAHEP2003,069(2003)].

[168] I. G. Moss and C. Xiong, *On the consistency of warm inflation,* JCAP **0811**, 023 (2008).

[169] S. Das, *Note on single-field inflation and the swampland criteria,* Phys. Rev. **D99**, 083510 (2019).

[170] S. Das, *Warm Inflation in the light of Swampland Criteria,* Phys. Rev. **D99**, 063514 (2019).

[171] M. Motaharfar, V. Kamali, and R. O. Ramos, *Warm inflation as a way out of the swampland,* Phys. Rev. **D99**, 063513 (2019).

[172] S. Das, G. Goswami, and C. Krishnan, *Swampland, Axions and Minimal Warm Inflation,* (2019).

[173] R. Brandenberger, V. Kamali, and R. O. Ramos, *Strengthening the de Sitter swampland conjecture in warm inflation,* (2020).

[174] G. Obied, H. Ooguri, L. Spodyneiko, and C. Vafa, *De Sitter Space and the Swampland,* (2018).

[175] H. Ooguri, E. Palti, G. Shiu, and C. Vafa, *Distance and de Sitter Conjectures on the Swampland,* Phys. Lett. **B788**, 180–184 (2019).

[176] P. Agrawal, G. Obied, P. J. Steinhardt, and C. Vafa, *On the Cosmological Implications of the String Swampland,* Phys. Lett. **B784**, 271–276 (2018).

[177] W. H. Kinney, S. Vagnozzi, and L. Visinelli, *The zoo plot meets the swampland: mutual (in)consistency of single-field inflation, string conjectures, and cosmological data,* Class. Quant. Grav. **36**, 117001 (2019).

[178] M. Morikawa, *Classical fluctuations in dissipative quantum systems,* Phys. Rev. D **33**, 3607–3612 (1986).

[179] E. Calzetta and B. L. Hu, *Nonequilibrium quantum fields: Closed-time-path effective action, wigner function, and boltzmann equation,* Phys. Rev. D **37**, 2878–2900 (1988).

[180] M. Gleiser and R. O. Ramos, *Microphysical approach to nonequilibrium dynamics of quantum fields,* Phys. Rev. **D50**, 2441–2455 (1994).

[181] J. Berges, *Introduction to nonequilibrium quantum field theory,* AIP Conf. Proc. **739**, 3–62 (2004).

[182] J. Rammer, *Quantum field theory of non-equilibrium states* (2007).

[183] E. A. Calzetta and B.-L. B. Hu, *Nonequilibrium Quantum Field Theory* (2008).

[184] K.-c. Chou, Z.-b. Su, B.-l. Hao, and L. Yu, *Equilibrium and Nonequilibrium Formalisms Made Unified,* Phys. Rept. **118**, 1–131 (1985).

[185] N. Landsman and C. van Weert, *Real and Imaginary Time Field Theory at Finite Temperature and Density,* Phys. Rept. **145**, 141 (1987).

[186] T. Altherr, *Introduction to thermal field theory,* Int. J. Mod. Phys. A **8**, 5605–5628 (1993).

[187] A. K. Das, *Finite Temperature Field Theory* (World Scientific, New York, 1997).

[188] M. Le Bellac, *Thermal Field Theory*, Cambridge Monographs on Mathematical Physics (Cambridge University Press, 1996).

[189] J. Yokoyama and A. D. Linde, *Is warm inflation possible?* Phys. Rev. D **60**, 083509 (1999).

[190] M. Bastero-Gil, A. Berera, R. O. Ramos, and J. G. Rosa, *Warm Little Inflaton,* Phys. Rev. Lett. **117**, 151301 (2016).

[191] M. Bastero-Gil, A. Berera, R. O. Ramos, and J. G. Rosa, *Towards a reliable effective field theory of inflation,* (2019).

[192] L. M. H. Hall and I. G. Moss, *Thermal effects on pure and hybrid inflation,* Phys. Rev. **D71**, 023514 (2005).

[193] M. Bastero-Gil, A. Berera, and N. Kronberg, *Exploring the Parameter Space of Warm-Inflation Models,* JCAP **1512**, 046 (2015).

[194] C. P. Burgess, M. Majumdar, D. Nolte, F. Quevedo, G. Rajesh, and R.-J. Zhang, *The Inflationary brane anti-brane universe,* JHEP **07**, 047 (2001).

[195] H. Mishra, S. Mohanty, and A. Nautiyal, *Warm natural inflation,* Phys. Lett. **B710**, 245–250 (2012).

[196] M. Bastero-Gil and A. Berera, *Determining the regimes of cold and warm inflation in the SUSY hybrid model,* Phys. Rev. D **71**, 063515 (2005).

[197] M. Bastero-Gil, A. Berera, T. P. Metcalf, and J. G. Rosa, *Delaying the waterfall transition in warm hybrid inflation,* JCAP **03**, 023 (2014).

[198] S. Bartrum, A. Berera, and J. G. Rosa, *Warming up for Planck,* JCAP **06**, 025 (2013).

[199] J. C. Bueno Sanchez, M. Bastero-Gil, A. Berera, and K. Dimopoulos, *Warm hilltop inflation,* Phys. Rev. D **77**, 123527 (2008).

[200] R. Cerezo and J. G. Rosa, *Warm Inflection,* JHEP **01**, 024 (2013).

[201] L. Visinelli, *Natural Warm Inflation,* JCAP **09**, 013 (2011).

[202] R. Herrera, S. del Campo, and C. Campuzano, *Tachyon warm inflationary universe models,* JCAP **10**, 009 (2006).

[203] M. Bastero-Gil, S. Bhattacharya, K. Dutta, and M. R. Gangopadhyay, *Constraining Warm Inflation with CMB data,* JCAP **1802**, 054 (2018).

[204] V. Kamali, *Warm pseudoscalar inflation,* Phys. Rev. D **100**, 043520 (2019).

[205] K. V. Berghaus, P. W. Graham, and D. E. Kaplan, *Minimal Warm Inflation,* JCAP **03**, 034 (2020).

[206] S. del Campo and R. Herrera, *Warm inflation in the DGP brane-world model,* Phys. Lett. B **653**, 122–128 (2007).

[207] M. Cid, S. del Campo, and R. Herrera, *Warm inflation on the brane,* JCAP **10**, 005 (2007).

[208] M. Bastero-Gil, A. Berera, and J. G. Rosa, *Warming up brane-antibrane inflation,* Phys. Rev. D **84**, 103503 (2011).

[209] R. Herrera, N. Videla, and M. Olivares, *Warm intermediate inflation in the Randall–Sundrum II model in the light of Planck 2015 and BICEP2 results: a general dissipative coefficient,* Eur. Phys. J. C **75**, 205 (2015).

[210] X.-M. Zhang and J.-Y. Zhu, *Warm inflation in loop quantum cosmology: a model with a general dissipative coefficient,* Phys. Rev. D **87**, 043522 (2013).

[211] X.-M. Zhang and j.-Y. Zhu, *Extension of warm inflation to noncanonical scalar fields,* Phys. Rev. D **90**, 123519 (2014).

[212] Z.-P. Peng, J.-N. Yu, X.-M. Zhang, and J.-Y. Zhu, *Consistency of warm k-inflation,* Phys. Rev. D **94**, 103531 (2016).

[213] R. Herrera, *G-Warm inflation,* JCAP **05**, 029 (2017).

[214] M. Sharif and I. Nawazish, *Warm intermediate inflation in $f(R)$ gravity,* Astrophys. Space Sci. **362**, 30 (2017).

[215] M. Sharif and I. Nawazish, *Warm logamediate inflation in Starobinsky inflationary model,* International Journal of Modern Physics D **27**, 1750191 (2018).

[216] M. Sharif and A. Ikram, *Warm Inflation in $f(G)$ Theory of Gravity,* J. Exp. Theor. Phys. **123**, 40–50 (2016).

[217] M. Jamil, D. Momeni, and R. Myrzakulov, *Warm Intermediate Inflation in $F(T)$ Gravity,* Int. J. Theor. Phys. **54**, 1098–1112 (2015).

[218] S. del Campo, R. Herrera, and D. Pavon, *Cosmological perturbations in warm inflationary models with viscous pressure,* Phys. Rev. D **75**, 083518 (2007).

[219] S. del Campo, R. Herrera, D. Pavn, and J. Villanueva, *On the consistency of warm inflation in the presence of viscosity,* JCAP **08**, 002 (2010).

[220] L. Akhtari, A. Mohammadi, K. Sayar, and K. Saaidi, *Viscous warm inflation: Hamilton–Jacobi formalism,* Astropart. Phys. **90**, 28–36 (2017).

[221] M. Bastero-Gil, A. Berera, and R. O. Ramos, *Shear viscous effects on the primordial power spectrum from warm inflation,* JCAP **1107**, 030 (2011).

[222] S. Bartrum, M. Bastero-Gil, A. Berera, R. Cerezo, R. O. Ramos, and J. G. Rosa, *The importance of being warm (during inflation),* Phys. Lett. **B732**, 116–121 (2014).

[223] P. A. R. Ade *et al.*, *Planck 2015 results. XIII. Cosmological parameters,* Astron. Astrophys. **594**, A13 (2016).

[224] P. A. R. Ade *et al.*, *Planck 2015 results. XX. Constraints on inflation,* Astron. Astrophys. **594**, A20 (2016).

[225] https://wiki.cosmos.esa.int/planck-legacy-archive/images/1/1a/Baseline_params_table_2015_limit95.pdf.

[226] L. Book, M. Kamionkowski, and F. Schmidt, *Lensing of 21-cm Fluctuations by Primordial Gravitational Waves,* Phys. Rev. Lett. **108**, 211301 (2012).

[227] R. Arya and R. Rangarajan, *Study of warm inflationary models and their parameter estimation from CMB,* Int. J. Mod. Phys. D **29**, 2050055 (2020).

[228] B. J. Carr, *Primordial black holes as a probe of cosmology and high energy physics,* Lect. Notes Phys. **631**, 301–321 (2003).

[229] B. J. Carr, *Primordial black holes: Do they exist and are they useful?* in "59th Yamada Conference on Inflating Horizon of Particle Astrophysics and Cosmology Tokyo, Japan, June 20-24, 2005," (2005).

[230] B. J. Carr, *Primordial black holes: Recent developments,* eConf **C041213**, 0204 (2004).

[231] M. Yu. Khlopov, *Primordial Black Holes,* Res. Astron. Astrophys. **10**, 495–528 (2010).

[232] A. M. Green, *Primordial Black Holes: sirens of the early Universe,* Fundam. Theor. Phys. **178**, 129–149 (2015).

[233] M. Sasaki, T. Suyama, T. Tanaka, and S. Yokoyama, *Primordial black holes - perspectives in gravitational wave astronomy,* Class. Quant. Grav. **35**, 063001 (2018).

[234] J. Garca-Bellido, *Primordial Black Holes,* PoS **EDSU2018**, 042 (2018).

[235] S. W. Hawking, *Black hole explosions,* Nature **248**, 30–31 (1974).

[236] S. W. Hawking, *Particle Creation by Black Holes,* Commun. Math. Phys. **43**, 199–220 (1975). [,167(1975)].

[237] B. N. Vainer and P. D. Naselskii, *Observable consequences of the evaporation of low-mass primordial black holes,* Sov. Astron. Lett. **3**, 76–78 (1977).

[238] Y. B. Zeldovich, A. A. Starobinskii, M. Y. Khlopov, and V. M. Chechetkin, *Primordial black holes and the deuterium problem,* Sov. Astron. Lett. **3**, 110–112 (1977).

[239] K. Kohri and J. Yokoyama, *Primordial black holes and primordial nucleosynthesis. 1. Effects of hadron injection from low mass holes,* Phys. Rev. **D61**, 023501 (2000).

[240] A. M. Green, *Supersymmetry and primordial black hole abundance constraints,* Phys. Rev. **D60**, 063516 (1999).

[241] M. Lemoine, *Moduli constraints on primordial black holes,* Phys. Lett. **B481**, 333–338 (2000).

[242] M. Yu. Khlopov, A. Barrau, and J. Grain, *Gravitino production by primordial black hole evaporation and constraints on the inhomogeneity of the early universe,* Class. Quant. Grav. **23**, 1875–1882 (2006).

[243] B. J. Carr, K. Kohri, Y. Sendouda, and J. Yokoyama, *New cosmological constraints on primordial black holes,* Phys. Rev. **D81**, 104019 (2010).

[244] B. J. Carr and J. E. Lidsey, *Primordial black holes and generalized constraints on chaotic inflation,* Phys. Rev. **D48**, 543–553 (1993).

[245] H. I. Kim and C. H. Lee, *Constraints on the spectral index from primordial black holes,* Phys. Rev. **D54**, 6001–6007 (1996).

[246] A. M. Green and A. R. Liddle, *Constraints on the density perturbation spectrum from primordial black holes,* Phys. Rev. **D56**, 6166–6174 (1997).

[247] A. S. Josan, A. M. Green, and K. A. Malik, *Generalised constraints on the curvature perturbation from primordial black holes,* Phys. Rev. **D79**, 103520 (2009).

[248] D. N. Page and S. W. Hawking, *Gamma rays from primordial black holes,* Astrophysical Journal **206**, 1–7 (1976).

[249] J. H. MacGibbon and B. J. Carr, *Cosmic rays from primordial black holes,* Astrophys. J. **371**, 447–469 (1991).

[250] B. Carr, F. Kuhnel, and M. Sandstad, *Primordial Black Holes as Dark Matter,* Phys. Rev. **D94**, 083504 (2016).

[251] G. Ballesteros and M. Taoso, *Primordial black hole dark matter from single field inflation,* Phys. Rev. **D97**, 023501 (2018).

[252] B. Carr and F. Kuhnel, *Primordial Black Holes as Dark Matter: Recent Developments,* (2020).

[253] A. M. Green and B. J. Kavanagh, *Primordial Black Holes as a dark matter candidate,* (2020).

[254] B. Paczynski, *Gravitational microlensing by the galactic halo,* Astrophys. J. **304**, 1–5 (1986).

[255] A. Gould, *Femtolensing of gamma-ray bursters,* Astrophysical Journal **386**, 5–7 (1992).

[256] M. R. S. Hawkins, *Gravitational microlensing, quasar variability and missing matter,* Nature **366**, 242–245 (1993).

[257] B. J. Carr, *Pregalactic black hole accretion and the thermal history of the Universe,* Monthly Notices of the Royal Astronomical Society **194**, 639–668 (1981).

[258] M. Ricotti, J. P. Ostriker, and K. J. Mack, *Effect of Primordial Black Holes on the Cosmic Microwave Background and Cosmological Parameter Estimates,* Astrophys. J. **680**, 829 (2008).

[259] Y. Ali-Hamoud and M. Kamionkowski, *Cosmic microwave background limits on accreting primordial black holes,* Phys. Rev. **D95**, 043534 (2017).

[260] S. Wang, Y.-F. Wang, Q.-G. Huang, and T. G. F. Li, *Constraints on the Primordial Black Hole Abundance from the First Advanced LIGO Observation Run Using the Stochastic Gravitational-Wave Background,* Phys. Rev. Lett. **120**, 191102 (2018).

[261] M. Raidal, V. Vaskonen, and H. Veerme, *Gravitational Waves from Primordial Black Hole Mergers,* JCAP **1709**, 037 (2017).

[262] T. Nakama, J. Silk, and M. Kamionkowski, *Stochastic gravitational waves associated with the formation of primordial black holes,* Phys. Rev. **D95**, 043511 (2017).

[263] S. Wang, T. Terada, and K. Kohri, *Prospective constraints on the primordial black hole abundance from the stochastic gravitational-wave backgrounds produced by coalescing events and curvature perturbations,* Phys. Rev. **D99**, 103531 (2019).

[264] J. Garca-Bellido, *Massive Primordial Black Holes as Dark Matter and their detection with Gravitational Waves,* J. Phys. Conf. Ser. **840**, 012032 (2017).

[265] P. Kanti, *Black holes in theories with large extra dimensions: A Review,* Int. J. Mod. Phys. A **19**, 4899–4951 (2004).

[266] J. H. MacGibbon, *Can Planck-mass relics of evaporating black holes close the universe?* Nature **329**, 308–309 (1987).

[267] S. W. Hawking, I. G. Moss, and J. M. Stewart, *Bubble Collisions in the Very Early Universe,* Phys. Rev. **D26**, 2681 (1982).

[268] H. Kodama, M. Sasaki, and K. Sato, *Abundance of Primordial Holes Produced by Cosmological First-Order Phase Transition,* Progress of Theoretical Physics **68**, 1979–1998 (1982).

[269] I. G. Moss, *Singularity formation from colliding bubbles,* Phys. Rev. D **50**, 676–681 (1994).

[270] C. J. Hogan, *Massive Black Holes generated by Cosmic Strings,* Phys. Lett. **143B**, 87–91 (1984).

[271] S. W. Hawking, *Black Holes From Cosmic Strings,* Phys. Lett. **B231**, 237–239 (1989).

[272] R. R. Caldwell, A. Chamblin, and G. W. Gibbons, *Pair creation of black holes by domain walls,* Phys. Rev. **D53**, 7103–7114 (1996).

[273] S. Rubin, M. Khlopov, and A. Sakharov, *Primordial black holes from nonequilibrium second order phase transition,* Grav. Cosmol. **6**, 51–58 (2000).

[274] M. Khlopov and A. Polnarev, *Primordial black holes as a cosmological test of grand unification,* Physics Letters B **97**, 383 – 387 (1980).

[275] V. Canuto, *On the origin of Hawking mini black-holes and the cold early Universe,* Monthly Notices of the Royal Astronomical Society **184**, 721–725 (1978).

[276] L. J. Hall and S. D. H. Hsu, *Cosmological production of black holes,* Phys. Rev. Lett. **64**, 2848–2851 (1990).

[277] K. Jedamzik and J. C. Niemeyer, *Primordial black hole formation during first order phase transitions,* Phys. Rev. D **59**, 124014 (1999).

[278] B. J. Carr, J. H. Gilbert, and J. E. Lidsey, *Black hole relics and inflation: Limits on blue perturbation spectra,* Phys. Rev. D **50**, 4853–4867 (1994).

[279] B. Carr, K. Dimopoulos, C. Owen, and T. Tenkanen, *Primordial Black Hole Formation During Slow Reheating After Inflation,* Phys. Rev. D **97**, 123535 (2018).

[280] A. Kalaja, N. Bellomo, N. Bartolo, D. Bertacca, S. Matarrese, I. Musco, A. Raccanelli, and L. Verde, *From Primordial Black Holes Abundance to Primordial Curvature Power Spectrum (and back),* JCAP **10**, 031 (2019).

[281] M. Boudaud and M. Cirelli, *Voyager 1 $e^{\pm}$ Further Constrain Primordial Black Holes as Dark Matter,* Phys. Rev. Lett. **122**, 041104 (2019).

[282] A. Katz, J. Kopp, S. Sibiryakov, and W. Xue, *Femtolensing by Dark Matter Revisited,* JCAP **12**, 005 (2018).

[283] H. Niikura *et al.*, *Microlensing constraints on primordial black holes with Subaru/HSC Andromeda observations,* Nat. Astron. **3**, 524–534 (2019).

[284] F. Capela, M. Pshirkov, and P. Tinyakov, *Constraints on primordial black holes as dark matter candidates from capture by neutron stars,* Phys. Rev. D **87**, 123524 (2013).

[285] T. Harada, C.-M. Yoo, and K. Kohri, *Threshold of primordial black hole formation,* Phys. Rev. **D88**, 084051 (2013). [Erratum: Phys. Rev.D89,no.2,029903(2014)].

[286] A. Escriv, C. Germani, and R. K. Sheth, *A universal threshold for primordial black hole formation,* (2019).

[287] A. R. Liddle and D. H. Lyth, *Cosmological Inflation and Large-Scale Structure,* Cambridge University Press (2000).

[288] A. R. Liddle and D. H. Lyth, *The Cold dark matter density perturbation,* Phys. Rept. **231**, 1–105 (1993).

[289] W. H. Press and P. Schechter, *Formation of galaxies and clusters of galaxies by selfsimilar gravitational condensation,* Astrophys. J. **187**, 425–438 (1974).

[290] J. Garcia-Bellido, A. D. Linde, and D. Wands, *Density perturbations and black hole formation in hybrid inflation,* Phys. Rev. **D54**, 6040–6058 (1996).

[291] E. Bugaev and P. Klimai, *Formation of primordial black holes from non-Gaussian perturbations produced in a waterfall transition,* Phys. Rev. D **85**, 103504 (2012).

[292] S. Clesse and J. Garca-Bellido, *Massive Primordial Black Holes from Hybrid Inflation as Dark Matter and the seeds of Galaxies,* Phys. Rev. D **92**, 023524 (2015).

[293] S. M. Leach, I. J. Grivell, and A. R. Liddle, *Black hole constraints on the running mass inflation model,* Phys. Rev. **D62**, 043516 (2000).

[294] K. Kohri, D. H. Lyth, and A. Melchiorri, *Black hole formation and slow-roll inflation,* JCAP **04**, 038 (2008).

[295] M. Drees and E. Erfani, *Running-Mass Inflation Model and Primordial Black Holes,* JCAP **1104**, 005 (2011).

[296] H. Motohashi and W. Hu, *Primordial Black Holes and Slow-Roll Violation,* Phys. Rev. **D96**, 063503 (2017).

[297] L. Alabidi and K. Kohri, *Generating Primordial Black Holes Via Hilltop-Type Inflation Models,* Phys. Rev. D **80**, 063511 (2009).

[298] K. Kohri, C.-M. Lin, and T. Matsuda, *Primordial black holes from the inflating curvaton,* Phys. Rev. **D87**, 103527 (2013).

[299] M. Kawasaki, N. Kitajima, and T. T. Yanagida, *Primordial black hole formation from an axionlike curvaton model,* Phys. Rev. D **87**, 063519 (2013).

[300] K. Ando, K. Inomata, M. Kawasaki, K. Mukaida, and T. T. Yanagida, *Primordial black holes for the LIGO events in the axionlike curvaton model,* Phys. Rev. D **97**, 123512 (2018).

[301] M. Kawasaki, N. Sugiyama, and T. Yanagida, *Primordial black hole formation in a double inflation model in supergravity,* Phys. Rev. D **57**, 6050–6056 (1998).

[302] R. Saito, J. Yokoyama, and R. Nagata, *Single-field inflation, anomalous enhancement of superhorizon fluctuations, and non-Gaussianity in primordial black hole formation,* JCAP **0806**, 024 (2008).

[303] K. Dimopoulos, T. Markkanen, A. Racioppi, and V. Vaskonen, *Primordial Black Holes from Thermal Inflation,* JCAP **1907**, 046 (2019).

[304] T. Bringmann, C. Kiefer, and D. Polarski, *Primordial black holes from inflationary models with and without broken scale invariance,* Phys. Rev. **D65**, 024008 (2002).

[305] P. Ivanov, P. Naselsky, and I. Novikov, *Inflation and primordial black holes as dark matter,* Phys. Rev. **D50**, 7173–7178 (1994).

[306] M. Drees and E. Erfani, *Running Spectral Index and Formation of Primordial Black Hole in Single Field Inflation Models,* JCAP **1201**, 035 (2012).

[307] K. Kohri and T. Terada, *Primordial Black Hole Dark Matter and LIGO/Virgo Merger Rate from Inflation with Running Spectral Indices: Formation in the Matter- and/or Radiation-Dominated Universe,* Class. Quant. Grav. **35**, 235017 (2018).

[308] S. Young, C. T. Byrnes, and M. Sasaki, *Calculating the mass fraction of primordial black holes,* JCAP **1407**, 045 (2014).

[309] A. M. Green, *Pitfalls of a power-law parametrization of the primordial power spectrum for primordial black hole formation,* Phys. Rev. **D98**, 023529 (2018).

[310] R. Arya, A. Dasgupta, G. Goswami, J. Prasad, and R. Rangarajan, *Revisiting CMB constraints on warm inflation,* JCAP **1802**, 043 (2018).

[311] M. C. Lopresto, *Some Simple Black Hole Thermodynamics,* Phys. Teacher **41**, 299–301 (2003).

[312] J. D. Barrow, E. J. Copeland, and A. R. Liddle, *The cosmology of black hole relics,* Phys. Rev. D **46**, 645–657 (1992).

[313] B. J. Carr, J. H. Gilbert, and J. E. Lidsey, *Black hole relics and inflation: Limits on blue perturbation spectra,* Phys. Rev. **D50**, 4853–4867 (1994).

[314] P. Chen, *Might dark matter be actually black?* (2003). ArXiv:astro-ph/0303349.

[315] Y. Bai and N. Orlofsky, *Primordial Extremal Black Holes as Dark Matter,* Phys. Rev. D **101**, 055006 (2020).

[316] Y. Aharonov, A. Casher, and S. Nussinov, *The Unitarity Puzzle and Planck Mass Stable Particles,* Phys. Lett. B **191**, 51 (1987).

[317] R. J. Adler, P. Chen, and D. I. Santiago, *The Generalized uncertainty principle and black hole remnants,* Gen. Rel. Grav. **33**, 2101–2108 (2001).

[318] P. Chen, *Inflation induced Planck-size black hole remnants as dark matter,* New Astron. Rev. **49**, 233–239 (2005).

[319] F. Scardigli, C. Gruber, and P. Chen, *Black Hole Remnants in the Early Universe,* Phys. Rev. D **83**, 063507 (2011).

[320] P. Bokulich, *Black hole remnants and classical vs. quantum gravity,* Philosophy of Science **68**, S407–S423 (2001).

[321] P. Chen, Y. C. Ong, and D.-h. Yeom, *Black Hole Remnants and the Information Loss Paradox,* Phys. Rept. **603**, 1–45 (2015).

[322] B. V. Lehmann, C. Johnson, S. Profumo, and T. Schwemberger, *Direct detection of primordial black hole relics as dark matter,* JCAP **1910**, 046 (2019).

[323] J. Pearson, *Computation of Hypergeometric Functions,* Dissertation, MSc in Mathematical Modelling and Scientific Computing, University of Oxford (2009).

List of Publications

Thesis related Publications

1. **R. Arya**, A. Dasgupta, G. Goswami, J. Prasad and R. Rangarajan,
   Revisiting CMB constraints on warm inflation
   JCAP 02 (2018) 043, arXiv:1710.11109 [astro-ph.CO].

2. **R. Arya** and R. Rangarajan,
   Study of warm inflationary models and their parameter estimation from CMB
   International Journal of Modern Physics D 29 (2020) 08, 2050055, arXiv:1812.03107 [astro-ph.CO].

3. **R. Arya**,
   Formation of Primordial Black Holes from Warm Inflation
   JCAP 09 (2020) 042, arXiv:1910.05238 [astro-ph.CO].

Other Publications

1. **R. Arya**, N. Mahajan and R. Rangarajan,
   Gravitino production in a thermal Universe revisited
   Physics Letters B 772, 258 (2017), arXiv:1608.03386 [astro-ph.CO].

Conference Proceedings

1. **R. Arya**, N. Mahajan and R. Rangarajan,
   Gravitino production in a thermal Universe
   Springer Proceedings in Physics 203 (2018), 551-554.
   Contribution to: 22nd DAE-BRNS High Energy Physics Symposium, 2016.

2. **R. Arya** and R. Rangarajan,

   Estimation of the Parameters of Warm Inflationary Models

   Contribution to: 23rd DAE-BRNS High Energy Physics Symposium, 2018

   (To be published).

3. **R. Arya**

   Primordial Black Holes from Warm Inflation

   Springer Proceedings in Physics 248 (2020), 67-73.

   Contribution to: International Workshop on Frontiers in High Energy Physics

   (FHEP - 2019).